

Universiteit
Leiden
The Netherlands

Wrapping up : nidovirus membrane structures and innate immunity

Oudshoorn, D.

Citation
Oudshoorn, D. (2017, December 28). *Wrapping up : nidovirus membrane structures and innate immunity*. Retrieved from https://hdl.handle.net/1887/59466

Version:	Not Applicable (or Unknown)
License:	Licence agreement concerning inclusion of doctoral thesis in the Institutional Repository of the University of Leiden
Downloaded from:	https://hdl.handle.net/1887/59466

Note: To cite this publication please use the final published version (if applicable).

Cover Page



Universiteit Leiden



The following handle holds various files of this Leiden University dissertation:
http://hdl.handle.net/1887/59466

Author: Oudshoorn, D.
Title: Wrapping up : nidovirus membrane structures and innate immunity
Issue Date: 2017-11-28



WRAPPING UP

NIDOVIRUS MEMBRANE STRUCTURES AND INNATE IMMUNITY

Diede Oudshoorn

WRAPPING UP

NIDOVIRUS MEMBRANE STRUCTURES AND INNATE IMMUNITY

Diede Oudshoorn

PhD Thesis, Leiden University, 2017

ISBN: 978-90-8890-563-6

The work described in this dissertation was performed in the Departments of Medical Microbiology and Molecular Cell Biology of the Leiden University Medical Center.

Cover: EM micrograph of chemically fixed HuH-7 cells by Diede Oudshoorn

Lay-out and printing: Sidestone Press, Leiden, The Netherlands

WRAPPING UP

NIDOVIRUS MEMBRANE STRUCTURES AND INNATE IMMUNITY

PROEFSCHRIFT

ter verkrijging van
de graad van Doctor aan de Universiteit Leiden,
op gezag van Rector Magnificus prof. mr. C.J.J.M. Stolker,
volgens besluit van het College voor Promoties
te verdedigen op dinsdag 28 november 2017
klokke 13:45 uur

door

Diede Oudshoon
geboren te Warmond
in 1989

Promotor: Prof. dr. E.J. Snijder

Co-promotores: Dr. Ir. M. Kikkert
Dr. M. Bárcena

Leden promotiecommissie:

Prof. dr. S.H. van der Burg
Prof. dr. A.J. Koster
Prof. dr. A.H. Meijer
Dr. I. Romero-Brey (Universiteit van Heidelberg; Duitsland)

TABLE OF CONTENTS

CHAPTER 1 **7**
General introduction

CHAPTER 2 **13**
Biogenesis and architecture of arterivirus replication organelles

CHAPTER 3 **37**
New insights in the biogenesis of arterivirus replication organelles

CHAPTER 4 **53**
Middle East respiratory syndrome-coronavirus nonstructural proteins 3 and 4 are required and sufficient to induce the formation of double-membrane vesicles

CHAPTER 5 **75**
Regulation of the innate immune system by ubiquitin and ubiquitin-like modifiers

CHAPTER 6 **91**
Antiviral innate immune response interferes with the formation of replication-associated membrane structures induced by a +RNA virus

CHAPTER 7 **111**
General discussion

References 121

Samenvatting 143
Curriculum vitae
List of publications

Chapter 1

General introduction

GENERAL INTRODUCTION

In recent years, the enormous impact virus outbreaks can have on public health has been illustrated by the epidemics of Zika virus in South America, Ebola virus in West Africa, and Middle East respiratory syndrome-coronavirus (MERS-CoV) in the Arabian Peninsula. Infections with such (re-)emerging viruses can have devastating effects for individuals, while at the same time having worldwide societal and economic impact. Virus outbreaks often accelerate research efforts in order to develop rapid and reliable diagnostic methods and ultimately find therapies and vaccines for life-threatening infections. For example, the severe acute respiratory syndrome-coronavirus (SARS-CoV) sparked renewed interest in research on coronaviruses (and by extension nidoviruses). The order *Nidovirales* currently encompasses four virus families, *Coronaviridae*, *Arteriviridae*, *Roniviridae* and *Mesoniviridae* (recently revised, for details see https://talk.ictvonline.org/taxonomy/). For the latter two, only a limited number of species have been discovered and the replication of these viruses remains to be studied in detail (1-3). The arterivirus family currently does not include known human pathogens. Instead, its members are known to infect livestock (equine arteritis virus (EAV) and porcine reproductive and respiratory syndrome virus (PRRSV)), rodents or non-human primates (simian hemorrhagic fever virus (SHFV) and related viruses) (4). EAV, being the prototypic as well as the first described arterivirus (5), has been well-studied (4, 6). During the past 25 years, PRRSV has posed a major threat to the swine industry worldwide (7, 8). Substantial research investments have been made to develop vaccines that may prevent PRRSV outbreaks (4, 9), although these are currently still insufficiently effective to control PRRSV spread. The molecular biology of EAV, the first nidovirus for which a reverse genetics system was developed (10), has been studied in considerable detail and the virus is considered a model for both other arteriviruses (like PRRSV) and the nidovirus order at large, including the distantly related coronaviruses (2). Knowledge gained from studies of EAV replication has been invaluable in enhancing our understanding of the molecular biology of other members of the order *Nidovirales*.

Currently the coronavirus family includes the largest number of classified members among the *Nidovirales* families, which are distributed over the genera *Alpha-*, *Beta-*, *Gamma-* and *Deltacoronavirus* (subfamily *Coronavirinae*) and the subfamily *Torovirinae* (https://talk.ictvonline.org/taxonomy/). In 2003, the previously unknown betacoronavirus causing SARS emerged and was the first coronavirus causing severe human disease with a potentially lethal outcome (11). Since then, no further SARS-CoV outbreaks have occurred, but a decade later another betacoronavirus that can cause severe SARS-like respiratory disease emerged in the Arabian Peninsula. This Middle East respiratory syndrome coronavirus (MERS-CoV) was first isolated from a human case in 2012 (12). The introduction of both SARS-CoV and MERS-CoV into the human population likely were zoonotic events, as close relatives of both viruses circulate in bats and dromedary camels, respectively (13). The two outbreaks have highlighted the potential threat that coronaviruses can pose to public health, which merits further research to dissect their replication and evolution. No specific strategies to control or prevent coronavirus infections are currently available (14), although

the MERS-CoV outbreak has sparked efforts to develop both vaccines and antiviral drugs (15). A better understanding of the fundamental aspects of coronavirus replication will help to design novel strategies to combat these infections.

Like all other +RNA viruses of eukaryotes, a group that includes important human pathogens like poliovirus, hepatitis C virus, dengue virus, and zika virus, nidoviruses replicate in the cytoplasm of the infected cell. After virus entry, the viral genome, which is of mRNA polarity, is released into the cytosol and can be directly translated by host ribosomes. Translation of +RNA virus genomes generally results in large polyproteins that are cleaved by viral and/or host proteases to release functional smaller subunits, such as the enzymes involved in RNA replication an capping. All +RNA viruses of eukaryotes modify intracellular membranes to accommodate their replication machinery (16-19). The viral RNA-synthesizing machinery is associated with these membrane structures, which will thus be referred to as 'replication organelles' (ROs) in this thesis. The viral ROs are thought to constitute a micro-environment that facilitates viral RNA synthesis. Furthermore, they could play a role in the spatial coordination of viral replication in the cell, by contributing to the compartmentalizing of certain steps of the viral cycle. Finally, ROs may aid in shielding replicating viral RNA from detection by the host cell's innate immune system. In the case of the arteriviruses and coronaviruses, the ROs mainly consist of a reticulovesicular network (RVN) of double-membrane vesicles (DMVs) that are interconnected with each other and (modified) ER membranes (20-22). RO formation is generally driven by specific viral proteins and their transient expression can in some cases suffice to induce the formation of very similar membrane structures (23-28). For arteriviruses, it has been shown that expression of two viral replicase subunits (non-structural protein (nsp) 2 and 3) results in the formation of DMVs similar to those observed during arterivirus infection (24). SARS-CoV DMV formation was claimed to require co-expression of three replicase subunits (nsp3, nsp4, and nsp6) (28). The biogenesis of nidovirus replication organelles will be reviewed extensively in **Chapter 2**.

RNA viruses can evolve very quickly, aided by their high mutation rate. This feature provides them with great adaptability, including the potential for host switching and the evasion of both the innate and the adaptive immune responses. While the adaptive immune response can develop towards specific viral epitopes, the innate immune system targets so-called pathogen-associated molecular patterns (PAMPs), which in the case of viruses can include double-stranded RNA, 5' triphosphate-bearing RNA, cytosolic DNA, or viral capsids. PAMPs can be recognized by cellular pathogen recognition receptors (PRRs), which subsequently induce the expression of interferon-stimulated genes (ISGs) in the infected as well as neighboring cells (29-31). The proteins expressed from ISGs restrict the replication of a whole range of viruses, either by targeting viral functions directly or by modulating host processes involved in virus replication, which leads to a so-called "antiviral state". The importance of the innate immune system is evident from the consequences of defects in – for example – the function of STAT1, a critical protein in the interferon-driven response to infection whose inactivation leads to severe susceptibility to viral infections in humans (32), illustrate the importance of the innate immune system. In line with the

everlasting evolutionary battle between pathogens and their hosts, viruses have developed numerous strategies to prevent the production of type I interferon, limit the effect of type I interferon signaling, or interfere with the antiviral effects of ISGs (33). Not surprisingly, ISGs (and other immunity-related genes) are among the fastest evolving genes (34), highlighting the continuing 'arms race' between pathogens and the innate immune system of their host.

THESIS OUTLINE

This thesis discusses the structure and function of the ROs of arteriviruses and coronaviruses, in particular details of their architecture, the viral factors required for their biogenesis, and novel insights regarding innate immune responses that may counter RO formation, possibly also targeting other +RNA viruses. In **Chapter 2** the current literature on +RNA virus ROs is reviewed, with a special focus on the membrane structures induced in cells infected with arteriviruses and coronaviruses, including their biogenesis and the viral proteins involved. **Chapter 3** further explores this topic and includes new data on the biogenesis of arteriviruses DMVs. Using electron tomography, intermediate structures were visualized that provide new clues on the sequence of membrane remodeling events leading to DMV formation. In addition, the effect on DMV formation was assessed when the third transmembrane nsp of EAV (nsp5) was co-expressed with nsp2 and nsp3. **Chapter 4** describes the identification of the viral proteins required for biogenesis of MERS-CoV DMVs. Although previous work on SARS-CoV led to the conclusion that all three transmembrane nsps (nsp3, nsp4 and nsp6) are required for DMV formation, electron microscopy and electron tomography studies now revealed that – for both MERS-CoV and SARS-CoV – co-expression of nsp3 and nsp4 sufficed to achieve DMV formation. Furthermore, these DMVs were organized in a RVN, similar to what has previously been observed in coronavirus-infected cells. This study also emphasized clear parallels between the viral proteins required for the biogenesis of the ROs of arteriviruses and coronaviruses. **Chapter 5** switches gears by reviewing the literature regarding the induction and regulation of the cellular innate immune response against viruses. The chapter is mainly focused on the pathways leading to the production of type I interferons and the role that post-translational modification with ubiquitin and other ubiquitin-like modifiers plays in the regulation of the innate immune response. Whether +RNA virus ROs may be targeted by the innate immune system is then explored in **Chapter 6**, which analyzes the impact of type I interferon treatment on the induction of DMV formation by arterivirus nsp2-3. Interferon-β treatment resulted in a sizeable reduction of the number of DMVs observed. Moreover, double-membrane sheets, a putative intermediate of DMV biogenesis, accumulated following Interferon-β treatment, which suggests that DMV biogenesis was impaired. Finally, **Chapter 7** summarizes the work presented in this thesis and discusses the findings in the broader context of +RNA-viral ROs.

Chapter 2

Biogenesis and architecture of arterivirus replication organelles

Diede Oudshoorn[1], Barbara van der Hoeven[1], Abraham J. Koster, Eric J. Snijder, Marjolein Kikkert, and Montserrat Bárcena

[1]These authors contributed equally to this study

The contents of this chapter were published, in modified form, as part of the review "Biogenesis and architecture of arterivirus replication organelles." (Virus Res. 2016 Jul 15;220:70-90) by B. van der Hoeven, D. Oudshoorn, A.J. Koster, E.J. Snijder, M. Kikkert and M. Bárcena.

ABSTRACT

All eukaryotic positive-stranded RNA (+RNA) viruses appropriate host cell membranes and transform them into replication organelles, specialized micro-environments that are thought to support viral RNA synthesis. Arteriviruses (order *Nidovirales*) belong to the subset of +RNA viruses that induce double-membrane vesicles (DMVs), similar to the structures induced by *e.g.* coronaviruses, picornaviruses and hepatitis C virus. In recent years, electron tomography has revealed substantial differences between the structures induced by these different virus groups. Arterivirus-induced DMVs appear to be closed compartments that are continuous with endoplasmic reticulum membranes, thus forming an extensive reticulovesicular network (RVN) of intriguing complexity. This RVN is remarkably similar to that described for the distantly related coronaviruses (also order *Nidovirales*) and sets them apart from other DMV-inducing viruses analyzed to date. This review summarizes the current knowledge and open questions regarding arterivirus replication organelles and discusses them in the light of the latest studies on other DMV-inducing viruses, particularly coronaviruses.

MEMBRANE MODIFICATIONS INDUCED TO ACCOMMODATE +RNA VIRUS REPLICATION

All positive-stranded RNA (+RNA) viruses of eukaryotes replicate their genome in the cytoplasm of the host cell using a common strategy characterized by the modification of host membranes into organelle-like structures that, for many +RNA viruses, have been directly implicated in viral RNA synthesis (reviewed in (18, 35, 36)). Although these virus-induced membrane structures, often referred to as viral replication organelles or replication structures, have been known for decades, their exact purpose remains enigmatic. Three major advantages of associating viral RNA synthesis with dedicated membranes have been proposed. Firstly, confining viral RNA synthesis in a specific compartment could generate an optimally suited micro-environment by concentrating the viral proteins and precursors necessary for the process. Furthermore, the anchoring of viral replication complexes to membranes creates a planar geometry for diffusion of metabolites and macromolecules, which can increase the efficacy of the enzymatic processes. Secondly, compartmentalization could provide a means to spatially separate and coordinate the different stages of the infectious cycle, such as genome translation, replication and packaging. Finally, during viral RNA synthesis several intermediate nucleic acid species such as double-stranded RNA (dsRNA) and 5′ triphosphate-containing RNAs are formed, which are potent activators of the host cell's innate immune response (29, 30). Insulation of these intermediates could therefore prevent or delay detection by the defense systems of the host cell (37). Clearly, these proposed functions are not mutually exclusive and, likely, +RNA viruses take advantage of multiple benefits associated with the compartmentalization of their replicative process.

Both viral and cellular factors are thought to be important for the biogenesis of +RNA viral replication organelles, although in most cases the specific players and processes involved remain poorly understood. Multiple +RNA viruses encode non-structural proteins (nsps) that include proven or predicted transmembrane domains and, for some of them, expression of a combination of such membrane-associated viral nsps has been shown to be necessary and sufficient for the induction of membrane modifications resembling those found in infected cells (23-28, 38, 39). Besides these viral proteins, a wide variety of host factors have been implicated in the formation and functioning of these structures (reviewed in (40, 41)). Their roles range from the recruitment of viral replication proteins to the induction of membrane modifications. Not surprisingly, the list of identified host factors includes proteins involved in lipid metabolism (e.g. phosphatidylinositol-4-phosphate (PI4P) kinases, fatty acid synthase), specific lipids (e.g. PI4P, sterols), and membrane-shaping proteins (e.g. reticulons and endosomal sorting complexes required for transport (ESCRT) proteins) (42-46).

Over the last decades, the replication organelles of a large number of +RNA viruses have been characterized using electron microscopy (EM). It has become apparent that, despite the large evolutionary distances between these viruses and the different cellular organelles they manipulate, all +RNA viruses infecting eukaryotic host cells seem to induce one of

Order	Family	Genus	Species[a]	DMVs[b]			Additional membranous structuresc	References
				Diameter (nm)	Membrane connections[d]	Open or closed to the cytosol		
Nidoviruses	*Arteriviridae*	*Arterivirus*	EAV	95[e]	DMV-ER, DMV-DMV, DMV-PM	Closed	PM	Knoops *et al.* (2012)[h]
			PRRSV	70-85	-	-	SMV	Metwally *et al.* (2010)
			LDV	100-300	-	-		Stueckemann *et al.* (1982)
			SHFV	100[f]	-	-	PM	Wood *et al.* (1970)
	Coronaviridae	*Alphacoronavirus*	HCoV-NL63	140-210	-	-		Orenstein *et al.* (2008)
			HCoV-229E	~200[g]	-	-		Lundin *et al.* (2014)
		Betacoronavirus	SARS-CoV	200-300	DMV-ER, DMV-DMV, DMV-CM	Closed	CM, VP	Knoops *et al.* (2008)[h]
			MHV	200-350	-	-	CM	Ulasli *et al.* (2010)
			MERS-CoV	150-320	-	-	CM	De Wilde *et al.* (2013)
		Gammacoronavirus	IBV	180[e]	Isolated DMVs / DMV-ER	Closed	ZM, spherules	Maier *et al.* (2013)[h]
Picornavirales	*Picornaviridae*	*Enterovirus*	CVB3	160[e]	Isolated DMVs	Closed / Open	SMT, MLV	Limpens *et al.* (2011)[h]
			PV	100-300	Isolated DMVs	Closed / Open	SMT, MLV	Belov *et al.* (2012)[h]
Unassigned	*Flaviviridae*	*Hepacivirus*	HCV	150[e]	Isolated DMVs / DMV-ER	Closed / Open	SMV, MLV	Romero-Brey *et al.* (2012)

two basic morphotypes of membrane modifications: invaginations or double-membrane vesicles. In the last decade, the study of the architecture of viral replication organelles has been stimulated further by the introduction of electron tomography (ET). ET enables the three-dimensional (3D) characterization of biological specimens at nanometer resolution by computationally combining images collected at different tilt angles in a transmission electron microscope (47). The first +RNA virus replication organelles characterized by ET were those induced by the nodavirus Flock House virus (FHV) (48). FHV induces invaginations in the outer mitochondrial membrane and therefore belong to the first morphotype of +RNA virus replication organelles. Using immuno electron microscopy (IEM) to detect BrUTP incorporated into viral RNA, the interior of these spherules was shown to contain newly-synthesized viral RNA that is thought to be exported to the cytosol through a neck-like channel of ~10 nm in diameter, which could be clearly visualized in the 3D reconstruction. Since this first study, the membrane modifications induced by, for example, coronaviruses (21, 49), arteriviruses (20), flaviviruses (50-54), hepaciviruses (36), togaviruses (55), picornaviruses (41, 56) and tombusviruses (57) have been characterized using ET.

The flavivirus dengue virus (DENV) provides another well-characterized example of virus-induced invaginations of cellular membranes (50) that, in this case, occur at the rough endoplasmic reticulum (ER). Despite the use of a different membrane donor organelle, the DENV-induced spherules share several characteristics with those generated during FHV infection. DENV-induced membrane invaginations are also open to the cytosol through a neck-like connection (~10 nm in diameter) and contain dsRNA. Apart from these invaginations, DENV infection also induces the formation of so-called convoluted membranes, which are continuous with the spherules through their connection with ER membranes and are speculated to be a reservoir of proteins and lipids used for DENV replication (50). The formation of ER invaginations that retain a connection to the cytosol has also been shown for other flaviviruses, like tick-borne encephalitis virus (53), West Nile virus (51), and Langat virus (52).

Table 1. (left page) Arteriviruses and other animal +RNA viruses inducing DMVs.

[a] Equine arteritis virus (EAV), porcine reproductive and respiratory syndrome virus (PRRSV), lactate dehydrogenase elevating virus (LDV), simian hemorrhagic fever virus (SHFV), human coronavirus NL63 (NL63), human coronavirus 229e (229e), severe acute respiratory syndrome coronavirus (SARS-CoV), mouse hepatitis virus (MHV), Middle East respiratory syndrome coronavirus (MERS-CoV), infectious bronchitis virus (IBV), coxsackievirus B3 (CVB3), poliovirus (PV), hepatitis C virus (HCV).

[b] DMV connections and openings are only specified when 3D studies are available. When different DMV subpopulations have been reported, the distinct features of these subpopulations are separated by a slash.

[c] Paired membranes (PM), single-membrane vesicle (SMV), convoluted membranes (CM), vesicle packets (VP), zippered membranes (ZM), single-membrane tubules (SMT), multilamellar vesicles (MLV).

[d] ER, endoplasmic reticulum

[e] Average diameter

[f] Modal diameter

[g] Not reported, estimate from published images

[h] 3D characterizations by electron tomography

The formation of cytopathic vacuoles (CPVs), which are modified endosomes and lysosomes of about 600-2000 nm in diameter that accommodate invaginations of their membranes, is a hallmark for togavirus infection. ET applied to cells infected with rubella virus (RUBV) showed that these CPVs also contain interconnected small vesicles, vacuoles and stacked membranes (55). Furthermore, RUBV recruits rough ER, mitochondrial, and Golgi membranes close to the CPVs, presumably to make use of the resources present in these organelles to fuel its genome replication. Early in infection, Semliki Forest virus and Sindbis virus (genus *Alphavirus*) induce plasma membrane invaginations that afterwards appear to be internalized through the endosomal pathway to produce the CPVs typical of togavirus-infected cells (58-61).

The morphotype of virus-induced invaginations seems to extend to plant +RNA viruses (reviewed in (62), for an ET characterization see (57)). The striking similarities in the morphology of these invaginations across widely different virus groups strongly suggest a highly conserved mechanism behind their formation. In this regard, brome mosaic virus (*Bromoviridae*), which induces invaginations into the ER, is one of the best studied models for this replication organelle morphotype (27, 63). The insights obtained into the biogenesis and function of BMV-induced spherules highlighted remarkable parallels with the assembly of retrovirus capsids, which could hint to an ancestral common mechanism to alter cellular membranes that may have been preserved even more broadly among viruses (64).

The architecture of the second morphotype of replication organelles is strikingly different compared to the invagination morphotype and consists of double-membrane vesicles (DMVs). In contrast with the virus-induced invaginations characterized so far, which have the same topology among different virus groups, viral DMVs with different architectures have been found. Thanks to ET, variations in DMV connectivity and topology, not only between different virus groups but sometimes also between subpopulations of DMVs induced by a specific virus, have become apparent (Table 1). Moreover, infection with viruses in this group often results in the formation of additional types of membrane modifications, thus creating complex scenarios in which the exact role of the different virus-induced structures and their interplay remains elusive (Table 1). An example are the structures induced by the picornaviruses coxsackievirus B3 (CVB3) and poliovirus (PV), two enteroviruses that first generate single-membrane tubular structures that appear to transform into DMVs later in infection, presumably through an enwrapping mechanism (56, 65).

Notably, whereas the replication organelles of all other members of the family Flaviviridae that have been analyzed so far belong to the invagination morphotype, hepatitis C virus (HCV), the prototype of the *Hepacivirus* genus, predominantly induces DMVs (23, 66). Although single-membrane vesicles could also be detected in HCV-infected cells, the presence of DMVs appeared to correlate with viral RNA replication (36, 67).These HCV DMVs were described as protrusions from the ER into the cytosol and were often still connected to the ER (23).

Other viruses that, like HCV, seem to use the ER as the membrane donor organelle and also generate DMVs are viruses belonging to the order *Nidovirales*. This order

currently encompasses four virus families, *Coronaviridae*, *Arteriviridae*, *Roniviridae* and *Mesoniviridae*. Only a limited number of species have been assigned to the latter two families thus far and many aspects of their replication remain to be studied in detail (1, 68). In contrast, coronaviruses have been studied extensively because of their role as veterinary pathogens and the large societal impact of the zoonotic disease outbreaks caused by severe acute respiratory syndrome coronavirus (SARS-CoV; 2003) and Middle East respiratory syndrome coronavirus (MERS-CoV; since 2012). Additionally, several established human coronaviruses are widespread in the population and frequently associated with common colds. During the past decade, detailed 3D ultrastructural characterizations of virus-induced replication structures have been published for a few nidoviruses, specifically, for the arterivirus equine arteritis virus (EAV) (20) and the coronaviruses SARS-CoV and infectious bronchitis virus (IBV) (21, 22, 69). This review focuses on arterivirus replication organelles. The fundamental analogies and differences between arteriviral and coronaviral replication organelles, as revealed by recent studies, will be analyzed in parallel and also in the wider context of DMV-inducing +RNA viruses. Finally, we will discuss some of the open questions and future research directions that, in our view, will be important to unravel the role of these remarkable structures.

ARTERIVIRUSES AND THE MEMBRANE REARRANGEMENTS THEY INDUCE

Arterivirus biology

Although the arterivirus prototype EAV was discovered in 1953 (5), the family *Arteriviridae* was not established until 1996 (70). The group was long comprised of four members: EAV, porcine reproductive and respiratory syndrome virus (PRRSV), simian hemorrhagic fever (SHFV) and lactase dehydrogenase-elevating virus (LDV). However, over the course of the last five years, several new (tentative) arteriviruses were discovered such as wobbly possum disease virus (WPDV), African pouched rat virus 1 and multiple new simian arteriviruses that are only distantly related to SHFV (4, 71-73). Because of their economic impact, EAV and PRRSV have been characterized most extensively and research on these viruses has provided the basis for most of our current understanding of arterivirus replication.

Arteriviruses have polycistronic +RNA genomes with sizes ranging from 13-16 kb (3). The two large 5′-proximal open reading frames (ORF1a and ORF1b), which encompass more than 60% of the genome space, encode the replicase or non-structural (poly)proteins (Fig. 1A). The 3′-proximal part of the genome contains an array of smaller ORFs encoding the structural proteins, which are expressed from a nested set of subgenomic (sg) mRNAs (Fig. 1A) (4). After virus entry, the genome is released into the cytosol and ORF1a can be directly translated into polyprotein 1a (pp1a). Genome translation can be extended using the downstream ORF1b reading frame when a -1 ribosomal frameshift (RFS) occurs just before the end of ORF1a. This event, which results in the synthesis of pp1ab, is promoted by a specific heptanucleotide shift site and an RNA pseudoknot structure (74, 75). The

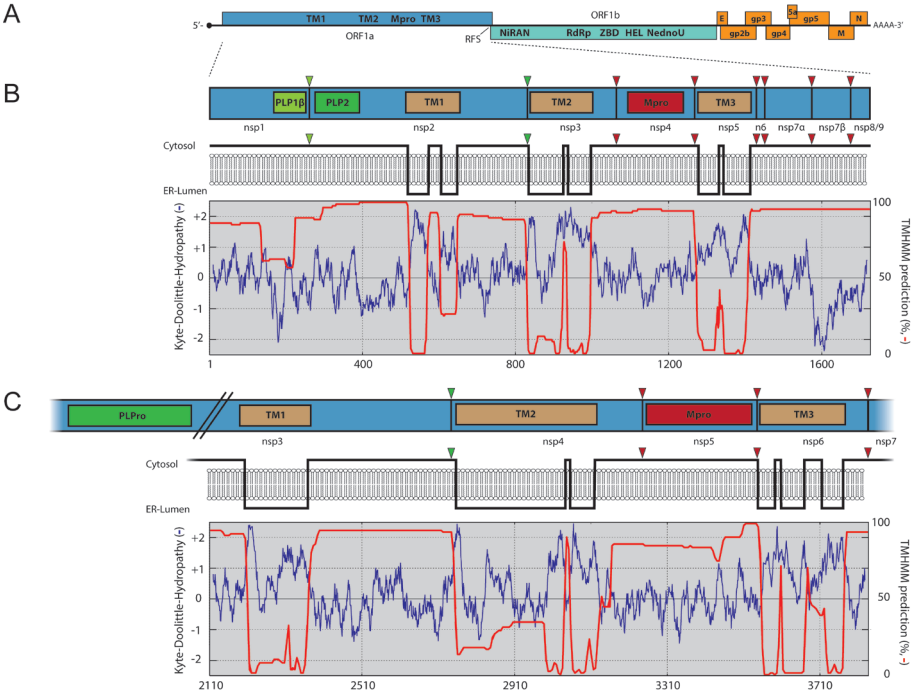


Fig. 1. Comparison of transmembrane non-structural proteins of arteri- and coronaviruses. (A) *Overview of the EAV genome organization with several conserved domains encoded in ORF1a and ORF1b indicated (see main text for details). The structural protein genes, such as those encoding the viral glycoproteins (GP), envelope (E), membrane (M) and nucleocapsid (N) proteins, are located in the 3'-proximal quarter of the genome (shown in orange).* **(B)** *The top panel presents a scaled schematic of EAV pp1a. The three proteases (PLP1β, PLP2 and M^{pro}) are indicated with colored boxes and their corresponding cleavage sites in pp1a with triangles. The middle panel shows a model of the membrane topology of EAV ORF1a based on a Kyte & Doolittle hydropathy plot (blue line) and TMHMM predictions (red line; the percentage on the right represents the probability for that part of the protein to be cytosolic), which are both shown in the lower panel.* **(C)** *SARS-CoV nsp3-7 region, represented as in B. The region encompassing the TM domains is shown using the same scale as used for EAV pp1a (amino acids 2110 – 3836 of SARS-CoV pp1a). SARS-CoV nsp3 has been truncated internally to include the protease corresponding to the nsp3/4 cleavage site. Kyte & Doolittle hydropathy plots were generated on web.expasy.org and TMHMM predictions using the Geneious software package both based on database sequences of EAV (NC_002532.2) and SARS-CoV (NC_004718.3).*

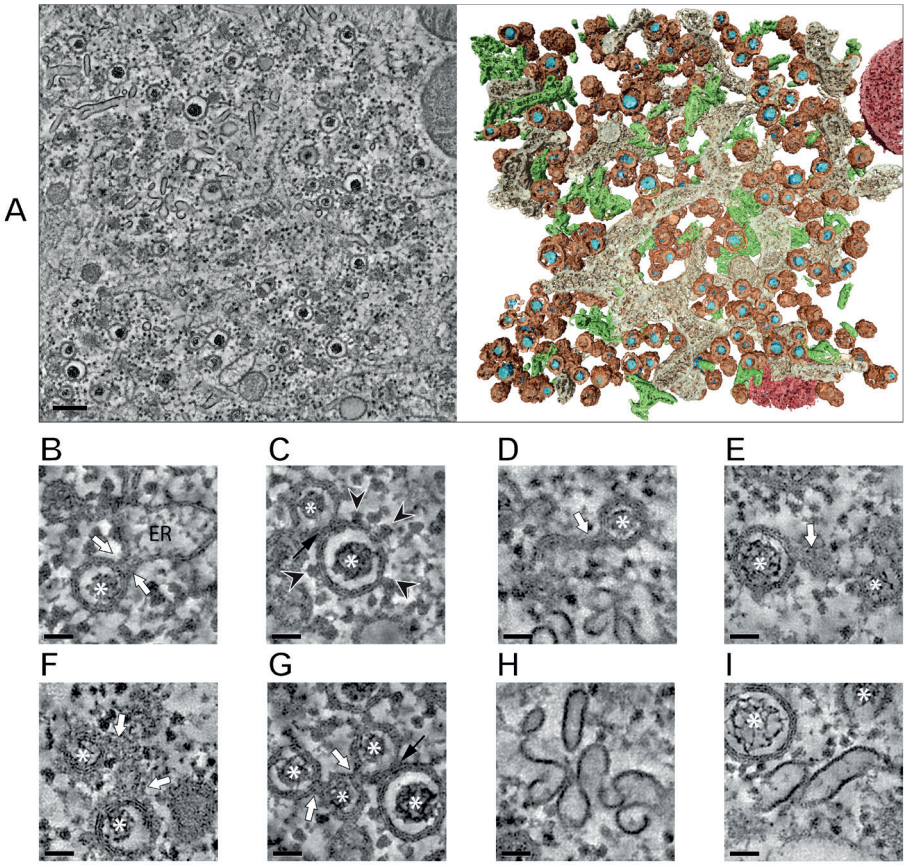
polyproteins pp1a and pp1ab contain the viral nsps, which are released by multiple internal proteases (76, 77). Together they are often referred to as the replicase, as they either are part of or support the functions of the so-called replication and transcription complex (RTC), the aggregate enzymes that replicate the viral genome and produce the sg mRNAs used to express the structural proteins.

The ORF1b-encoded subunits include the main enzymatic activities required for RNA replication, such as the RNA-dependent RNA polymerase (RdRp) and the helicase (4, 75, 78-81). The pp1a subunits seem to support the viral RNA replication more indirectly. Their functions include modulation of host gene expression, proteolytic activity required for polyprotein maturation, and modification of host cell membranes to accommodate viral RNA synthesis.

When considering nidoviruses at large, a conserved array of replicase domains can be defined, consisting of the viral main protease (M^{pro}) flanked by two transmembrane (TM) domains, the ORF1a/1b ribosomal frameshift site, a nidovirus RdRp-associated nucleotidyltransferase (NiRAN), the RdRp, a zinc-binding domain (ZBD), a superfamily 1 helicase (HEL) and, only in vertebrate nidoviruses, an endoribonuclease (NendoU) (3, 78, 81, 82). In all arteri- and coronavirus replicases, a third TM domain (TM1) is present upstream of the hydrophobic regions that flank M^{pro} (TM2 and TM3; Fig. 1A). Although many other virus groups contain some or most of these elements, the array of (TM1-)TM2-M^{pro}-TM3-RFS-NiRAN-RdRp-ZBD-HEL is nidovirus specific.

Arteriviruses encode multiple papain-like proteases (PLPs) and a 3C-like or chymotrypsin-like protease that is their M^{pro} (reviewed in (4, 76, 79)). The number of active PLP domains varies per virus species (e.g. 2 for EAV, 3 for PRRSV and LDV, and 4 for SHFV) and these proteases are all located upstream of TM1 in pp1a/pp1ab, where each of them processes a single downstream cleavage site (83). In the case of EAV, the PLPs located in nsp1 and nsp2 (called PLP1β and PLP2) both swiftly process a single site in the polyprotein (the nsp1/nsp2 and nsp2/nsp3 junctions, respectively; Fig. 1B). M^{pro} is located in nsp4 and processes the remainder of pp1a/pp1ab (the nsp3-8/nsp3-12 region; Fig. 1B). The C-terminal half of pp1a encompassing nsp3-8 can be processed following two different pathways, each yielding specific end products. The pathway used for nsp3-8 processing depends on the presence or absence of cleaved nsp2 (84). When free nsp2 is present, the nsp4/nsp5 junction can be cleaved, which yields the nsp5-7 and nsp5-8 cleavage products that, apart from the slow processing of the nsp7/nsp8 junction, do not seem to undergo further processing. In the absence of nsp2, the nsp4/5 junction remains uncleaved, but instead the nsp5/6, nsp6/7 and possibly the nsp7α/7β sites are processed (77, 84-86). In infected cells, the nsp4/5 junction is mostly cleaved, resulting in the majority of nsp5 being present in nsp5-7 and nsp5-8 cleavage products; however, cleavage of sites in nsp5-7, even though occurring in a minority of cases, is critical for virus replication (86).

For the three TM regions in pp1a of arteriviruses, located in nsp2, nsp3 and nsp5, the exact membrane topology has not been established in full experimental detail, but all of them are predicted to span the membrane multiple times (87, 88). Furthermore, it is assumed that both termini of each of these nsps must face the cytosol, where the viral proteases that



must have access to the cleavage sites are present (Fig. 1B) (89). Nevertheless, PRRSV TM1 in nsp2 was suggested to span the membrane 5 times after performing *in vitro* translation of nsp2 alone in the presence of artificial membranes (90). Such a topology, however, would appear to pose a major problem for polyprotein processing since PLP2 and the nsp2/3 cleavage site would reside on opposite sides of the membrane. The transmembrane nature of EAV TM2 in nsp3 was confirmed by engineering a site for N-linked glycosylation in the first predicted luminal loop, which was indeed glycosylated when pp1a was expressed transiently (89). This result strongly supports the nsp3 topology model that places the nsp2/3 cleavage site at the cytoplasmic side of the membrane. Translocation of the nsp2 C-terminal domain following polyprotein cleavage would be compatible with all these observations; however, evidence supporting this hypothesis remains to be obtained.

When the TM1-TM2-M^{pro}-TM3 regions of the arterivirus and coronavirus pp1a polyproteins are compared (Fig. 1), their general organization is strikingly similar, despite the 2.5-fold overall pp1a size difference between the two families. In both virus groups, the junction between the nsps containing TM1 and TM2 is cleaved by a PLP located in the TM1-containing nsp (PLP2 in nsp2 for arteriviruses and PLpro in nsp3 for coronaviruses)

Fig. 2. (right page) Electron tomography analysis of the EAV-induced RVN. (A) *Typical region containing EAV-induced structures in Vero E6 cells at 8 h post-infection (p.i.). Tomographic slice (10 nm thick) extracted from the dual-axis reconstruction of a 200-nm-thick section (left) (see also Supplementary movie S1), and corresponding surface-rendered model (right) displaying DMVs (membranes in brown, electron-dense cores in blue), ER (beige), EAV-induced tubular network (green), and mitochondria (red).* **(B-I)** *Close-ups illustrating detailed features of EAV-induced structures. The gallery consists of virtual thin slices extracted from tomograms of infected Vero E6 (B,C,D,G,H) and HuH-7 cells (E,F,I). In both cell lines, identical features were observed. EAV-induced DMVs often appear connected through their outer membrane (white arrows) to the ER (A), and ribosomes decorate their outer membrane (B, arrowheads), suggesting an ER origin for these membranes. Additional membrane connections of DMVs to paired membranes (D,E) or small complex membranous structures (F), and/or to other DMVs (G) are common. Close membrane-membrane interactions between different DMVs are also frequent (black arrows, C,G). The typical electron-dense cores inside the DMVs are indicated by asterisks. (H,I) Fragments of the tubular network induced by EAV. Note the difference between the single electron-dense layer of the tubular profiles and the trilaminar profile typical of lipid bilayers. This tubular network (in green in the model in 2A) is intertwined with EAV replication structures and contains the nucleocapsid protein (20). Scale bars, 200 nm (A), 50 nm (B-I). For experimental details on EAV-infected HuH-7 samples see* **Chapter 3**. *B,C,D,G: adapted from (20) with permission.*

Movie S1 *(available at http://www.sciencedirect.com/science/article/pii/S016817021630199X). Tomographic reconstruction of an area in EAV-infected VeroE6 cell exhibiting the typical DMV replication organelles. The video shows consecutive 1.2-nm-thick slices through the entire tomogram of the region presented in Fig. 2A.*



(91-94). The other TM-containing nsps (nsp3 and nsp5 for arteriviruses and nsp4 and nsp6 for coronaviruses) are both released from the polyprotein by the M^{pro} situated between TM2 and TM3 (76). Moreover, the predicted tetraspanning membrane topology of TM2 is very similar, with two ER luminal domains of which the N-terminal one is the largest (89, 95). The fact that the general arrangement of hydrophobic domains in pp1a is conserved between arteriviruses and coronaviruses probably points to a common, and important, function in virus replication.

Host membrane remodeling in arterivirus infection

The non-structural proteins containing the predicted TM domains (Fig. 1B,C) appear to be the main players in the modification of host cell intracellular membranes (24, 28, 88, 96). These proteins, together with several other nsps like the RdRp-containing nsp9 and the helicase-containing nsp10, were shown by immunofluorescence and IEM to localize to the same membrane structures in the perinuclear region of EAV-infected cells (88, 97, 98). This suggested that arterivirus RNA synthesis is associated with these intracellular membranes. When a crude membrane fraction was isolated from EAV-infected cells, the viral RTC was

retained and RNA synthesis could be reconstituted *in vitro*, which further supported the concept of membrane-associated viral RNA synthesis (99). Interestingly, this in vitro RTC activity was lost after detergent treatment, strongly suggesting that the RTC's functionality depends on the integrity of the membranes (99). Similar data has also been published for coronaviruses (94, 100-107).

The remarkable ability of arteriviruses to induce the formation of DMVs in the cytoplasm of infected cells was already observed by electron microscopy in the 1970's (108, 109) and has been noticed for all family members analyzed by EM to date (88, 110-114). These DMVs, with a diameter of about 100 nm (Table 1), appear in the perinuclear region of the cell and then proliferate in number giving rise to cytoplasmic clusters that often also show an increased presence of free ribosomes (20, 109, 110).

A significant breakthrough in our understanding of the complex architecture and spatial arrangement of arteriviral replication organelles was brought about by applying electron tomography to EAV-infected Vero E6 cells (20) (Fig. 2A, Supplementary movie S1). More recently these 3D imaging studies were expanded to HuH-7 cells in our laboratory (for experimental details, see **Chapter 3**) showing that the original observations were not unique for a single cell line (Fig. 2). Occasionally, neck-like connections between the endoplasmic reticulum and the outer membrane of DMVs had been observed in 2D images (88). However, the 3D analysis showed that these narrow connections are actually rather common. This type of connections (Fig. 2B, white arrows) pointed directly to the ER as the most likely membrane donor organelle, a notion further supported by the fact that ribosomes decorating the outer membrane of the DMVs were regularly observed in the tomograms (Fig. 2C, black arrowheads). Although DMVs are the most prominent and abundant EAV-induced membrane structures, other modified membranes in the form of short stretches of paired membranes or small complex membrane arrangements connecting DMVs to one another or to the ER, were also apparent in the tomograms (Fig. 2D-F). The large majority of the DMVs seemed to be connected to the ER, modified membranes, other DMVs or a combination of the above (Fig. 2B,D-G, white arrows). It should be pointed out that not all of these associations appeared as clear membranous connections but, instead, as tight membrane-membrane interactions that were particularly frequent between DMVs (Fig. 2C,G, black arrows). Only about 10% of the DMVs in the tomograms appeared as separate, free-floating vesicles and this may even be an overestimation since narrow connections in the top or bottom regions of the DMVs cannot be detected due to the intrinsically lower resolution of the tomograms along the Z axis (47). Therefore, the general concept that emerges from the 3D analysis is that of a large reticulovesicular network (RVN), consisting of DMVs and modified ER.

As an additional complexity, a few hours after the appearance of the first DMVs, a rather different EAV-induced structure could be observed between the clusters of DMVs. ET revealed that it consists of a network of branching tubular structures, with an average diameter of approximately 43 nm, (Fig. 2A, right panel; in green; Fig. 2H-I) lacking the typical trilaminar profile of lipid bilayers in EM, and thus most probably representing a proteinaceous structure. Using IEM, these tubules were found to abundantly label for the

arteriviral N protein (20). Similar tubules had been detected before in EAV-infected BHK-21 cells, both upon infection (111) and upon transfection with EAV RNA replicons (115). The formation of these tubules seems to depend on expression of the arteriviral N protein as they were absent when the transfected viral RNA lacked the N protein gene. Nevertheless, additional viral components are likely required in the process as N protein expression by itself appeared to be insufficient to generate tubules (115).

Together with the previously reported observation that similar tubules extended into budding virus particles (111), the data suggests that these structures are involved in virus assembly, a process that is still largely uncharacterized for arteriviruses. The fact that this tubular network appears entwined with the RVN could reflect an efficient way of spatially linking the synthesis and packaging of genomic RNA.

Our detailed 3D characterization of the ultrastructure of the EAV-induced RVN revealed additional interesting details with intriguing functional implications. For example, in the DMV interior a previously unreported electron dense core could clearly be distinguished (Fig. 2A, blue; Fig. 2B-I, asterisks). The detection of this core depended on the use of high-pressure freezing (HPF) followed by freeze substitution (FS) for EM sample preparation (20). In chemically fixed samples, the conventional technique used in all previous studies on arterivirus-induced membrane modifications, the DMV interior appeared mainly electron translucent. Using plunge-freezing followed by FS, a granular content became apparent but a dense core was only visible in HPF-FS samples. HPF-FS is considered the gold standard for the ultrastructural preservation of resin-embedded specimens as it has several advantages over alternative methods (116). In our comparison of different protocols for fixation of EAV-infected cells, it was evident that HPF-FS offered superior preservation, not only of the RVN but also of the cytosolic content and various cellular organelles (20).

The average diameter of the DMV cores (~50 nm) appears relatively constant during the course of infection and their individual size seems directly proportional to the size of the surrounding DMV. Interestingly, in IEM samples, these cores labeled strongly for dsRNA, a presumed intermediate in viral RNA replication (Fig. 3A). Consistent with this observation, these structures were shown by 2D and 3D electron spectroscopic imaging (ESI) to have a high phosphorus content (Fig. 3B-D). ESI is an EM technique that takes advantage of the fact that electrons that are inelastically scattered by different elements in the sample lose different amounts of energy. Using this principle, and by collecting images using only electrons that have suffered specific energy losses, images that reveal the location and concentration of a certain element, known as elemental maps, can be obtained (117). In this manner, the average phosphorous content of the cores was determined to be equivalent to about a dozen copies of the EAV RNA genome (20).

In view of the presence of dsRNA inside DMVs, it is tempting to speculate that the DMV interior is the site of viral RNA synthesis as this could provide a propitious environment that would also hide dsRNA replication intermediates from the innate immune sensors of the host. In analogy, for the other morphotype of +RNA virus-induced membrane alterations, the interior of the invaginated spherules seems to be the site of viral RNA synthesis (27, 48, 58, 60, 118, 119). However, these invaginations have openings to the cytosol that permit

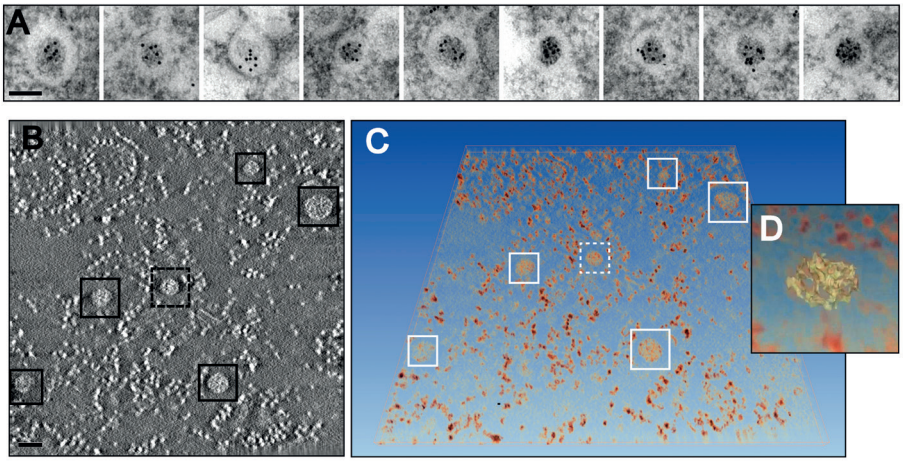


Fig. 3. Analysis of the cores in EAV-induced DMVs. (A) *Immunogold labeling for dsRNA in EAV-infected Vero E6 cells (7 h p.i.). The gallery of DMVs illustrates the strong labeling for dsRNA of the DMV core.* **(B-D)** *Analysis of the phosphorous content in EAV-infected Vero E6 cells (8 h p.i.) by 3D electron spectroscopy imaging (ESI). A tilt series of elemental map images for P was obtained using the jump-ratio approach as described in (20) from a 75-nm thick section of an infected cell.* **(B)** *Tomographic slice (~5 nm thick) extracted from the final ESI reconstruction, showing the high P content (higher intensity) of the DMV cores (boxed). The smaller brighter structures between DMV cores correspond to free ribosomes, also rich in P, which are always particularly abundant in the areas containing DMVs.* **(C)** *Direct volume rendering of the ESI tomogram showing the P-content in 3D.* **(D)** *Close-up of one of the DMV cores (discontinuous box in B and C), which is highlighted in yellow in isosurface display mode. The resulting isosurface, generated at an intensity threshold level that revealed isolated ribosomes, suggests a thread-like structure of the core RNA content. Scale bars, 100 nm. Adapted from (20) with permission.*

the necessary import of substrates and export of RNA products, whereas in the case of EAV DMVs the inner membrane defines a closed compartment, apparently sealed from the cytosol, thus creating a topological conundrum with respect to RNA synthesis.

The situation is further complicated by the fact that, according to immunolabeling experiments, key replicase subunits, like nsp3 and the RdRp-containing nsp9, localize to DMVs and surrounding RVN membranes but only rarely to the core of DMVs (20). At this point it is important to note that the presence of neither dsRNA nor nsps may be bona fide markers for the localization of the active site of viral RNA synthesis. For example, only a small part of the abundantly expressed nsps is likely to be involved in active RNA-synthesizing complexes, as previously calculated for HCV (120). Likewise, abundant labeling of DMV cores could reflect accumulation of dsRNA intermediates rather than active RNA synthesis. A less ambiguous alternative to pinpoint viral RNA synthesis is by metabolic labeling of nascent viral RNA followed by EM detection. This latter approach was followed in the past for EAV (88) by transfecting cells with Br-UTP, after which labeling with a Br-U-specific antibody revealed some signal associated with DMV membranes. However, the size of the DMVs, relatively small when considering the distance that separates the gold markers from

the original epitopes (up to ~30 nm), the limited sample preservation and the qualitative nature of the analysis precluded an accurate localization of the active RTC. Furthermore, signal in the cytosol was also observed, probably reflecting the fact that the labeling times may have been too long to prevent the migration of newly-synthesized RNA.

Comparison with coronavirus-induced membrane modifications

In the wider context of the order *Nidovirales*, coronaviruses constitute the only other family for which the putative replication organelles have been analyzed in some detail. Coronavirus-induced membrane alterations were first described in the 1960's (121, 122) and have been further investigated in the past decade. In all cases examined so far, also coronaviruses were shown to induce the formation of DMVs. This includes members of three of the four genera of the coronavirus family: alphacoronaviruses (123, 124), betacoronaviruses (21, 106, 125-128), and gammacoronaviruses (22). Considering the pervasiveness of DMVs across the coronavirus and arterivirus families, it seems plausible that this is a shared trait that would extend to other nidoviral families not yet characterized. A striking difference between arterivirus and coronaviruses DMVs concerns their size: coronaviruses induce DMVs that are, on average, around twice the diameter of those in arterivirus-infected cells (Table 1, Fig. 4A), which corresponds to a ~8 fold difference in DMV volume.

The betacoronavirus SARS-CoV was the second +RNA virus for which the virus-induced membrane modifications were characterized in 3D by electron tomography (Fig. 4B) (21). This study uncovered DMVs that were connected through their outer membrane with other DMVs and the ER, together forming an RVN of modified ER membranes that is topologically comparable to that described for EAV in the previous section (20). The remarkable similarities between these two distantly-related nidoviruses suggested that the RVN architecture may be a universal feature among nidoviruses. This idea, however, has been challenged by a recent tomographic study of the structures formed upon infection of primary cells with the gammacoronavirus IBV (Fig. 4C) (22). Remarkably, in these tomographic studies, most of the IBV-induced DMVs were found to be isolated vesicles: no DMV-DMV connections were observed and only a small proportion of DMVs appeared to be connected to the ER. Additionally, and in contrast to the case of EAV- and SARS-CoV-induced DMVs, ribosomes were not found to be associated with the outer membrane of IBV-induced DMVs. Whether these features represent specific differences for gammacoronaviruses or also apply to some of the other nidovirus (sub)groups remains to be analyzed. In any case, the RVNs generated by SARS-CoV and EAV appear to be a unique example of highly-interconnected membrane modifications among the +RNA viruses that induce DMVs (Table 1). The overall DMV connectivity is decidedly more limited in the case of HCV, for which direct membranous connections between DMVs were not observed (23). In terms of connectivity, enterovirus-induced modifications appear to be at the opposite end of the spectrum relative to nidoviral RVNs, as all of them seem to be isolated compartments with no membranous connections between them or any cellular organelle (56, 65).

A common characteristic of coronavirus-infected cells, which is absent in cells infected with arteriviruses, is the formation of relatively disorganized assemblies of tangled, partially

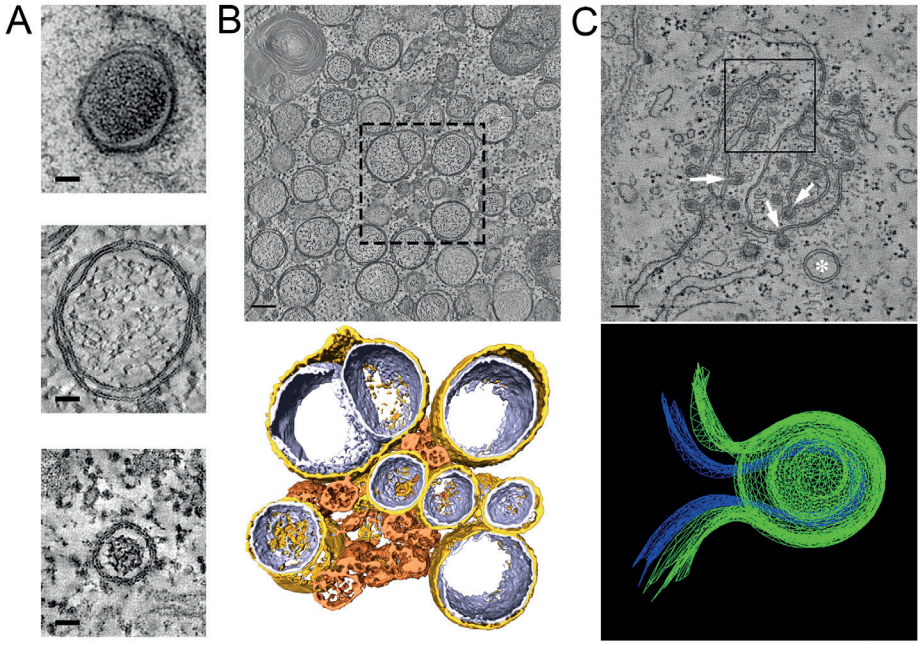


Fig. 4. Coronavirus-induced membrane structures. (A) *Gallery of nidovirus-induced DMVs represented to scale. The panel shows DMVs in cells infected with (from top to bottom) IBV (CK cells, HPF-FS), SARS-CoV (Vero E6, plunge-freezing and FS) and EAV (HuH-7 cells, HPF-FS). The top image is a 2D projection, while the middle and bottom images are virtual slices (2 nm thick) extracted from tomograms.* **(B)** *Membrane modifications induced by SARS-CoV infection in Vero E6 cells (7 h p.i.). The top panel is a 2-nm thick virtual slice from a tomogram. The boxed area represents the region that was used for the 3D surface rendering in the lower panel. In this model, gold represents the outer membrane of the DMV is colored in gold, the inner membrane in silver, and CM in bronze.* **(C)** *Membrane modifications induced by IBV infection in CK cells (16 h p.i., chemical fixation) The upper panel is a virtual slice taken from a tomogram in a region rich in IBV-induced zippered membranes where a DMV (white asterisk) is also present. These zippered membranes often curve to form spherules with a neck that connects their interior to the cytosol (white arrows). The upper spherule in the boxed region was used to create the 3D mesh model presented in the lower panel. Blue represents the inner membrane and green the outer membrane of the spherule. Scale bars, 50 nm (A), 100 nm (B,C). A,B: adapted from (21). A,C: adapted from (22).*

double membranes. These structures, now mostly referred to as convoluted membranes (CM), were already described for mouse hepatitis virus (MHV) in 1965 as 'reticular inclusions' (122). Since then, they have been further characterized for several betacoronaviruses including MHV (127), SARS-CoV (21) and the recently emerged Middle East Respiratory Syndrome coronavirus (MERS-CoV) (128). DMV formation seems to precede CM formation, since the latter has been observed predominantly at later time points after infection (21, 127, 128). CM are found in close proximity to the DMVs, but only their 3D characterization in SARS-CoV-infected cells unambiguously showed the presence of neck-like membranous connections between the CM and surrounding DMVs and ER cisternae (21), which make the

CM also an integral part of the coronavirus-induced RVN. Notably, CM have been described so far only for cells infected with betacoronaviruses and could be a feature restricted to this genus. In the few ultrastructural studies of cells infected with alphacoronaviruses, CM were not reported (123, 124); however, these studies focused on virus morphogenesis and DMVs, respectively, and therefore it is unclear whether CM may have been present. For the gammacoronavirus IBV, a thorough search for this structure was reported to be unsuccessful (22).

Interestingly, in cells infected with the gammacoronavirus IBV, a distinct and novel membranous structure was described consisting of double-membrane spherules that were continuous with zippered ER cisternae and had a channel of 4.4 nm in diameter connecting them to the cytosol (Fig. 4C) (22). Although these spherules are delineated by two membranes instead of one, their size (~60 nm) and overall configuration with an opening to the cytosol was very reminiscent of the single-membrane invaginations induced by a large number of +RNA viruses (see section 1). Based on this similarity, the authors proposed that viral RNA synthesis would take place inside these spherules. This possibility, which requires further experimental corroboration, is particularly attractive in view of the closed configuration of the DMVs found in coronavirus infection. Both for IBV- and SARS-CoV-infected cells, the tomograms revealed DMVs in which the inner membrane seems to be fully sealed with no apparent openings to the cytosol. This makes it difficult to envision how viral RNA synthesis could take place (at least exclusively) inside these vesicles. This situation is completely analogous to the case of the EAV-induced DMVs discussed in the previous section and the parallels extend to the localization of different viral markers by IEM. Most of the dsRNA signal in SARS-CoV-infected cells was shown to map to the inner compartment of the DMVs, whereas the bulk of the labeling for several replicase proteins was located predominantly in the surrounding CM (21). The CM in MHV-infected cells also abundantly labeled for several nsps (127). The experiments using metabolic labeling of newly-synthesized viral RNA, which could be crucial to pinpoint the actual site of viral RNA synthesis, are restricted so far to MHV. IEM detection of newly-synthesized RNA using BrUTP as a probe revealed signal associated to the regions of DMV clusters, but the results are difficult to interpret due to the limited sample preservation that resulted in a clear loss of the DMV content and, possibly, also of the CM (125). In a recent study, using incorporation of ethynyl uridine into RNA and its detection through click-chemistry followed by light microscopy (129), a loss of colocalization between the ethynyl-uridine and the dsRNA signal was observed as infection progressed. The ethynyl uridine-containing foci, which early in infection overlapped with the dsRNA signal, became dispersed in the cytoplasm late in MHV infection. This prompted the idea that RNA synthesis could take place, at least during these later stages, in regions of the cell distant from those containing DMVs. The interpretation of these results at the ultrastructural level, however, is not possible in the absence of a parallel EM characterization.

Overall, the question of the actual site of viral RNA synthesis for arteriviruses and coronaviruses appears more enigmatic than ever and it is certainly a key issue to be addressed in the future. New studies that meet the challenge of achieving shorter labeling

times without critically reducing signal levels, and that combine improved ultrastructural preservation with quantitative analyses, will be crucial to accurately determine the location of the active RTC. Meanwhile, multiple scenarios remain possible, as originally discussed in (21). If viral RNA synthesis does take place exclusively inside DMVs, a yet unknown mechanism of material exchange with the cytosol should exist, perhaps in the form of a proteinaceous channel spanning the two membranes, similar to the TIM/TOM export complex in mitochondria (130). The visualization of such a channel may be possible using advanced techniques like cryo-EM and cryo-ET, which preserve molecular resolution (47). On the other hand, if such an exchange mechanism is not present, alternative locations for anchoring the RTC appear necessary. These locations could include the cytosolic face of the DMV outer membrane, but also other membrane structures induced by nidoviruses (e.g. the CM in betacoronaviruses, the open double-membrane spherules of the gammacoronavirus IBV, paired membranes in arteriviruses), and/or even other subcellular membrane structures. In this alternative scenario the DMVs may not even play a critical role in viral RNA synthesis at all, a possibility that may be supported by recent observations with temperature-sensitive MHV mutants. This study could not establish a direct correlation between the number of DMVs and MHV RNA synthesis (131), which would have been expected if DMVs would be the sole site of viral RNA synthesis. The fact that DMVs have been detected by EM a few hours later than the onset of viral RNA synthesis could also argue in the same direction; however, this could also simply be due to EM limitations. Incipient modifications, which would likely be rare, would be even less frequent in the cell sections prepared for EM and could easily go undetected.

The biogenesis of arterivirus and coronavirus DMVs

A crucial aspect for better understanding virus-induced replication organelles, and possibly for the design of antiviral strategies that target them, is to uncover the steps leading to their formation and, ultimately, to determine the exact nature of the molecular interactions of the viral and host players involved. Compared to DMVs, the +RNA virus-induced invaginations are much better understood in this respect. Mechanistically, their formation entails the induction of negative curvature (i.e. a concave membrane, bending away from the cytosol) on the host membrane-donor organelle to yield a vesicle budding into the luminal space. This negative curvature is compensated by positive curvature (i.e. convex membrane, bent towards the cytosol) at the membranous neck that keeps the vesicle attached to the organelle and connects its interior to the cytosol. Detailed studies on BMV replication organelles have greatly helped to establish a model system for the molecular players and mechanisms involved in molding the membranes to form this type of invaginations (63, 132, 133). While the BMV case illustrates the significant progress in understanding the mechanisms involved in producing virus-induced invaginations, our insight into the generation of viral DMVs lags well behind. This is in part due to the more complex architecture of a DMV compared to a single-membrane structure, which implies a more elaborate formation process that would encompass several membrane remodeling steps including fission events. In the context of nidovirus-induced DMV formation, two

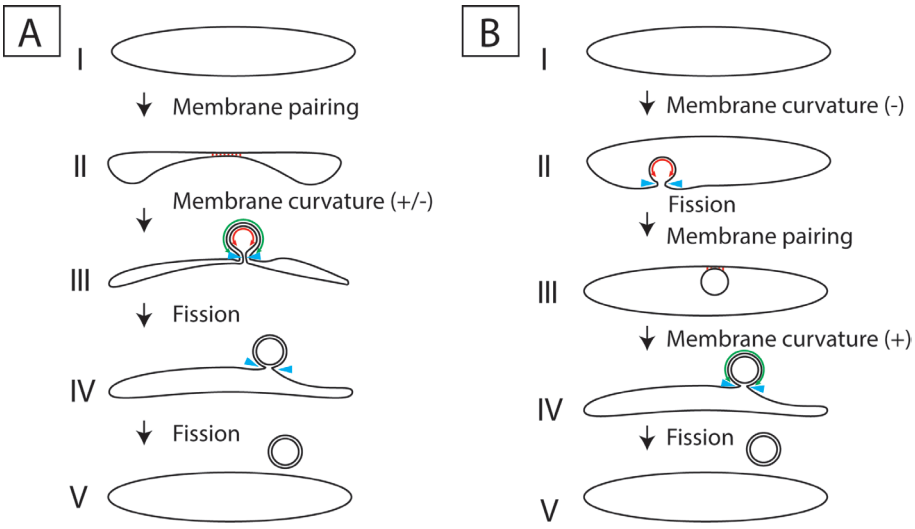


Fig. 5. Mechanisms proposed for DMV biogenesis. (A) *Different stages in remodeling of ER membranes that would result in DMVs by an enwrapping mechanism. This process would start with the pairing of membranes, which then would start curving until this curvature becomes so pronounced that a double-membrane vase-like compartment is formed. Finally, through a fission event of the inner membrane a closed compartment is formed, while the outer membrane is still continuous with the ER. An additional fission event of the outer membrane would sever the connection with the ER and give rise to a detached DMV.* **(B)** *An alternative mechanism that would result in DMV formation is double budding. The first step in this process would be the formation of an invagination in an ER membrane, which then buds into the ER lumen through a fission event. The resulting luminal single-membrane vesicle could subsequently interact with the ER membrane to form stretches of paired membranes. Induction of additional curvature would enable the vesicle to bud out of the ER, thereby acquiring a second membrane. Notice that stages IV and V would be topologically identical in both routes and that similar membrane remodeling events are required for both mechanisms: membrane pairing (represented by red lines), positive and negative membrane curvature (green and red double arrows, respectively) and membrane fission (blue arrowheads).*

alternatives have been proposed: enwrapping (also known as protrusion and detachment) and double budding (88) (Fig. 5).

In the enwrapping model (Fig. 5A) the first crucial step is the pairing of two lipids bilayers in the membrane donor organelle (likely the ER for nidoviruses). These paired membranes would then progressively curve to form a DMV that is still connected to the cytosol in a vase-like configuration. In this step, the outer and inner membranes acquire opposite curvature (positive and negative, respectively). As curvature increases, the opening would get narrower and, eventually, the DMV may be sealed by fission to give rise to an inner compartment containing cytosolic material and an outer lipid bilayer that is still continuous with the ER. The alternative mechanism, the double-budding model (Fig. 5B), would start with the budding of a single-membrane vesicle (SMV) into the lumen of the membrane donor organelle and, therefore, would involve the induction of negative curvature in the ER and

fission to release the SMV into the lumen. A second budding event, this time towards the cytosol, would make this vesicle emerge from the ER while acquiring its outer membrane. In this second step, the SMV and the ER would establish membrane-pairing interactions and positive curvature would be induced. This process would result in a DMV outer membrane that is still continuous with the ER, essentially identical to that formed in the enwrapping model. In both models, an additional fission event could lead to the pinching off of a free DMV.

Membrane pairing, fission and induction of both positive and negative membrane curvature are key features of both models, and in fact they only differ in the order in which these events occur. Membrane pairing could be mediated by protein-protein interactions across the lumen. For EAV, this could be potentially achieved by the predicted luminal domains of the transmembrane proteins nsp2 and nsp3, two non-structural proteins that have been shown to engage in a strong interaction (89, 134). Regarding curvature, several processes that can drive bending of cellular membranes have been described (reviewed in (135)). One of them is the generation of asymmetry in the bilayer by differential insertion of proteins or irregularly-shaped lipids, which act as wedges that deform the membrane. Self-oligomerization of transmembrane or soluble scaffold proteins can also result in the induction of membrane curvature. While we currently do not know how arteriviruses and coronaviruses accomplish membrane bending, it seems likely that the transmembrane viral nsps play a prominent role. Other factors could also be involved, for example, a change in lipid composition or homeostasis, as shown for other DMV-inducing viruses. Enteroviruses and HCV alter the lipid composition of the membranes recruited for the formation of replication organelles, which become enriched in phosphatidylinositol-4-phosphate (PIP4) by the specific recruitment of PI4P-kinases (PI4KIIIβ in enteroviruses, PI4KIIIα in HCV), which seems essential for viral replication (42, 44). Whether any of the PI4K variants play a role during arterivirus and coronavirus infection would be highly informative and is currently under investigation in our group. A recent siRNA library screen targeting the human kinome in fact identified some proteins involved in the metabolism of complex lipids as factors relevant for SARS-CoV replication. Interestingly, the PI4P-kinases, which appear essential for the replication of other DMV-inducing viruses, did not show an effect on SARS-CoV replication in this study (136).

A link with autophagy?

Double-membrane structures are not without precedent in the cell. Organelles delimited by a double membrane in eukaryotic cells include the nucleus, mitochondria and autophagosomes. Although much larger in size (0.5-1.5 μm in diameter), autophagosomes have a similar appearance as virus-induced DMVs. Autophagosome formation (reviewed in (137)) is a central process in the macroautophagy pathway (hereafter autophagy) (138) and involves the formation of a double-membrane sheet, known as the phagophore, which wraps and sequesters cytoplasmic material, sometimes even whole organelles or bacteria. Recently, it has become clear that the cargo for degradation in autophagosomes is selected specifically by autophagy receptors which bind to the selected cellular components and

recruit them to the growing autophagosomal membranes (139). Closure of the phagophore yields the autophagosome, which fuses with late endosomes or lysosomes after maturation to deliver its cargo for degradation and recycling of the engulfed macromolecular components.

Autophagy can be triggered by stress, starvation and infection. While autophagy can act as a cellular defense mechanism for virus clearance in response to infection, several viruses have evolved strategies to avoid or even subvert the autophagy pathway for their own benefit (140-142). The parallels between autophagosomes and virus-induced DMVs elicited the hypothesis of a link between autophagy and DMV biogenesis, postulating that DMVs may represent modified autophagosomes.

Infection with arteriviruses and coronaviruses can induce autophagy (143-148) but conflicting results on the relationship between autophagy and nidovirus replication have been published, possibly due in part to the differences in the cell lines used. Knock-down of Atg5, an essential protein in the autophagy pathway, was first reported to inhibit MHV replication and preclude the formation of DMVs in embryonic stem cells (143), but later these effects were not observed in bone marrow-derived macrophages and primary mouse embryonic fibroblasts (MEF) (149), or MEF cells lacking another key autophagy protein, Atg7 (150). For the avian coronavirus IBV, it was shown that viral replication is not affected by either inhibition or activation of autophagy in monkey kidney cells (Vero) (49, 144). Of note, IBV infection induced autophagy in mammalian cells but not in avian cell lines (49), which emphasizes the potential influence of the cell type on the study of the interplay between viral infection and autophagy and, possibly, the consequences of a virus-host mismatch. Likewise, the replication of the arterivirus EAV in Vero cells did not seem to be affected by either Atg7-dependent autophagy or the alternative Atg5/Atg7-independent autophagy pathway (148). However, for the arterivirus PRRSV, progeny titers were moderately reduced in another monkey kidney cell line (MARC-145) treated with the autophagy inhibitor 3-methyladenine or when autophagy genes were silenced, whereas activation of autophagy with rapamycin had the opposite effect (145-147). Whether these results are dependent on the cell line used or reflect a particularity of PRRSV remains to be investigated. Overall, the data gathered in the last decade seems to strongly suggest that autophagy, or at least the canonical autophagy pathway, is not essential for arterivirus and coronavirus replication and whether it plays a role in DMV biogenesis is therefore unclear. Such a role has not been established for other DMV-inducing viruses either. Whereas in the case of HCV conflicting reports make the influence of autophagy in viral replication rather unclear, for enteroviruses, autophagy appears to have only limited impact on replication. However, autophagy seems to be critically linked to virus assembly, maturation and the non-lytic release of new enterovirus particles (151-153).

Induction of autophagy is often monitored using the autophagy marker LC3 (microtubule-associated protein 1 light chain 3), a key player in autophagosome formation and recruitment of specific cargo for degradation. Upon exposure to autophagy stimuli, the cytosolic form (LC3-I) is converted into a lipidated form (LC3-II) by covalent binding to phosphatidylethanolamine, which is present in the autophagosomal membranes (138).

In light microscopy images, this LC3 relocation is reflected in the formation of puncta of fluorescently tagged LC3. Using this approach, the IBV nsp6 replicase protein (but not other IBV nsps) was shown to be capable of inducing autophagosome formation when individually expressed (49, 144). This effect was also described for nsp6 of MHV and SARS-CoV, as well as the arteriviral PRRSV nsp5-7 (144). The autophagosomes induced by these proteins appeared to be smaller in size than normal autophagosomes, as judged from light-microscopy images, and therefore closer to viral DMVs (154). However, in contrast with individually expressed nsp6, IBV infection did not induce LC3 relocalization and autophagic signaling in avian cells (49). Therefore the relevance of this nsp6 feature in the context of infection remains unclear,

One of the reasons to relate autophagy to nidovirus replication was the reported colocalization of LC3 with viral replicase proteins or dsRNA in light microscopy images of cells infected with MHV (143, 150), SARS-CoV (105, 149), PRRSV (147) and EAV (148), although some other studies with SARS-CoV and IBV could not confirm this finding (106, 144). Without accompanying EM data, extrapolating this colocalization, which appears to be partial in confocal images, to the specific ultrastructural location of LC3 is problematic, even more so in the case of coronaviruses considering the variety of membrane structures that they induce during infection (see section 2.3). Ultrastructural studies using IEM, which are limited so far in the case of EAV to chemically-fixed BHK-21 cells at late time points in infection (148), would be essential to establish whether LC3 is associated with virus-induced modifications and, specifically, with DMVs.

Interestingly, data obtained using EAV- and MHV-infected cells indicated that the non-lipidated form of LC3 (LC3-I), which is inactive in autophagosome formation, would be the one that is recruited from the cytosol and that partially colocalizes with viral nsps (148, 150). Silencing of LC3 was reported to reduce EAV and MHV replication and this effect could be reversed by transfecting a non-lipidable form of LC3 in MHV-infected cells (150). This was considered reminiscent of EDEMosomes, a class of short-lived small vesicles that appear to depend on LC3-I recruitment (155, 156). EDEMosomes have been proposed to serve as a mechanism to tune down the ER-associated protein degradation (ERAD) machinery, which targets misfolded proteins, by transporting some ERAD regulators, like EDEM1 (ER degradation-enhancing α-mannosidase-like protein 1) or OS-9 (osteosarcoma amplified 9), away from the ER for their disposal (155). Exploring these analogies further, EDEM1 and OS-9 were found to partially colocalize with dsRNA in MHV-infected cells, which was interpreted as recruitment of these proteins to DMVs (150). Similarly, dsRNA and EDEM-1 showed some degree of colocalization in EAV-infected cells (148). It was therefore proposed that the ERAD-tuning pathway would supply the membranes for the biogenesis of viral DMVs (150). The direct conversion of EDEMosomes into DMVs, however, seems difficult to envision, as it would entail the transformation of smooth single-membrane vesicles of about 150 nm in diameter (155) into DMVs that can reach 300 nm in diameter in the case of coronaviruses and whose outer membranes are decorated with ribosomes. The recruitment to virus-induced modifications of some components of the ERAD machinery during arterivirus and coronavirus infection is, nevertheless, plausible, but its functional

significance may well be completely unrelated to DMV biogenesis and needs to be further investigated using in-depth EM analysis and molecular biology approaches.

CONCLUSIONS AND FUTURE PERSPECTIVES

The replication organelles induced by +RNA viruses are examples of the remarkable level of sophistication in host membrane manipulation that viruses can achieve. Their complex architecture, revealed by electron tomography, poses additional challenges, for example concerning DMV structure-function interpretation. In this respect, arteriviruses and coronaviruses represent perhaps the most intriguing case (Table 1). The RVNs that EAV and SARS-CoV induce are intricate labyrinths of modified membranes that have no parallel in the +RNA virus world thus far. Additionally, and in contrast with other +RNA viruses that induce mixed populations of open and closed DMVs, the closed configuration of nidovirus-induced DMVs defies the straightforward concept of viral RNA synthesis occurring inside these compartments, and puts at the forefront the open question of the location of the viral enzyme complexes actively engaged in replication/transcription. Until this question is unambiguously answered experimentally, multiple possibilities remain open, from a scenario in which RNA synthesis would take place solely inside DMVs while a still undetected macromolecular channel would accomplish the necessary import/export processes, to a situation in which the active nidoviral RTC would be located in alternative sites and the DMVs would not even play any direct role in viral RNA synthesis. Along these lines, the possibility of DMVs simply being a by-product of the high expression levels of the viral non-structural proteins cannot be completely discarded. However, even if the DMVs are not critically involved in viral RNA synthesis, less passive roles seem also plausible. These RNA-containing structures could perhaps be used to shield an excess of viral RNA from the cellular innate immune sensors and/or be the result of the subversion of cellular pathways for the benefit of virus replication. Clearly, additional experimental data are required to provide key information on the precise role of nidovirus-induced DMVs, which may well extend to other +RNA viruses.

Acknowledgements

We are grateful to Kèvin Knoops and Helena Maier for kindly providing high-resolution originals for some of the figures in this chapter. This work was supported in part by the Netherlands Organization for Scientific Research through a TOP grant from the Council for Chemical Sciences (NWO-CW grant 700.57.301 to EJS and AJK) and a MEERVOUD grant (NWO-ALW grant 836.10.003 to MB) from the Council for Earth and Life Sciences.

Chapter 3

New insights in the biogenesis of arterivirus replication organelles

Diede Oudshoorn[1], Barbara van der Hoeven[1], Abraham J. Koster, Eric J. Snijder , Marjolein Kikkert and Montserrat Bárcena

[1] These authors contributed equally to this study

The contents of this chapter were published, in modified form, as part of the review "Biogenesis and architecture of arterivirus replication organelles." (Virus Res. 2016 Jul 15;220:70-90) by B. van der Hoeven, D. Oudshoorn, A.J. Koster, E.J. Snijder, M. Kikkert and M. Bárcena.

ABSTRACT

All positive-strand RNA (+RNA) viruses of eukaryotes modify cellular membranes into replication organelles to facilitate their replication. The most prominent replication-associated membrane structures induced in cells infected with nidoviruses (including arteri- and coronaviruses) are double-membrane vesicles (DMVs). Using the equine arteritis virus (EAV) model for nidovirus replication and electron tomography, we obtained new data regarding the biogenesis of arterivirus-induced DMVs and uncovered numerous putative intermediates in DMV formation. We generated cell lines that can be induced to express specific EAV replicase proteins and showed expression of the transmembrane proteins nsp2 and nsp3 induced the formation of DMVs that constitute a reticulovesicular network (RVN) and are comparable in terms of architecture to those formed during viral infection. Co-expression of the third EAV transmembrane protein (nsp5), expressed as part of a self-cleaving polypeptide that mimicked viral polyprotein processing in infected cells, led to the formation of DMVs whose size was more homogenous and closer to what is observed upon EAV infection, suggesting a regulatory role for nsp5 in modulating membrane curvature and DMV formation.

INTRODUCTION

Double-membrane vesicles (DMVs) are the most prominent membrane structures formed upon nidovirus infection. However, the process of DMV biogenesis is still poorly understood. DMV biogenesis is mechanistically complex, probably involving a defined sequence of events (see **Chapter 2**) and multiple players including the membrane donor organelle (the endoplasmic reticulum in the case of nidoviruses), host protein factors involved and viral proteins required (discussed below). Unraveling the different stages of membrane transformation, and the underlying molecular interactions, will be essential for a full understanding of arterivirus DMV biogenesis. Addressing some of these questions in the context of virus-infected cells is complicated by the (potential) number of viral players involved and the fact that targeting the viral proteins with mutagenesis often leads to defects that inhibit or block viral replication. The development of so-called "surrogate systems for DMV formation", however, does create the possibility to address these questions by essentially uncoupling the expression of the viral proteins under study from their expression from a viable viral genome. In such systems, ectopic expression of a subset of viral proteins is used to mimic the formation of membrane structures that resemble those found during infection, although they obviously lack the viral RNA-synthesizing enzyme complexes associated with these structures in infected cells. For a number of viruses this approach has proven to be productive and, in many cases, instrumental for a better understanding of the biogenesis of virus-induced replication organelles (23-28, 38, 39). These systems can be expanded by using site-directed mutagenesis of the proteins that are expressed in order to probe the relevance of specific residues, protein domains or interactions.

For EAV, this approach has been instrumental in the identification of the proteins that are likely driving the conversion of specific intracellular membranes into viral replication organelles. Initially, the expression of EAV nsp2-7 in BHK-21 cells was shown to give rise to membrane rearrangements that were similar to those found in infected cells (88). The minimal set of viral proteins required for DMV formation was later narrowed down to nsp2 and nsp3 (24) and, since then, expression of these two proteins has been considered a useful surrogate system to mimic and study EAV-induced membrane modifications. Although these studies highlighted the key role of EAV nsp2 and nsp3 in DMV formation, the ultrastructural analysis was limited to 2D electron microscopy of chemically fixed samples. Therefore, the question of whether the detailed architecture of the DMVs induced upon co-expression of nsp2 and nsp3 was comparable to that of the DMVs found in infected cells remained unanswered. Furthermore, although nsp2 and nsp3 were shown to suffice to induce DMV formation, it was unknown whether the third transmembrane protein (nsp5) plays a role during arterivirus DMV biogenesis. In order to address these questions, we now carried out an electron tomographic characterization of the structures induced by different combinations of EAV-encoded non-structural proteins using two protein expression systems and samples prepared by high-pressure freezing (HPF) followed by freeze substitution (FS).

Clear intermediate structures that could support or argue against one of two models for arterivirus-induced DMV biogenesis (described in **Chapter 2**, Fig. 5) have not been visualized so far. Historically, the so-called enwrapping model has been favored due to the detection of short stretches of tightly paired membranes (88, 112), which could constitute a specific feature of this mechanism. Using ET on EAV-infected cells, we now found several intermediates compatible with either of the (non-mutually exclusive) DMV biogenesis models. The particularly frequent observation of tightly paired ER membranes suggests that enwrapping is at least a key process of DMV biogenesis.

RESULTS & DISCUSSION

Expression of EAV nsp2-3 using a Sindbis virus-based vector

We first analyzed the membrane modifications induced by EAV nsp2 and nsp3 using a Sindbis virus-based expression system, essentially identical to that used in previous studies in BHK-21 cells (24, 89). Alphaviruses like Sindbis virus also alter cellular membranes (see **Chapter 2**); however, they modify endosomes, lysosomes and the plasma membrane (59, 61, 157) and therefore are thought not to interfere with arterivirus-induced DMV formation. The system consisted of an RNA replicon (SINrep5) in which a foreign gene (a self-cleaving EAV nsp2-3 polypeptide C-terminally fused to enhanced GFP (eGFP)) replaced the ORF encoding the structural polyprotein of Sindbis virus and was expressed to high levels from a subgenomic mRNA (158). The eGFP tag on nsp3 enabled the application of correlative light and electron microscopy (CLEM), an emerging methodology that allows imaging of the same sample both by light microscopy and high-resolution EM (159). In order to carry out CLEM, we used a freeze-substitution protocol that minimizes staining to preserve the fluorescence throughout EM sample preparation (160). The eGFP signal facilitated the quick identification of transfected cells and, more specifically, the localization of nsp3-eGFP positive sites in the EM sections (Fig. 1A-C). In all these areas, some circular double-membrane profiles typical of DMVs were readily observed (Fig. 1C, white asterisks).

Intriguingly, numerous irregular structures that were also delineated by two tightly apposed membranes were readily apparent in the regions containing membrane modifications (Fig. 1C, black arrows). Electron tomography revealed that this type of irregular structures consists of strikingly long stretches of paired membrane sheets (Fig. 1D, black arrows) which appear to derive from the ER, with which they are continuous (Fig. 1E,F). Although the majority of the circular double-membrane profiles observed in 2D projection images were found to be closed DMVs upon tomographic analysis (Fig. 1D, white arrow) and thus analogous to those found in EAV infection, many apparent DMVs turned out to be patches of these membrane sheets that locally curved creating a secluded internal space reminiscent of a DMV but still continuous with the cytosol (Fig. 1G). In fact, these DMV-like structures, which could be easily mistaken for bona fide DMVs in 2D projection images, appeared to be part of a large network of double-membrane sheets weaving through the perinuclear area of the cytoplasm (Supplementary movie 2).

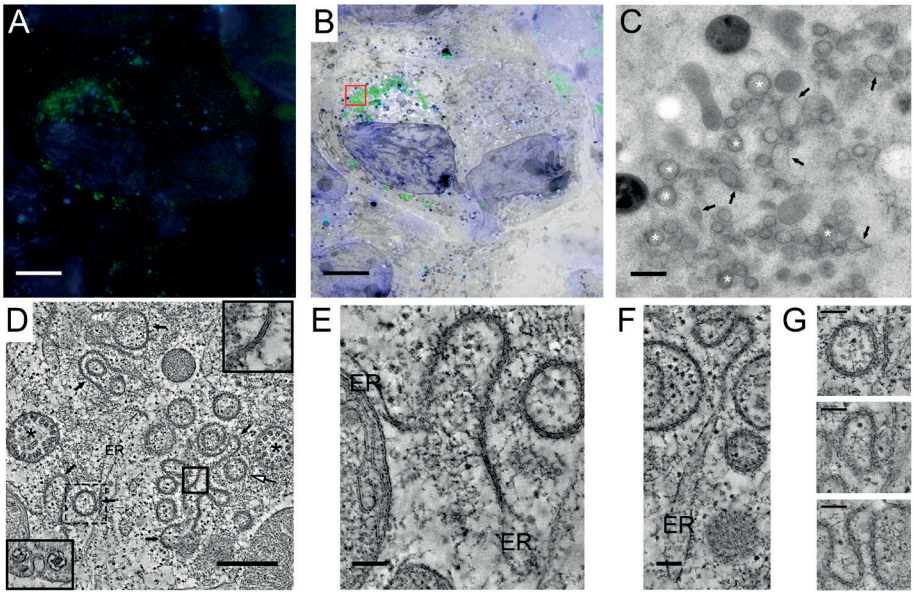


Fig. 1. Characterization of membrane structures induced by EAV nsp2-3 expression from a Sindbis virus-based replicon. (A-C) *Correlative light-electron microscopy (CLEM) analysis of transfected cells expressing an eGFP-tagged self-cleaving nsp2-3 polyprotein.* **(A)** *Fluorescence microscopy image of a 200 nm section on an EM grid showing nuclear DNA staining and a clear cytosolic eGFP signal.* **(B)** *Merging of the fluorescence image and the corresponding electron microscope images.* **(C)** *Higher magnification image of the boxed area in panel B, showing the structures underlying the eGFP signal. Several circular profiles typical of DMVs are clearly visible (white asterisks), as well as other more irregular double-membrane structures (black arrows).* **(D-G)** *3D architecture of nsp2-3 induced membrane rearrangements.* **(D)** *Tomographic slice (2 nm thick) of EAV nsp2-3-induced structures (see also Supplementary movie S2). These consist of the characteristic double-membrane vesicles (white arrow), as well as double-membrane sheets (black arrows) that are particularly abundant in this region. The membrane structures induced by Sindbis non-structural proteins are also visible (black asterisks), and consist of invaginations in modified endosomes that have a neck-like channel connecting their interior with the cytosol, (lower left inset). The inset at the upper right corner is a close-up of the boxed area in (D) (continuous line) and highlights the two tightly-apposed membranes that form these structures.* **(E,F)** *Gallery of tomographic slices (6 nm thick) highlighting the continuity of the paired-membrane sheets with ER cisternae.* **(G)** *Tomographic slices through the structure highlighted in (D) with a dashed box (relative z height of the slices, from top to bottom: 0, 35 and 60 nm). Notice how at one level (top image) the structure appears indistinguishable from a closed DMV, while the successive tomographic slices reveal that it is actually open to the cytosol and more akin to a highly curved fragment of the paired membrane sheet network to which it is connected. Scale bars, 10 µm (A-B), 500 nm (C-D); 100 nm (E-G).*

Movie S2 *(available at http://www.sciencedirect.com/science/article/pii/S016817021630199X). Tomography of the membrane structures induced by nsp2-3-eGFP expression from a SINrep5 replicon in HuH-7 cells. The movie shows consecutive slices (1.2 nm thick) through the reconstruction of the area displayed in Fig. 1D.*

This profusion of membrane sheets is a phenomenon that had been described before in the SINrep5nsp2-3 expression system, but only when a mutation creating an N-linked glycosylation site was introduced in the first luminal loop of nsp3 (T873N) (89) and not in cells expressing wild-type EAV nsp2-3 (24, 89). The reasons for this discrepancy are unclear and, although it may be partially attributed to the lack of 3D data in previous studies, it could also be related to differences in the experimental set-up. In any case, these differences were not related to the cell line used, nor were they due to the eGFP tag on nsp3 since similar double-membrane sheet networks were detected using BHK-21 and Vero E6 cells and the same construct lacking the eGFP fluorescent tag (data not shown).

Cell lines for the inducible expression of EAV nsps2-3 and nsp2-7

In order to avoid possible undesired side-effects derived from the expression of Sindbis virus non-structural proteins and to obtain a surrogate system that is more convenient, reproducible and suitable for a wider range of experimental setups, we created stable cell lines which can be induced to express the self-cleaving EAV nsp2-3 polyprotein from a cytomegalovirus (CMV) promoter.

Clusters of DMVs were readily observed 24 hours after induction of expression in HuH-7 cells (Fig. 2A, white asterisks). Both the inner and outer membranes of these DMVs were decorated with ribosomes (Fig. 2B,C, black arrows), which, as in the infected cell, hints at the ER as the membrane donor for DMV formation. In fact, some of these DMVs showed a direct connection with ER cisternae, with which they were continuous through their outer membrane (Fig. 2D). As in the case of DMVs found in infected cells, neck-like membrane connections between DMVs were detected in the tomograms (Fig. 2E, black arrowheads). Finally, the similarities with DMVs observed in EAV infection extended to the closed nature of these compartments, as no openings could be detected in the DMVs induced by nsp2-3 expression in this system.

Despite these general similarities, some anticipated differences with the structures found in infected cells were apparent. No tubular proteinaceous structures (**Chapter 2**; Fig. 2H,I) were detected, which is in agreement with the notion that their formation depends on N protein expression (20, 115). Also, the DMVs formed upon expression of nsp2-3 lack the electron dense core that is typical of the DMVs in EAV-infected cells. The absence of this structure is consistent with the interpretation that the DMV cores that appear in infected cells, which have a high phosphorus content and label for dsRNA (**Chapter 2**; Fig. 3), contain viral RNA. The content of the nsp2-3-induced DMVs appears quite similar to the surrounding cytosolic material, although slightly more electron dense and, like the cytosol, it contains densities that may be free ribosomes (Fig. 2D,E white circles). Taken together, our results show that the expression of nsp2-3 suffices to reproduce the double-membrane architecture, topology and connectivity of the DMVs found in infected cells, and therefore constitutes a useful system to study these features of the EAV-induced RVN. This also implies that the membrane-remodeling capacities necessary to generate the RVN reside in these two arteriviral nsps, likely with the assistance of recruited host factors.

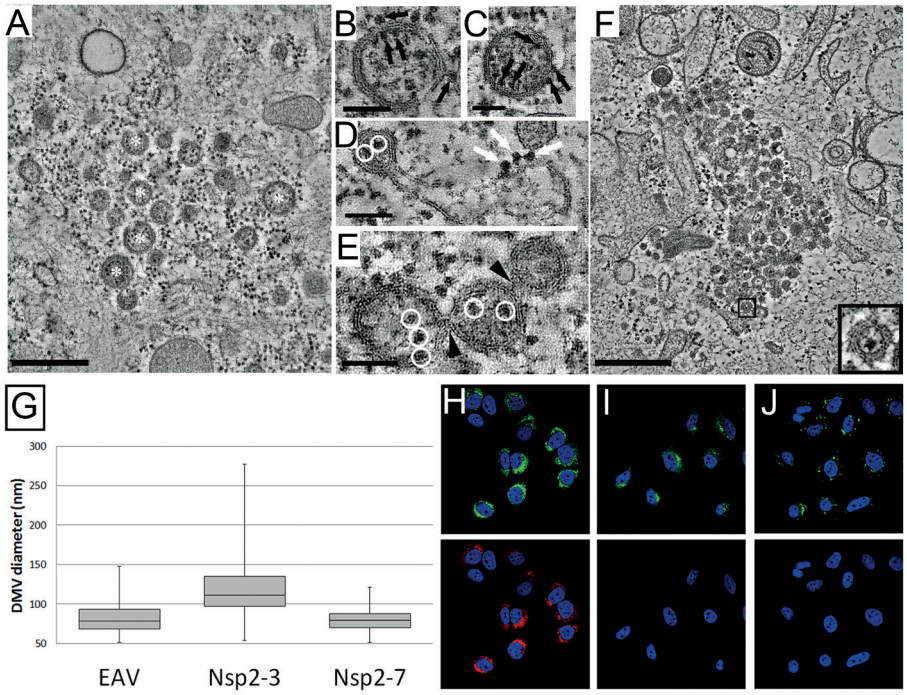


Fig. 2. Characterization of membrane structures induced after EAV nsp2-3 and nsp2-7 expression using inducible HuH-7 cell lines. (A) *Tomogram slice (2 nm thick) showing an overview of the structures induced upon nsp2-3 expression. The structures consist of DMVs, some of which are indicated by white asterisks. Note that the membrane sheet network observed in the SINrep5 expression system (Fig. 7) is absent.* **(B-E)** *Close-up tomographic slices (6 nm thick) highlighting several features of the DMVs induced by nsp2-3 expression.* **(B,C)** *Ribosomes decorate both the inside and the outside of the DMVs (black arrows).* **(D)** *An example of membrane continuity between rough ER and DMV, similar to what is found for DMVs induced in EAV infection (Fig. 2B). The ribosomes decorating the surface of the ER membrane are indicated by white arrows, while the ribosomes in the interior of the vesicle are encircled in white. Another feature, highlighted in* **(E)**, *is the propensity for the DMV to form interconnections similar to those found in EAV-induced DMVs (black arrowheads).* **(F)** *Virtual slice (2 nm thick) showing an overview of the typical structures seen upon induction of nsp2-7 expression, which consist of clusters of DMVs. The inset shows a close-up of the DMV in the boxed area, which appears to contain a ribosome.* **(G)** *Boxplot illustrating the diameter distribution for DMVs induced by EAV infection, nsp2-3 expression and nsp2-7 expression in HuH-7 cells, as measured from the tomographic reconstructions from samples prepared in parallel in the same experiment. The middle of the boxplot represents the median value for each population, the bottom and top of the boxplot represent the first and third quartile respectively. The whiskers extend to the minimum and maximum measured values.* **(H-J)** *Immunofluorescence labeling of viral markers in EAV-infected HuH-7 cells (H) and in the inducible HuH-7 cell lines expressing nsp2-3 (I) or nsp2-7 (J). A perinuclear nsp2 labeling (top, green) was apparent in the three experimental conditions, while dsRNA signal (bottom, red) was only detected in EAV-infected cells. Scale bars, 500 nm (A,I); 100 nm (B-E).*

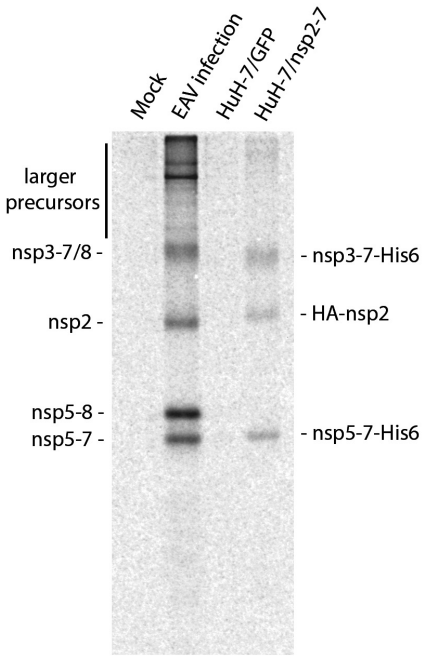


Fig. 3. Figure comparing the polyprotein processing during EAV infection and in HuH-7/tetR/nsp2-7 cells. *EAV infected and mock HuH-7 cells as well as HuH-7/tetR/nsp2-7 cells and control HuH-7/tetR/eGFP were metabolically labeled with 100 µCi/mL 35S methionine and 35S cysteine (EXPRE35S35S Protein Labeling Mix; Perkin-Elmer) for 4-10 hours post infection or tetracycline induction. Immunoprecipitation was performed as described previously with an antiserum raised for amino acids 1508-1727 (nsp7-8) of pp1a (134). Cleavage products observed during EAV infection are indicated on the left side and for nsp2-7 expressing cells on the right side.*

The results with this nsp2-3 expression system raise the question of the role in DMV formation, if any, of the third (presumed) transmembrane subunit of the arterivirus replicase: nsp5. To investigate this, using the same approach as above, we created a stable inducible HuH-7 cell line expressing nsp2-7. Since most nsp5 molecules in infected cells are present in the form of nsp5-7 or nsp5-8 processing intermediates (77, 84), expression of a self-cleaving nsp2-7 was chosen to mimic the course of events in infected cells most closely (Fig. 3). As in the case of nsp2-3, induction of nsp2-7 expression gave rise to the appearance of DMV clusters in close proximity to the ER (Fig. 2F). Notably, these DMVs observed in HuH-7 cells at 24 h after induction were strikingly smaller than those observed upon expression of nsp2 and nsp3 only. A detailed DMV size comparison was carried out using the 3D-reconstructions (Fig. 2G, Table 1). This method provides a much more reliable estimate of vesicle sizes than 2D measurements because, inevitably, not every DMV is fully contained in a cell section. Only a 3D analysis allows exclusion of DMVs whose equator is not present in the cell section. In this manner, the average diameter of the nsp2-7-induced DMVs was determined to be 79 nm (±13 nm, n=145) versus 119 nm (±32 nm, n=145) for nsp2-3-induced DMVs. The average size difference between the two populations, which translates into a decrease in DMV volume of about 70%, was found to be statistically significant using an independent two-sample *t*-test (Table 1). Remarkably, expression of nsp2-7 seems to bring the average diameter of the DMVs closer to the average diameter of DMVs formed in EAV infection (83 ±21 nm, n=145). Additionally, the population of nsp2-7-induced DMVs appeared to be significantly more homogenous in size than the DMVs

	n	Median	Average	Standard deviation	p-value[a]	p-value[b]	p-value[c]
EAV infection	145	78	83	21	-	<0.001	<0.05
Nsp2-3	145	111	119	32	<0.001	-	<0.001
Nsp2-7	145	80	79	13	<0.05	<0.001	-

Table 1. Diameters of DMVs in EAV infection, nsp2-3 expression and nsp2-7 expression.

[a] *Comparison with diameters of DMVs formed upon EAV infection.*

[b] *Comparison with diameters of DMVs formed upon nsp2-3 expression.*

[c] *Comparison with diameters of DMVs formed upon nsp2-7 expression.*

produced upon expression of just nsp2 and nsp3, where particularly large DMVs (up to ~270 nm in diameter) were detected (Fig. 2G). The DMVs in the nsp2-7-expressing cell line also lacked the electron dense core typical of DMVs formed upon EAV infection, although their content appeared slightly more electron dense than the surrounding cytosolic material. The dark content often seemed to correlate with the presence of densities that resembled ribosomes (Fig. 2F, inset). In any case, immunofluorescence microscopy confirmed that this darker interior is not due to the presence of dsRNA. As expected for systems lacking viral RNA replication, no dsRNA signal could be detected in cells expressing either nsp2-3 or nsp2-7, in contrast with the abundant dsRNA labeling found in EAV-infected HuH-7 cells (Fig. 2H,I,J).

Overall, our results show that, while nsp2 and nsp3 are capable of inducing all the membrane-remodeling steps required to generate the virus-induced RVN, the presence of additional nsps can modulate the process and produce DMVs more similar in size to those found in EAV-infected cells. The significantly smaller DMVs found upon nsp2-7 expression relative to those induced by nsp2-3 suggest a role for the extra proteins in enhancing the curvature of the membranes used for DMV formation, while the narrower size distribution suggests a tighter regulation of the process. Although several additional nsps and intermediates are expressed in the nsp2-7 system, it seems likely that, nsp5, given its presumed transmembrane nature, is the primary cause of the observed differences.

Comparison with the role of coronavirus nsps in membrane remodeling

In terms of host cell membrane remodeling, the coronaviral non-structural proteins 3, 4 and 6 that contain three conserved transmembrane domains (TM1, TM2 and TM3) are considered to be the functional equivalents of arterivirus nsp2, nsp3 and nsp5, respectively (78). A recent study addressed the question of the membrane-remodeling abilities of the SARS-CoV proteins nsp3, nsp4 and nsp6, using (co-)transfection of plasmids encoding separate nsps to express them either individually or in various combinations, followed by an ultrastructural analysis of the cells by EM (28). In this experimental set-up, co-expression of these three nsps appeared to be required for the formation not only of DMVs but also of structures resembling the CM that are typical of SARS-CoV infection (**Chapter 2**; Fig. 4B). This outcome differs from the results obtained with arteriviruses, where expression of

just nsp2 and nsp3 was sufficient, as described above, for the formation of closed DMVs in the expression systems tested. The corresponding combination of coronavirus nsps, namely SARS-CoV nsp3 and nsp4, gave rise to membrane structures termed maze-like bodies, which consisted of clusters of curved parallel-running profiles of ER-derived paired membranes (28). Interestingly, these were interspersed with circular profiles delineated by a double membrane. The circular profiles had an average diameter similar to the average spacing of the curved parallel double-membrane profiles (~80 nm), and they were interpreted, respectively, as cross or longitudinal sections of double-membrane walled tubules. However, in the absence of 3D-EM data, the authors recognized that is was not possible to firmly establish this point. In our opinion, the circular double-membrane profiles may alternatively represent DMVs interspersed with regions of paired membranes sheets, similar to what is observed upon expression of EAV nsp2-3 in the Sindbis virus-based expression system (Fig. 1). This is a particularly interesting possibility as it would imply that, both for arteriviruses and coronaviruses, the proteins containing TM1 and TM2 would be sufficient to induce DMV formation. In this alternative scenario, the nsp comprising TM3 may merely have a modulating role in DMV formation and, in coronaviruses, could be important for the generation of CM.

In any case, the presence of maze-like bodies reflects that expression of coronavirus nsp3 in combination with nsp4 is able to induce membrane-pairing, which is likely an essential step in DMV formation. The membrane pairing observed in the maze-like bodies appeared to strictly depend on the co-expression of nsp3 and nsp4, suggesting that it could be the result of heterotypic interactions between these proteins (28). This type of interaction between nsp3 and nsp4 has been biochemically detected by mammalian two-hybrid assay (161) and co-immunoprecipitation (162), and may resemble the nsp2-nsp3 interaction documented for arteriviruses (89, 134).

Additional experiments provided some interesting hints regarding the specific domains that could be important for the nsp3-nsp4 interaction possibly leading to membrane-pairing. The co-expression of MHV nsp4 and a C-terminal fragment of nsp3 that contained the two predicted transmembrane domains changed the localization of these proteins from the ER to discrete perinuclear foci (162). At the ultrastructural level, the two nsps mapped to regions of highly curved, ER-derived membranes that were vaguely reminiscent of the maze-like bodies described by Angelini *et al.* (2013) (96). Using truncated mutants, the critical regions for the relocation of these proteins to foci could be narrowed down to the luminal loop of nsp3 and the first luminal loop of nsp4 (96). This large N-terminal nsp4 loop contains ten conserved cysteines, which could be important in inter- or intra-molecular interactions. Mutations in each of these cysteines severely impaired the relocation of nsp4 and the nsp3 C-terminal fragment, suggesting an important direct or indirect role of these cysteines in the nsp3-nsp4 interaction (96). Like the coronavirus nsp4, the corresponding arterivirus protein (nsp3) contains a cluster of four conserved cysteine residues in its first luminal loop, and each of them appeared to be critical for DMV formation and virus replication (89). The latter study also showed, by mutating a catalytic residue in PLP2 (H332Y), that the cleavage between nsp2 and nsp3, although essential for virus replication, was dispensable for DMV

formation in an expression system. When expressed from the SINrep5 vector in BHK-21 cells, an nsp2-3 construct containing an N glycosylation site in the cysteine-containing loop induced the abundant formation of curved paired membranes, which was interpreted as partial inhibition of DMV formation (89). These modifications, however, closely resemble the results now obtained using wild-type nsp2-3 expressed from a Sindbis virus-based vector and therefore perhaps reflect peculiarities of this expression system rather than an effect of the mutation. This latter possibility seems to be supported by preliminary results for this mutant when expressed in an inducible HuH-7 cell line, in which long curved paired membranes could not be detected whereas regular DMV clusters were present (data not shown).

One major difference between studies on coronaviruses and arteriviruses (24, 88, 89), is that coronavirus nsps were expressed independently from separate plasmids, whereas arterivirus proteins were expressed as (more natural) self-cleaving polyproteins. Obviously, the former poorly mimics the situation in infected cells and could influence the course of events during which translation, polyprotein cleavage, nsp translocation, and membrane remodeling occur, likely in a defined order. Also processing intermediates could play an important role in membrane rearrangement, for example, by keeping nsps in close proximity to each other to favor key interactions in the membrane remodeling process. Additionally, it should be noted that proteins made from polyproteins are produced at equimolar ratios, something that is virtually impossible to control when co-transfecting multiple plasmids. Unfortunately, the exceptionally large size of coronavirus nsp3 (~2000 amino acids long) has so far complicated the production of the nsps from a self-cleaving polyprotein in an expression system. Future studies that overcome this technical difficulty may be pivotal to definitively establish the similarities and differences between coronaviruses and arteriviruses regarding the membrane-remodeling abilities of their nsps.

Intermediates of DMV biogenesis

We now have performed an extensive tomographic analysis that uncovered the 3D structure of some distinct intermediates that further support an enwrapping mechanism for DMV formation. These intermediates (observed in EAV-infected HuH-7 cells) include relatively long stretches of paired ER membranes that represent sheets according to the 3D analysis and could reflect the first step in DMV formation through enwrapping (Fig. 4A). In order to transform these sheets into DMVs, curvature must be induced and paired-membrane sheets with different degrees of curvature could indeed be detected in the tomograms (Fig. 4B). A (putative) even more advanced stage, in which the paired curved sheet is already transformed into a nascent DMV that is not yet completely sealed, is shown in Fig. 4C,D.

Given the similarities between arterivirus- and coronavirus-induced DMVs and the presumed common ancestry of their replicase proteins, including the subunits likely to drive the membrane modifications, it is tempting to speculate that the enwrapping mechanism could also be used for the formation of DMVs in coronavirus infection. In this regard, there are some striking similarities between the intermediate paired-membrane structures shown here for EAV and the zippered ER membranes recently documented for

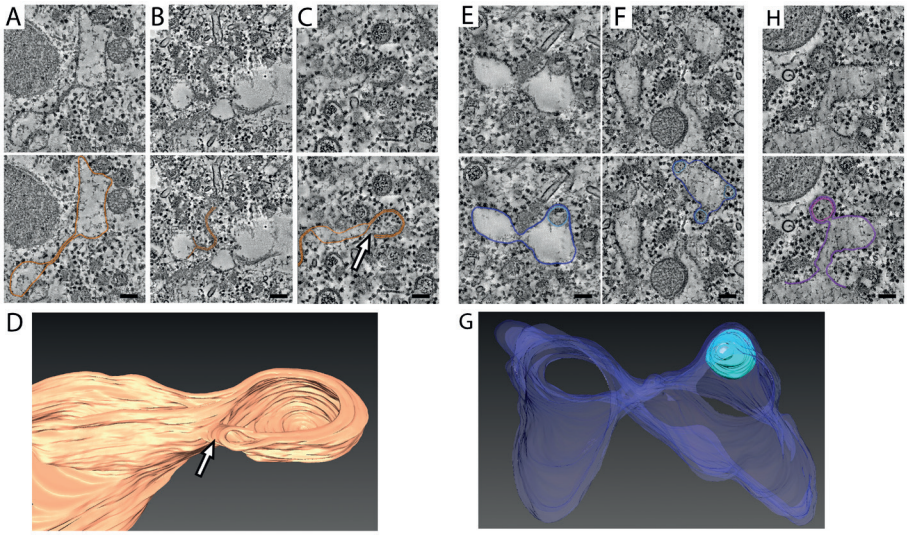


Fig. 4. Putative intermediate structures in the formation of DMVs. *The grayscale top images are virtual slices (6 nm thick) extracted from tomograms of EAV-infected HuH-7 cells.* **(A-C)** *Putative intermediates of an enwrapping process. The membranes of interest are highlighted in orange in the lower images. (A) Paired ER membranes, possibly corresponding to the stage sketched in* **Chapter 2** *Fig. 5A as II. This type of paired membranes could progressively curve (B) to form a vase-like double-membrane compartment (C, D) (stage represented in* **Chapter 2***; Fig.5A as III) with an opening to the cytosol (white arrows).* **(D)** *3D-surface rendering of the structure shown in panel C.* **(E-F)** *Structures compatible with intermediates in a double-budding mechanism. In the lower panels, the membranes are highlighted in dark blue (ER) and light blue (luminal vesicle). These structures could represent a stage between III and IV in* **Chapter 2***; Fig.5B, in which a luminal vesicle interacts with an ER membrane that curves towards the cytosol, possibly to form the outer membrane of a nascent DMV.* **(G)** *3D surface-rendered model of the structure shown in panel E.* **(H)** *Example of a DMV that is connected to the ER though it lacks the electron dense core usually seen in DMVs. The membranes are highlighted with purple (ER membranes) and pink (inner vesicle). Scale bars, 100 nm.*

the gammacoronavirus IBV (**Chapter 2**; Fig. 4C). These zippered membranes also appear to curve, forming open double-membrane spherules that, nevertheless, were ruled out as DMV precursor by Maier *et al.* due to their much smaller size (~60 nm in diameter versus ~180 nm for IBV DMVs) and their different appearance (22). Interestingly, the tomographic analysis of cells infected with the enteroviruses CVB3 and PV revealed putative intermediate structures supporting an enwrapping mechanism for the biogenesis of the DMVs induced by these viruses (56, 65). Taken together, these results suggest that enwrapping may well be a general route used for the generation of virus-induced DMVs.

Nevertheless, in our search for intermediates that could shed light on the biogenesis of EAV-induced DMVs, we also detected structures in infected HuH-7 cells that would be compatible with a double-budding mechanism. These consisted of sealed SMVs contained in the ER lumen and closely apposed to the ER membrane to possibly recruit the

second membrane through membrane pairing (Fig. 4E,F,G). We cannot discard, however, an alternative scenario in which these luminal SMVs would result from a distension of the connection between an already formed DMV and the ER. Although the putative double-budding intermediates were considerably rarer in our tomograms than the structures that would fit with the enwrapping model, this lower frequency cannot be directly translated into a quantitative assessment about the prevalence of the two mechanisms, as it could simply reflect that double-budding is a faster process that is therefore under-represented in the snapshots that EM provides. Overall, our data suggests that the enwrapping mechanism plays an important role in DMV formation but is also compatible with a model in which both enwrapping and double-budding would coexist. In this regard, it is interesting to emphasize that the fundamental difference between the two proposed mechanisms is simply the order in which essentially the same membrane reshaping events would take place (**Chapter 2**; Fig. 5). It is therefore conceivable that, having the molecular mechanism required for these steps in place, both paths could be used by the virus for the ultimate goal of forming DMVs.

An interesting feature of all putative nascent DMVs observed in the tomograms (Fig. 4C,E,F) is that they lack the electron-dense core that is typical of most DMVs found in EAV infected cells. However, occasionally fully-formed DMVs that do not contain such a core could also be detected. DMVs lacking and containing a core are indistinguishable in size and both types often appear to be connected to the ER (Fig. 4H). In our view, they could well represent early and later stages in the existence of a DMV. In this scenario, the DMV content would be initially identical to the surrounding cytosolic material. Once fully formed and closed, the DMV would accumulate electron-dense material. The exact nature of this material remains unclear although one of its components must be dsRNA.

CONCLUSIONS AND FUTURE PERSPECTIVES

The biogenesis of the DMVs formed upon nidovirus infection is an aspect that we are just beginning to address. The results presented here for EAV document clear putative intermediates in DMV formation by enwrapping of paired ER membranes as well as structures also compatible with a double-budding mechanism. This suggests that, maybe more than a strict sequence of events, the virus could "direct" basic membrane remodeling events (e.g. membrane pairing and induction of membrane curvature) that could be used in different routes ultimately leading to the same (or similar) structures. Viral proteins are likely to drive RVN biogenesis with the aid of host factors that, in the case of nidoviruses, remain to be identified. It seems clear now that both in arteri- and coronaviruses the TM1- and TM2-containing nsps are sufficient to produce membrane pairing (24, 28) and, in arteriviruses, also suffice for the formation of DMVs that have a comparable architecture to those found in infection. Our results suggest that the TM3-containing nsp, which has been proposed to be essential for DMV formation in coronaviruses (28), would merely have a curvature-modulating role in DMV biogenesis in the case of arteriviruses. Similar electron tomography studies with coronaviral nsp expression systems may help to firmly establish the similarities

and differences between arterivirus- and coronavirus-induced DMV formation. This kind of 3D-ultrastructural studies, possibly complemented with similar analyses *in vitro* using membrane model systems (163), could be a significant step towards the mechanistic dissection of the role of the nsps and their different domains in RVN biogenesis.

The stable inducible cell lines ectopically expressing EAV nsps that we present in this study, besides closely mimicking the morphology of DMVs in EAV-infected cells, open multiple possibilities for future research. These 'surrogate systems', inducibly expressing self-cleaving nsp constructs, could be employed, for example, to investigate the interplay between the virus-induced membrane structures and different host factors and pathways (e.g. innate immunity, autophagy), to study how viral proteins affect cellular lipid homeostasis, as well as in the search for new antiviral drugs that specifically target viral replication organelles.

Acknowledgements

We thank Ronald Limpens for general technical assistance and discussions. This work was supported in part by the Netherlands Organization for Scientific Research through a TOP grant from the Council for Chemical Sciences (NWO-CW grant 700.57.301 to EJS and AJK) and a MEERVOUD grant (NWO-ALW grant 836.10.003 to MB) from the Council for Earth and Life Sciences.

MATERIALS AND METHODS

Cells, virus, and infections

HuH-7 cells were cultured in Dulbecco's modified Eagle's medium supplemented with 8% fetal calf serum, non-essential amino acids (PAA), L-glutamine (PAA)), and penicillin/streptomycin (PAA). Cells were infected with a cell-culture-adapted EAV Bucyrus isolate (5). Infections were carried out with a multiplicity of infection of 10 and incubated at 37°C for 12 h before further processing.

Construction of EAV expression vectors

EAV polyprotein constructs were assembled in pDONR201 (Invitrogen) based on the previously described full-length cDNA clone of EAV pEAN511(89). Constructs for the expression of nsp2 and nsp3 contained amino acids 261-1063 of EAV pp1a with an HA-tag fused to the N-terminus of nsp2. The C-terminus of nsp3 lacked the final glutamic acid of nsp3 and was instead fused to either a His6 tag or enhanced GFP (eGFP). Polyprotein constructs of EAV pp1a nsp2-7 (amino acids 261-1676, lacking the last glutamic acid of nsp7) were fused to an HA-tag at the N-terminus and His6 tag at the C-terminus. Using gateway cloning, polyprotein constructs, as well as eGFP controls, were shuttled to either a modified Sindbis replicon vector based on SINrep5 (158) in which a gateway cassette was inserted into the multiple cloning site (pSR5-DEST) or the lentivirus vector pLenti6.3/TO/V5-DEST (Invitrogen).

Transfections

pSR5 constructs were linearized with XhoI followed by *in vitro* RNA synthesis using a SP6 mMESSAGE mMACHINE kit (Thermo). Cells were transfected using AMAXA electroporation with 1 µg SR5 RNA for each 1x106 cells and incubated at 37°C for 24 hours until analysis.

Generation of stable inducible cell lines

Lentivirus particles of pLenti6.3 constructs and pLenti3.3/tetR (Invitrogen) were generated as described previously (136). HuH-7 cells were transduced first with Lenti3.3/tetR lentivirus particles and selected using 500 µg/ml G418 (PAA) to insert the tetR gene for tetracycline-regulated expression (164). After complete selection cells were transduced again with different Lenti6.3 constructs and selected using 12.5 µg/ml Blasticidin-S (PAA). Expression of recombinant EAV constructs was induced for 24 hours using 1µg/ml tetracycline (Invitrogen) prior to fixation and further analysis.

Immunofluorescence and light microscopy

Cells were fixed at indicated time points with 3% paraformaldehyde in a phosphate-buffered saline (PBS) solution, permeabilized with 0.1% Triton X-100 in PBS and then immunolabeled with nsp2-specific rabbit antisera (previously described in (165)) and a mouse monoclonal antibody specific for dsRNA (MAb J2) (166, 167). These were detected, respectively, using a goat anti-rabbit immunoglobulin conjugated to Alexa Fluor 488 and a donkey anti-mouse immunoglobulin conjugated to a Cy3 fluorophore (Jackson). Imaging was done using a Leica SP8 confocal laser scanning microscope, which was equipped with a 63x objective (NA 1.40; 1 Airy Unit) and a Leica HyD hybrid detector.

Electron microscopy sample preparation

HuH-7 cells grown on sapphire discs (Leica) were either infected with EAV, transfected with Sindbis virus replicons or, in the case of the transduced HuH-7 cell lines, induced to express EAV nsp constructs as described above and subsequently high-pressure frozen with a Leica EM PACT2 and freeze-substituted as previously described (20) using an AFS2 (Leica) equipped with a freeze substitution processor robot. The freeze substitution medium consisted of 2% osmium tetroxide, 1% glutaraldehyde and 10% H2O in acetone. The samples were then kept at -90°C for 9h after which the temperature was raised by 23.33°C/h to -20°C. This temperature was kept for 1 h after which the temperature was again raised by -20°C/h to 0°C. After 1 h at this temperature the samples were washed first with cooled down acetone and again at room temperature. The samples were then embedded in epoxy LX-112 resin and polymerized at 60°C for 48 h.

For CLEM samples, the freeze substitution method described by (160, 168) was used to preserve the eGFP signal. Samples were maintained at a temperature of -90°C in 0.1% uranyl acetate in acetone for 48h. The temperature was then raised by 5°C/h to -45°C at which point the samples were washed with acetone and resin infiltration was started by adding increasing concentrations of Lowicryl (Polysciences, Inc., USA) in acetone (10, 25, 50 and 75%) that were kept on the sample for 4 h each, while the temperature was slowly

raised to -25°C. The 75% Lowicryl in acetone was then exchanged with 100% Lowicryl in three infiltration steps of 10 h each. Polymerization by ultra-violet (UV) light was started -25°C and maintained for 48 h. The temperature was then raised 5°C/h to 20°C. UV light illumination was then maintained for an additional 48 h.

For all the samples, 200 nm sections were cut with a UC6 ultramicrotome (Leica). The sections for CLEM were picked up on finder grids coated only with carbon (F1 200 mesh, Electron Microscopy Sciences). Parallel bar copper grids (R100, Electron Microscopy Sciences) covered with a carbon-coated formvar layer were used for tomography samples, which were then additionally counter-stained by incubating the grids with uranyl acetate (120 min) and lead citrate (10 min).

Electron microscopy and electron tomography

EM data was collected on FEI Tecnai12 BioTWIN and TWIN microscopes operated at 120kV and equipped with Eagle 4k cooled slow-scan charge couple device (CCD) cameras. Grids for tomography were inserted into a dual-axis tomography holder (Fischione). SerialEM (169) and Xplore3D (FEI company) acquisition software packages were used to collect images covering 130° around the specimen in 1° increments around two perpendicular axes. The pixel size at the specimen level was 1.2 nm (BioTWIN data) or 1 nm (TWIN data). Alignment of the tilt-series and tomogram reconstruction by weighted back-projection were done using IMOD software (170). The 3D surface renderings of the tomograms were manually generated using the AMIRA visualization software (FEI Visualization Sciences Group) using a Wacom tablet and pen.

Correlative light and electron microscopy (CLEM)

Grids containing sections for CLEM were incubated with a Hoechst 33342 solution for 15 minutes to stain the nucleus of the cells in order to aid with the correlations. The grids were then washed, dried and subsequently mounted on a glass-slide in a drop of water with the section side facing up. This was then covered with a coverslip to enable oil immersion imaging, which was performed with a DM 5500 wide-field microscope (Leica) equipped with a 40x (NA 1.25) objective and a photometrics Coolsnap HQ B/W camera. The position on the grid of the fluorescence images was logged by using the marks on the finder grid. After light microscopy imaging the grids were dismounted from the glass-slide, dried at room temperature and transferred to the EM, where the logged positions were traced back. The overlay of the fluorescent and EM images was made in Photoshop using the nuclei in both images as reference points.

Chapter 4

Middle East respiratory syndrome-coronavirus nonstructural proteins 3 and 4 are required and sufficient to induce the formation of double-membrane vesicles

Diede Oudshoorn, Kevin Rijs, Ronald W.A.L. Limpens, Kevin Groen, Abraham J Koster, Eric J Snijder, Marjolein Kikkert, Montserrat Bárcena

Revised manuscript accepted for publication in mBio (mBio 8(6) e01658-17)

ABSTRACT

Betacoronaviruses such as Middle East Respiratory Syndrome-Coronavirus (MERS-CoV) are important pathogens causing potentially lethal infections in humans and animals. Coronavirus RNA synthesis is thought to be associated with replication organelles (ROs) consisting of modified endoplasmic reticulum membranes. These are transformed into double-membrane vesicles (DMVs) that contain viral double-stranded RNA, convoluted membranes, and other membranous elements, together forming a reticulovesicular network. Previous evidence suggested that the non-structural proteins (nsps) 3, 4, and 6 of the Severe Acute Respiratory Syndrome-Coronavirus (SARS-CoV), which contain transmembrane domains, are required for DMV formation. We have now expressed MERS-CoV replicase self-cleaving polyprotein fragments encompassing nsp3-4 or nsp3-6, as well as co-expressed nsp3 and nsp4 of either MERS-CoV or SARS-CoV, to characterize the membrane structures induced. Using electron tomography, we found that, for both MERS-CoV and SARS-CoV, co-expression of nsp3 and nsp4 is clearly required and sufficient to induce DMVs. DMV formation was similar when MERS-CoV nsp3 and nsp4 were co-expressed either as individual proteins or as a self-cleaving nsp3-4 precursor. Moreover, using polyprotein expression, we established that cleavage of the nsp3/nsp4 junction is essential for MERS-CoV DMV formation. Addition of the third MERS-CoV transmembrane protein, nsp6, did not seem to affect DMV formation, while its impact on the formation of other RO elements remains to be further investigated. These findings provide important insight into the formation of coronavirus ROs and establish strong similarities with RO formation by other nidoviruses, specifically the arteriviruses.

Importance

The replication of all plus-stranded RNA viruses of eukaryotes is thought to take place at cytoplasmic membranous replication organelles (ROs). One of the most prominent types of viral ROs induced by a number of these viruses, including coronaviruses, are double-membrane vesicles (DMVs) that contain viral double-stranded RNA. In this study, using electron microscopy and tomography, we explored which viral proteins are required for the formation of MERS- and SARS-coronavirus-induced DMVs. We found that co-expression of two of the three transmembrane subunits of the coronavirus replicase polyprotein, non-structural proteins (nsps) 3 and 4, is required and sufficient to induce DMV formation. In contrast to a previous report, the third transmembrane protein, nsp6, seems to be dispensable. Moreover, release of nsp3 and nsp4 from the polyprotein by proteolytic maturation is essential for DMV formation. These findings provide a strong basis for further research on the biogenesis and functionality of coronavirus ROs.

INTRODUCTION

Coronaviruses are positive-strand RNA viruses that can pose serious zoonotic threats to human health, as evidenced by the emergence of severe acute respiratory syndrome coronavirus (SARS-CoV) in 2002 (171, 172) and, more recently, the Middle East respiratory syndrome coronavirus (MERS-CoV). Since the start of the outbreak in 2012, MERS-CoV has continued to circulate in the Arabian Peninsula (12, 173), which to date has led to almost 2,000 laboratory-confirmed human infections with a lethality rate of about 35% (http://www.who.int/emergencies/mers-cov/en/). Coronaviruses, members of the order *Nidovirales*, have the largest known positive-strand RNA genomes, ranging from 26 to 33.5 kb (13, 78, 174). The 5′-proximal two-thirds of the genome contains the replicase gene that consists of two open reading frames (ORF1a and ORF1b). ORF1a translation yields polyprotein 1a (pp1a; roughly 4,000-4,500 amino acid (aa) residues long), which, following a -1 ribosomal frameshift, can be extended with the ORF1b-encoded polyprotein to yield pp1ab (6,700-7,200 aa residues in total). The pp1a and pp1ab polyproteins contain the enzymes of the RNA-synthesizing complex that drives viral genome replication and subgenomic mRNA synthesis (175). The replicase polyproteins are co- and post-translationally processed into 15 or 16 nonstructural proteins (nsps) by two or three ORF1a-encoded proteases (76, 176-179). Depending on the coronavirus, one or two papain-like proteases (PLpro) that reside in nsp3 process the part of the polyproteins upstream of nsp4. In all coronaviruses, the region downstream of nsp4 is cleaved by the 3C-like cysteine protease or main protease (M^{pro}) located in nsp5 (Fig. 1A) (76, 176-179).

Coronaviruses, like all positive-strand RNA viruses of eukaryotes, hijack intracellular membranes to form replication organelles (ROs) (16-19, 180). These generally reside in the perinuclear region of the cell and are assumed to constitute micro-environments that promote viral RNA synthesis, while possibly shielding replicative intermediates, such as double-stranded RNA, from detection by the innate immune system. The most prominent membrane structures induced after coronavirus infection are double-membrane vesicles (DMVs) (21, 22, 106, 123-128, 181), which appear to contain double-stranded RNA, a well-known marker of positive-strand RNA virus replication (21, 167). DMVs are not only formed during the replication of coronaviruses, but are also a central component of the ROs induced by numerous other plus-stranded RNA viruses such as hepatitis C virus (HCV), and enteroviruses like poliovirus and coxsackievirus (23, 56, 65). Most of our current knowledge of coronavirus ROs has been gained through electron microscopy (EM) studies of members of the genus *Betacoronavirus*, which includes SARS-CoV, MERS-CoV, and mouse hepatitis virus (MHV) (21, 106, 125-128). Electron tomography (ET) studies of SARS-CoV-infected cells showed that DMV outer membranes are often interconnected and also connected with the endoplasmic reticulum (ER) and/or with another virus-induced structure called convoluted membranes (CM) (21). Together, they form an elaborate reticulovesicular network (RVN), for which the ER probably serves as the membrane donor organelle (21).

The three main coronaviral proteins likely responsible for RO formation are the membrane-spanning nsp3, nsp4, and nsp6 subunits (Fig. 1A) (16, 182). Each of these spans

the membrane multiple times (2, 4, and 6 times, respectively) and they have 1, 2, and 3 luminal loops, respectively, with both nsp3 and nsp4 having a large luminal loop (95, 183-185). Mutagenesis studies showed that the first luminal loop of MHV nsp4 is critical for viral replication (186, 187). Furthermore, nsp4 of both MHV and SARS-CoV contains sites (2 and 1 respectively) for N-linked glycosylation in the first luminal loop of nsp4 (95, 185, 188). When both these sites were mutated in MHV nsp4 (186, 188), the virus was attenuated in cell culture and DMV formation was impaired, suggesting that nsp4 plays a critical role in coronaviral RO formation. The combined membrane-spanning regions of these proteins (i.e. including all luminal loops and flanking transmembrane domains) are commonly referred to as TM1, TM2, and TM3, respectively. Nsp3, nsp4, and nsp6 are non-conventional transmembrane proteins in the sense that they are derived from a polyprotein and do not contain N-terminal signal sequences for co-translational membrane insertion. It is currently unknown how their membrane insertion is facilitated and whether polyprotein cleavage precedes (or is required for) translocation across the ER membrane. To a certain extent, nsp2, nsp3, and nsp5 of the distantly related arteriviruses (also members of the *Nidovirales* order) can be considered equivalent to coronavirus nsp3, nsp4, and nsp6, in terms of their relative position in the replicase polyprotein and their membrane-spanning properties. For arteriviruses, expression of nsp2 and nsp3 alone was necessary and sufficient for the formation of double-membrane structures strikingly resembling the DMVs observed in infected cells (24). Co-expression of nsp5 reduced the size of the induced DMVs, but did not change their overall architecture (180). In the case of coronaviruses, it was recently reported that the transient co-expression of SARS-CoV nsp3, nsp4, and nsp6 led to the formation of DMVs (28). Cells co-expressing nsp3 and nsp4 alone contained so-called maze-like bodies, consisting of paired ER membranes (zippered ER) and some circular profiles that were interpreted as cross-sections of double-membrane tubules. Therefore, it was concluded that nsp6 is essential for the biogenesis of SARS-CoV DMVs, whereas nsp3 and nsp4 can mediate the pairing of membranes that are likely an intermediate in DMV formation (28).

In the current study, we examined the role of MERS-CoV nsps in betacoronavirus RO biogenesis. Using EM and ET, we found that MERS-CoV nsp3 and nsp4, either co-expressed from separate plasmids or expressed as a self-cleaving polyprotein fragment (nsp3-4), are essential and sufficient for the formation of DMVs that assemble into an RVN. Addition of the third transmembrane subunit of the MERS-CoV replicase, nsp6, did not alter the overall morphology of the induced DMVs. When the nsp3-4 polyprotein remained uncleaved, this prevented the formation of DMVs while membrane pairing did still occur, suggesting that proteolytic processing coordinates DMV formation in time and/or space. To compare our results with previous work, we used ET to analyze the 3D structure of the maze-like bodies induced upon co-expression of SARS-CoV nsp3 and nsp4, and established that also in the case of SARS-CoV these proteins suffice for DMV formation. Our results provide important new insights in the biogenesis of coronavirus ROs and suggest the conservation of certain principles underlying RO formation among distantly related members of the order *Nidovirales*.

RESULTS

MERS-CoV nsp3 and nsp4 co-localize in the perinuclear region of the cell

To study whether the transmembrane nsps of MERS-CoV are able to induce DMV formation, we expressed nsp3 and nsp4 from a CAG promoter (189) either by co-transfection of cells with plasmids encoding individual proteins or by transfection with a single plasmid encoding a self-cleaving nsp3-4 polyprotein fragment (Fig. 1A). Constructs were codon-optimized for expression in human cells, (potential) splice sites were eliminated, and the encoded proteins were equipped with HA, myc, or V5 tags at their termini. The constructs were transfected into 293T cells to verify protein expression and processing (Fig. 1B). The wild-type nsp3-4 polyprotein was fully cleaved into mature nsp3 and nsp4, as was previously described (190). As a control, a mutant in which the nsp3/nsp4 cleavage site was inactivated (G2739A/G2740A; GG>AA; (191)) was included to generate the non-cleaved precursor. Interactions between nsp3 and nsp4 were previously shown to occur for MHV and SARS-CoV (161, 162) and we assessed whether this was also the case for the corresponding MERS-CoV proteins. To this end, 293T cells were transfected with a construct expressing HA-nsp3-myc or nsp4-V5, or co-transfected with both constructs. Expression products were labeled metabolically with [^{35}S]methionine and [^{35}S]cysteine, and subsequently immunoprecipitated with either HA- or V5-specific antibodies (Fig. 1C). Upon immunoprecipitation with the HA-specific antiserum, nsp4-V5 was brought down when HA-nsp3 was present (left panel). Conversely, when using the V5-specific antibody, HA-nsp3 was co-immunoprecipitated when nsp4-V5 was present (right panel). These findings demonstrated that these two MERS-CoV proteins interact and further supported the notion that this is a common feature of coronaviruses. When using immunofluorescence microscopy, separate expression of nsp3 or nsp4 in HuH-7 cells yielded a reticular labeling pattern, with some more intense foci in the perinuclear region of the cell, suggesting that – in the absence of the other – either protein localized at least partially to the ER (Fig. 1D). This reticular pattern (but without the foci) has been described previously upon transient expression of MHV and SARS-CoV nsp4 (95, 96), whereas full-length SARS-CoV nsp3 was reported to localize to foci similar to those we observed (28). When co-expressing MERS-CoV nsp3 and nsp4, or when expressing the self-cleaving nsp3-4 polyprotein, the reticular pattern was much less pronounced and both proteins mainly co-localized in foci in the perinuclear region (Fig. 1D lower panels). This was in agreement with the finding that MERS-CoV nsp3 and nsp4 interact and also suggested that this interaction strongly promotes their recruitment to the foci in the perinuclear region. However, the resolution of light microscopy does not allow drawing conclusions about the ultrastructure of the subcellular structures in which these proteins accumulate.

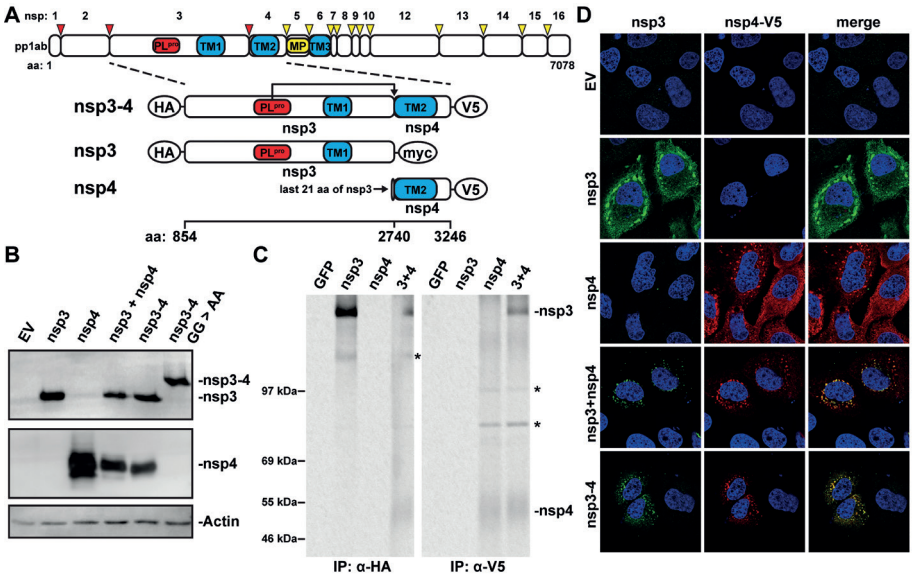


Fig. 1. MERS-CoV nsp3 and nsp4 interact with each other. (A) *Scaled schematic overview of MERS-CoV pp1ab and nsp3-4 constructs. Amino acid numbers refer to the MERS-CoV pp1ab sequence. The expected cleavage of nsp3/nsp4 junction by PL^{pro} is indicated. The epitope tags used at the termini of the constructs are indicated with ovals. TM = transmembrane region.* **(B)** *293T cells were transfected with MERS-CoV nsp3-4 plasmids or empty pCAGGS vector (EV) and analyzed by Western blotting 20 hours post transfection. Nsp3 was detected with α-SARS-CoV nsp3 serum that cross-reacts with MERS-CoV nsp3 (128) and nsp4 was detected with α-V5 monoclonal antibody.* **(C)** *Constructs expressing MERS-CoV nsp3, nsp4 or a GFP control were transfected into 293T cells, which were metabolically labeled with [^{35}S] methionine/cysteine from 4 to 20 hours post transfection. Lysates were immunoprecipitated with the indicated antibodies, separated on a SDS-PAGE gel and visualized using phosphor imaging. Bands not corresponding to expected protein size in Western Blot were indicated with asterisks. The ± 130kDa band in the nsp3 IP was also observed in Western Blot. Nsp4 bands in IP were fuzzy likely due to the relatively high hydrophobicity of the protein.* **(D)** *HuH-7 cells were transfected with the indicated plasmids and localization of MERS-CoV nsp3 and nsp4 was analyzed using immunofluorescence labeling and confocal microscopy at 24 hours post transfection. Nsp3 was detected with α-SARS-CoV-nsp3 serum and nsp4 with α-V5 monoclonal antibody.*

MERS-CoV nsp3 and nsp4 are required and sufficient to induce DMV formation

The next step was to determine whether nsp3 and nsp4 could induce the formation of double-membrane structures similar to those observed during infection. As a reference, MERS-CoV-infected HuH-7 cells were analyzed by EM. The membrane structures that were previously described in high-pressure frozen and freeze-substituted Vero cells infected with MERS-CoV (128) were readily apparent at 10 h post infection (p.i.) in chemically fixed HuH-7 cells (Fig. 2A). Numerous DMVs were found (red asterisks), often adjacent to areas containing CM. The DMV interior appeared electron-translucent, a difference with cryo-

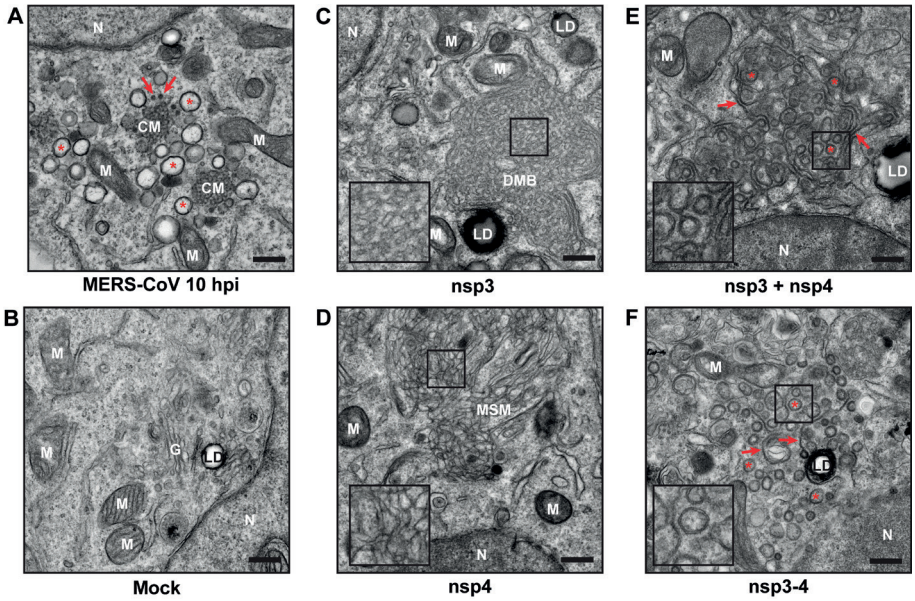


Fig. 2. MERS-CoV nsp3 and nsp4 induce modification of intracellular membranes. (A) *HuH-7 cells were infected with MERS-CoV or mock infected* **(B)** *and analyzed at 10 h p.i. using EM. Several DMVs are indicated with red asterisks and several spherules are indicated with red arrows.* **(C-F)** *HuH-7 cells were transfected either with constructs expressing individual nsps (C,D) or both nsp3 and nsp4, following either co-transfection with two plasmids (nsp3 + nsp4) or expression of a self-cleaving precursor (nsp3-4) (E/F), and analyzed using EM at 24 hours post transfection. (E,F) Some stretches of zippered-ER are indicated with red arrows and several DMVs are indicated with red asterisks. (A-F) N = nucleus; G = Golgi; M = mitochondria; LD = lipid droplet; CM = convoluted membranes; DMB = disordered-membrane body; MSM = clusters of modified single-membranes; all scale bars represent 500 nm.*

fixed samples (128) that can likely be attributed to the different sample preparation method as the contents of SARS-CoV induced DMVs are easily lost upon chemical fixation (106). Occasionally some small(er) circular structures were observed that seemed similar in size to the spherules recently described for the gammacoronavirus infectious bronchitis virus (red arrows) (22). None of these structures were found in mock-infected control samples (Fig. 2B).

When HuH-7 cells expressed either nsp3 or nsp4, areas containing modified membranes were observed, which likely corresponded to the foci observed in fluorescence microscopy (Fig. 1D). In nsp3-expressing cells (Fig. 2C), we detected large regions, usually several microns in diameter, of disordered membrane bodies (DMB), which were similar to those previously observed after SARS-CoV nsp3 expression (28). The membrane structures clustering in these DMBs were reminiscent of the surrounding ER cisternae, with which they were frequently connected, suggesting that DMBs consisted of clustered ER-derived membranes. Upon expression of MERS-CoV nsp4, large clusters of modified single membranes (MSM) were observed (Fig. 2D), but these structures seemed more

irregular when compared to those induced by nsp3 (Fig. 2C). The expression of SARS-CoV nsp4 did not result in changes in intracellular membrane morphology (28), in contrast with our present observations following MERS-CoV nsp4 expression. Whether this reflects differences between the experimental setups used or an actual difference between these viral proteins remains to be determined.

When MERS-CoV nsp3 and nsp4 were expressed in the same cell, either by co-transfection or by expression of the self-cleaving nsp3-4 polyprotein, a remarkably different set of membrane structures was observed (Fig. 2E,F). A combination of circular double-membrane profiles (red asterisks) and paired membranes (red arrows) was present in both cases, suggesting that the combined expression of MERS-CoV nsp3 and nsp4 is sufficient to induce DMV formation. There was no apparent difference between the structures resulting from co-expression of nsp3 and nsp4 versus expression of the self-cleaving nsp3-4 polyprotein (Fig. 2E,F), but in both cases the circular profiles were significantly smaller than the ones observed in MERS-CoV infected cells (average diameters 146 and 148 nm, respectively, versus 252 nm in infection) (Sup Fig. 1).

To verify that DMVs are indeed formed upon expression of nsp3 + nsp4 and nsp3-4, we analyzed the 3D architecture of these membrane structures using ET, which confirmed that multiple circular profiles indeed corresponded to DMVs (Supplementary movies 3 and 4, Fig. 3A). We found no openings connecting the DMV interior and the cytosol, similar to what was observed previously in tomographic analysis of coronavirus-infected cells (21, 22). The tomograms corroborated the structural similarity between the membrane structures induced by co-transfection with nsp3 and nsp4 constructs and by expression of the nsp3-4 polyprotein. The electron density of the DMV interior seemed similar to that of the surrounding cytoplasm and in this sense it was different from the DMVs observed in MERS-CoV infected cells (compare to Fig. 3A), which is likely due to the absence of other viral proteins and double-stranded RNA. In some cases, DMVs appeared to be contained in a larger double-membrane structure (Fig. 3B; red asterisks). Such structures have not been observed in coronavirus-infected cells so far and their formation could be linked to *e.g.* the absence of (viral) DMV content or levels of the nsp3 and nsp4 proteins. The paired membranes were often continuous with the ER (Fig. 3B) and resembled the so-called zippered ER that has been also observed in IBV-infected cells (22), although they have not been documented so far for betacoronavirus-infected cells. These paired membranes may represent an intermediate of DMV biogenesis. Further supporting this explanation, structures in which the zippered ER seemed to transform into a nascent DMV could be observed in the tomograms (Fig. 3B; red arrows). We also observed DMV-DMV, DMV-zippered ER, and DMV-ER connections (Fig. 3C; red arrows), and completely isolated DMVs were in fact rare. Together, these observations suggest that MERS-CoV nsp3 and nsp4 are capable of inducing the transformation of ER membranes into an RVN of modified ER and DMVs.

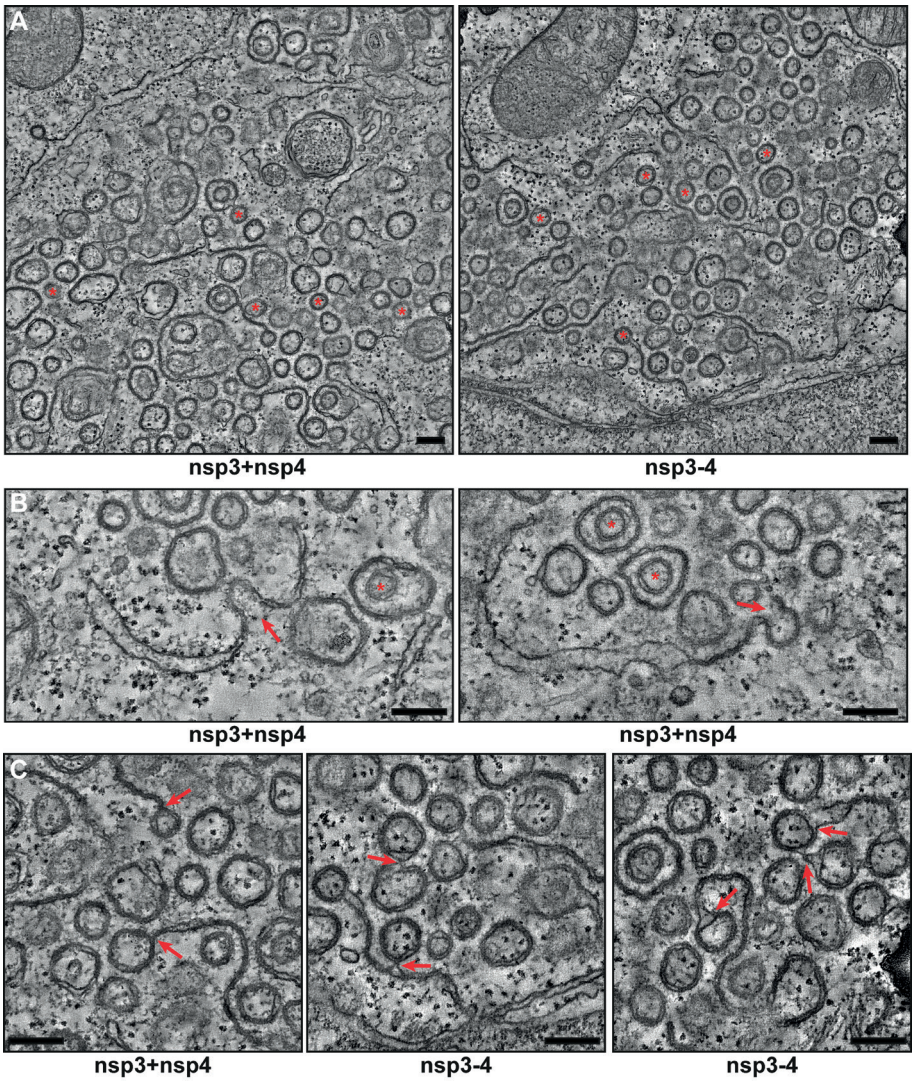


Fig. 3. MERS-CoV nsp3 and nsp4 induce the formation of DMVs that are organized in an RVN. *HuH-7 cells were co-transfected with constructs expressing nsp3 and nsp4 or the nsp3-4 precursor and fixed for ET analysis.* **(A)** *Overviews of reconstructed tomograms (available as supplementary movies S1 and S2, respectively) for both conditions. Some of the fully reconstructed closed DMVs are indicated with red asterisks.* **(B)** *Zippered-ER curving into putative intermediates during DMV biogenesis (indicated with red arrows) is shown. Two DMVs that are enclosed within other DMVs are indicated with red asterisks.* **(C)** *Examples of connections between DMVs and (zippered) ER (indicated with red arrows). All the images are virtual 5 nm thick slices from the reconstructed tomograms. All scale bars represent 250 nm.*

MERS-CoV nsp6 does not alter DMV morphology

The DMVs induced by expression of MERS-CoV nsp3-4 largely mimicked those observed during infection. However, the additional RVN elements that have been observed in this and previous studies of coronavirus-infected cells (CM and spherules) were not detected. To investigate whether nsp6, the third transmembrane subunit of the coronavirus replicase, plays a role in their formation or affects DMV formation, we extended the expressed polyprotein fragment to include nsp5 and nsp6. In addition to PLpro cleaving the nsp3/nsp4 site in this polyprotein fragment, the nsp5-based M^{pro} was expected to perform the cleavages at the nsp4/nsp5 and nsp5/nsp6 junctions. It should be noted, however, that the kinetics of polyprotein cleavage during MERS-CoV infection have not been documented; for example, it is unknown whether specific intermediates of polyprotein cleavage are long-lived and/or perform specific functions during MERS-CoV replication. Unfortunately, our efforts to investigate this matter in MERS-CoV-infected cells were hampered by technical difficulties arising from the insufficient levels of 35S-labelled pp1a/pp1ab subunits for immunoprecipitation analysis.

We therefore designed several polyprotein constructs encompassing the nsp3-6 region of MERS-CoV pp1a and tested their proteolytic processing as part of our evaluation of the impact of nsp6 expression on the formation of the coronavirus ROs (Fig. 4A). Upon expression of an HA-nsp3-6-V5 polyprotein and labeling with [^{35}S]methionine/cysteine, immunoprecipitation analysis showed that only a trace amount of fully cleaved nsp4 and nsp5 was present (Fig. 4B; lanes 3 and 8) and that most of the signal was present in larger precursors. Given the interaction between nsp3 and nsp4 (Fig. 1C) and the fact that the nsp5-6 precursor did not co-immunoprecipitate with the HA-tagged nsp3 (lane 3), we assumed the second, larger band to be co-precipitating nsp4-6 precursor. When a rabbit antiserum raised against a combination of MERS-CoV nsp5 peptides was used (lane 8), two precursors were pulled down. The smallest of these co-migrated with the nsp5-6 precursor (lane 13), which was expressed from an nsp5-6 construct carrying an nsp5/nsp6 cleavage site mutation (Q3553A). Based on its migration in the gel, a possible dimer of the nsp5-6 precursor was also observed, which co-migrated with nsp4-6 observed in lanes 3 and 8.

As in the nsp3- and nsp4-coding sequences used above, the codon usage of the nsp5 and nsp6 genes in our constructs was optimized for expression in human cells. One caveat is that this approach may eliminate rare codons that can reduce ribosome processivity during translation to promote proper protein folding, which can be particularly important for transmembrane proteins (192). Nsp6 is the coronavirus transmembrane nsp with the largest number of predicted membrane-spanning domains and its folding and proper membrane insertion might be linked to polyprotein processing. We therefore swapped the codon-optimized nsp6 gene for the original viral sequence. Furthermore, anticipating that the C-terminal V5-tag could be an issue, we restored the nsp6/7 cleavage site to yield the native nsp6 C-terminus after cleavage. Downstream of the short nsp7 peptide, GFP was fused to the C-terminus of the polyprotein so that its cleavage could be monitored (Fig. 4A; nsp3-6-GFP). This approach, however, only marginally improved the processing by M^{pro} as only small amounts of free nsp4, nsp5, and GFP were observed and most of the signal

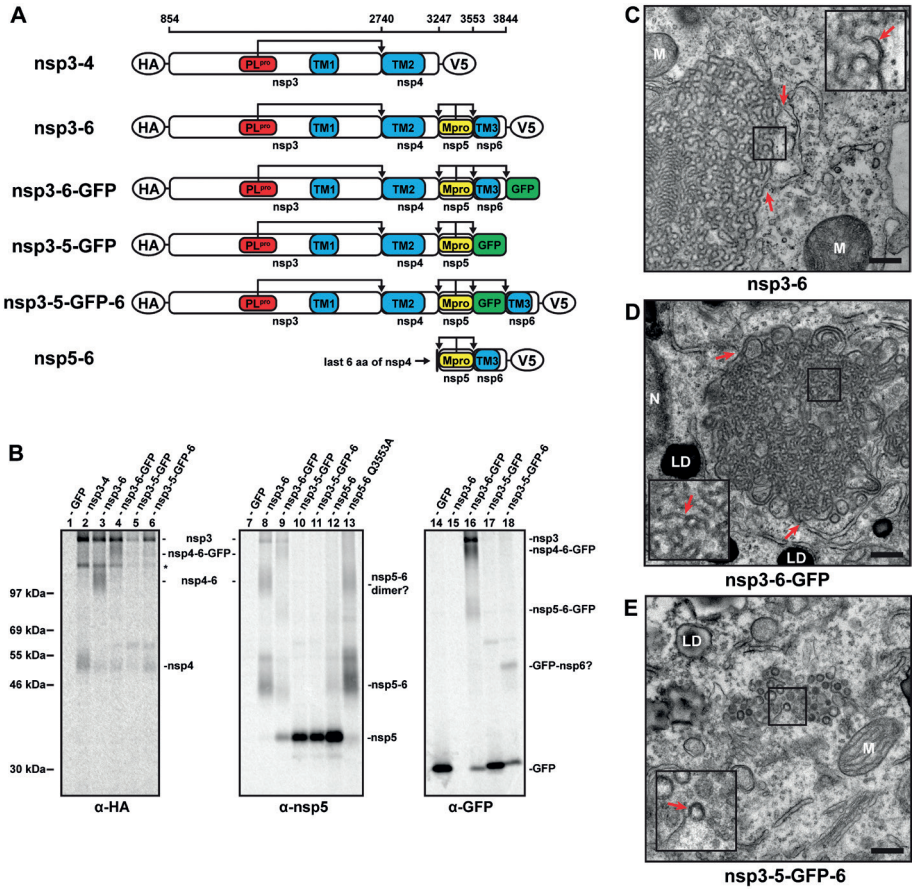


Fig. 4. Co-expression of MERS-CoV nsp6 does not alter DMV morphology. (A) *Scaled schematic overview of MERS-CoV nsp3-6 constructs. Amino acid numbers at the top are the positions in MERS-CoV pp1a. Expected cleavage sites by PL^{pro} and M^{pro} are indicated. TM = transmembrane domain, used epitope tags are indicated with ovals.* **(B)** *293T cells were transfected with indicated plasmids and metabolically labeled with [^{35}S]methionine/cysteine from 4 to 20 hours post transfection. Lysates were immunoprecipitated with indicated antibodies and separated on a SDS-PAGE gel. The ~130 kDa band in the nsp3 sample (indicated with an asterisk) is the same as in (Fig. 1C) and was also observed when only nsp3 was expressed. Nsp4 bands and putative nsp4- and nsp6-containing precursor bands were fuzzy, likely due to their relatively large hydrophobic domains. The different GFP bands around 30 kDa vary in size due to small variations in the length of the linker in the different polyprotein constructs.* **(C,D,E)** *HuH-7 cells were transfected with indicated plasmids and analyzed using EM at 24 hours post transfection. Red arrows indicate possible connections between the ER and the cubic membranes and some DMVs are indicated with red asterisks. The insets show some areas where the double membrane can be observed. N = nucleus; M = mitochondria; LD = lipid droplet; all scale bars represent 500 nm.*

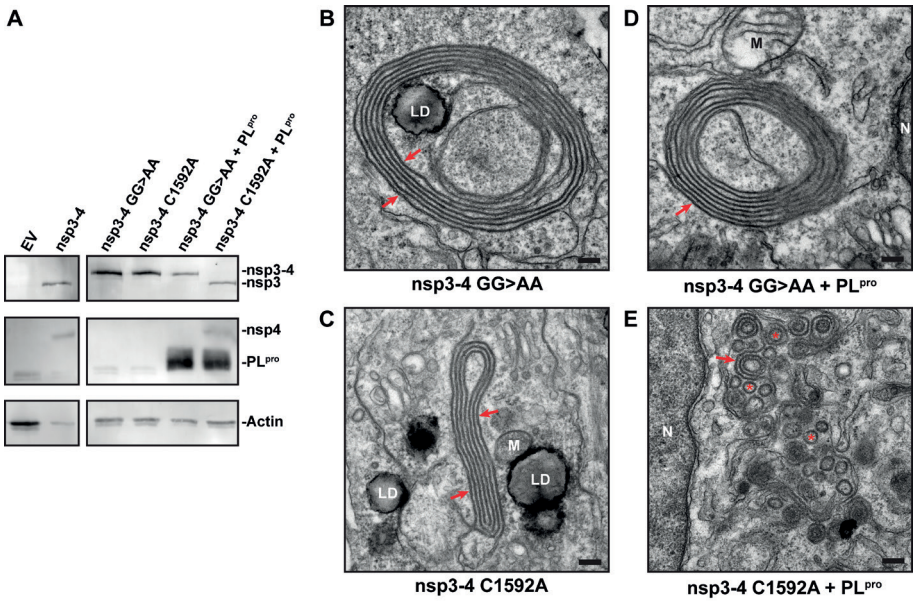


Fig. 5. Cleavage of MERS-CoV nsp3/nsp4 junction is essential for DMV formation. (A) *293T cells were transfected with indicated plasmids and analyzed using Western blotting. Nsp3 was detected with α-SARS-nsp3 serum and nsp4 with α-V5 monoclonal antibody.* **(B-E)** *HuH-7 cells were transfected with mutant nsp3-4 constructs individually (B/C) or co-transfected with the PL^{pro} domain of nsp3 (D/E) and analyzed using EM. Red arrows point at zippered-ER and in panel (E) some putative DMVs are indicated with red asterisks. N = nucleus; M = mitochondria; LD = lipid droplet; all scale bars represent 500 nm.*

was still present in the form of larger precursor proteins (Fig. 4B; lanes 9 and 16). We next checked whether M^{pro} was able to fully process the nsp4/nsp5 and nsp5/nsp6 junctions in other polyprotein configurations. To this end we used an nsp3-5-GFP polyprotein of which the nsp5/nsp6 junction was intact but followed, after a short nsp6 linker, by the GFP sequence (Fig. 4A; nsp3-5-GFP), and an nsp5-6 polyprotein carrying a small C-terminal nsp4 peptide at its N-terminus (Fig. 4A; nsp5-6). For both of these polyproteins, we observed near-complete proteolytic processing (Fig. 4B; lanes 10, 12, and 17), which suggested that in the case of nsp3-6-GFP the simultaneous expression of nsp4 and nsp6 impaired the kinetics of polyprotein processing. In an attempt to trigger efficient proteolytic processing of a polyprotein containing all three MERS-CoV transmembrane nsps, we duplicated the nsp5/nsp6 junction and inserted GFP between the two copies (Fig. 4A; nsp3-5-GFP-6). This polyprotein was processed reasonably efficiently, as mature nsp5 and a substantial amount of free GFP were observed, although some of the remaining signal may have corresponded to uncleaved GFP-nsp6 (Fig. 4B; lanes 11 and 18). Even though several questions remained regarding the identity of some of the larger cleavage products and the kinetics of polyprotein processing, the different MERS-CoV nsp3-6 constructs offered a useful tool to evaluate the effect of expressing nsp6 in addition to nsp3 and nsp4.

When the inefficiently processed nsp3-6 precursor was expressed in HuH-7 cells, we no longer found DMVs, but instead large areas of highly organized and curved membrane structures were seen (Fig. 4C). Similar structures were observed when the nsp3-6-GFP polyprotein was expressed (Fig. 4D). In both cases, the structures were connected to surrounding ER cisternae (Fig. 4C,D; red arrows) and, in contrast to the large single-membrane clusters observed in nsp3- or nsp4-expressing cells (Fig. 2C,D), they consisted of double membranes (Fig. 4C,D; red arrows in insets). The geometrical pattern in these large areas containing double-membrane structures is typical of cubic membranes (193). Possible triggers of cubic membrane formation are over-expression and/or misfolding of ER proteins, which can lead to protein and membrane aggregation, which possibly happened here. When we instead expressed the nsp3-5-GFP-6 polyprotein, which was almost fully processed (see above), rather than cubic membranes we observed putative DMVs together with zippered-ER (Fig. 4E). These membrane structures were very similar to the ones found in cells expressing just nsp3 and nsp4 (compare with Fig. 2E,F). The average size of these DMVs (146 nm) was very similar to that of DMVs induced by nsp3-4 expression (148 nm) (Sup Fig. 1). The circular profiles (putative DMVs) were detected in 33 out of 642 cell profiles analyzed; however, none of these regions contained CM or spherules. This suggests that, while nsp3 and nsp4 are necessary and sufficient for the rearrangement of intracellular membranes into DMVs, the presence of (cleaved) nsp6 does not suffice to trigger the formation of the additional membrane structures typical of MERS-CoV infection. Other viral components that are present during MERS-CoV replication, such as viral RNA or other viral proteins, might thus be required for the formation of convoluted membranes and spherules.

Cleavage of the MERS-CoV nsp3/nsp4 junction is essential for DMV formation

To gain more insight in the biogenesis of coronavirus DMVs, we set out to determine the role of the nsp3/nsp4 cleavage event. We surmised that the membrane modifications induced by an uncleaved nsp3-4 polyprotein could differ from those triggered by the (cleaved or co-expressed) nsp3 and nsp4 subunits. We transfected HuH-7 cells with plasmids encoding nsp3-4 carrying either a mutated nsp3/nsp4 cleavage site (GG>AA) or a catalytic site mutation in the nsp3 PL^{pro} domain (C1592A) that inactivates the protease (194). In both cases, only the uncleaved nsp3-4 precursor was observed (Fig. 5A). Interestingly, DMVs were no longer found and instead we detected concentric structures consisting of zippered ER that mostly lacked the pronounced curvature present in DMVs (Fig. 5B,C). Co-transfection of the cells with a plasmid encoding the active PL^{pro} domain restored the nsp3/nsp4 cleavage in the nsp3-4 C1592A mutant polyprotein, but not in the nsp3-4 polyprotein with the mutated cleavage site (Fig. 5A). Accordingly, expression of PLpro together with the nsp3-4 cleavage site mutant (Fig. 5D) did not alter the structures observed. In contrast, when trans-cleavage of the nsp3/nsp4 site, by co-expression of PLpro with the nsp3-4 C1592A polyprotein, was achieved, DMV formation was at least partially restored and resulted in a mixture of abundant DMV and zippered ER profiles (Fig. 5E), as observed before (Fig. 2E,F). Expression of PL^{pro} by itself did not have a membrane-remodeling effect. These results clearly showed

that the nsp3-4 precursor is able to induce the membrane pairing required to form zippered ER, but that cleavage of the nsp3/nsp4 junction is essential for the formation of DMVs.

SARS-CoV nsp3 and nsp4 are also sufficient to induce DMV formation

Recently it was reported that SARS-CoV nsp3, nsp4, and nsp6 are all required for the formation of DMVs when transiently expressed as individual subunits (28). In that study, co-expression of SARS-CoV nsp3 and nsp4, but not nsp6, led to the formation of so-called maze-like bodies (MLBs), large clusters of double-membrane structures that were interpreted as closely packed double-membrane tubules. In view of our data presented above (Fig. 2E,F), this suggested that the nsp3 and nsp4 subunits of MERS-CoV and SARS-CoV differ in their ability of to induce DMV formation. These observations could reflect fundamental differences in the biogenesis of the ROs of these two betacoronaviruses or, alternatively, could result from differences in the respective experimental setups used. Such technical differences could include the transfection method (lipofection in the SARS-CoV study versus electroporation in our MERS-CoV study) and the cell type used for the EM analysis (293T cells versus HuH-7 cells, respectively). Therefore, we co-expressed nsp3 and nsp4 of either virus in 293T cells transfected using lipofection. For MERS-CoV, co-expression of nsp3 and nsp4 led to the formation of numerous circular double-membrane profiles together with some zippered ER (Fig. 6A,B), which strongly resembled what we observed in HuH-7 cells. Co-expression of SARS-CoV nsp3 and nsp4 led to the formation of MLBs very similar to those observed previously (28) with areas of zippered ER, often clustered as regularly spaced profiles, and circular double-membrane profiles (Fig. 6C,D). Angelini *et al.* (28) previously postulated that these circular profiles likely were cross sections of double-walled tubules, of which the regularly spaced zippered ER profiles would then represent longitudinal sections. The fact that the spacing between clustered zippered ER profiles roughly coincided with the diameter of the circular profiles supported this interpretation. However, the authors also admitted that ET would be required to confirm their model. To determine whether the circular profiles in the MLBs represented tubular or vesicular structures, we now used ET to analyze several MLBs, two of which are shown in Fig. 6. In one of those images, zippered ER is the dominant structure (Supplementary movies 5; Fig. 6C) whereas the other mainly contained circular double-membrane profiles (Supplementary movie 6; Fig. 6D). In both tomograms, we could detect multiple double-membrane profiles that increase and decrease in diameter when progressing through the tomogram (indicated with green dots in the tomogram movie) and ultimately disappear, indicating that they represent vesicles rather than tubules. In fact, no tubular structures were observed in the tomograms. The presumed longitudinal views of tubular structures turned out to consist of zippered-ER winding through the MLB. Our results show that, also in the case of SARS-CoV, co-expression of nsp3 and nsp4 suffices for the induction of DMV formation and strongly suggests that this is a common feature among betacoronaviruses.

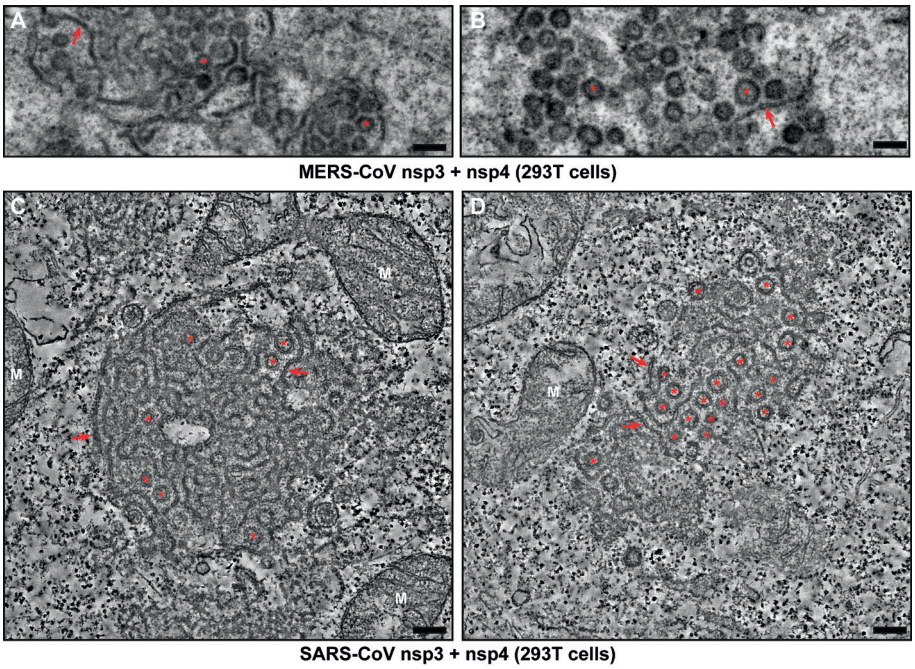


Fig. 6. SARS-CoV nsp3 and nsp4 also suffice to induce DMV formation. (A,B) *293T cells were co-transfected with plasmids encoding MERS-CoV nsp3 and nsp4 and fixed for conventional EM analysis 24 hours post-transfection. DMVs are indicated with red asterisks and red arrows point at zippered ER.* **(C,D)** *293T cells were co-transfected with plasmids encoding SARS-CoV nsp3 and nsp4 and fixed for ET analysis 24 hours post-transfection. Two virtual slices (8.5 nm) from reconstructed tomograms (available as supplementary movies S3 and S4 respectively) are shown. Red arrows indicate zippered-ER and red asterisks indicate all the DMVs that were fully reconstructed in the tomogram present in this virtual slice. All scale bars represent 250 nm.*

DISCUSSION

The generation of membranous organelles that support their replication machinery is a universal mechanism among positive-strand RNA viruses infecting eukaryotes. The formation of these ROs is induced by viral proteins (23, 25, 27), and appears to be also reliant on host factors, some of which have been identified as important players (41, 195). In this study, we sought to identify the viral proteins required to induce the formation of (beta)coronavirus DMVs, the most prominent membrane structure formed during coronavirus infection. Using ET, we found that co-expression of nsp3 and nsp4 of either SARS-CoV or MERS-CoV was required and sufficient to trigger the formation of ER-derived DMVs. Moreover, their 3D architecture was similar to what has been observed during betacoronavirus infection (21). The DMVs formed upon co-expression of nsp3 and nsp4 were closed, with no detectable opening connecting the DMV interior and the surrounding cytosol, whereas their outer membrane usually was continuous with those of other DMVs

and/or with (modified) ER. Our data importantly modify the conclusions of an earlier SARS-CoV study (28), which was based on the transient co-expression of SARS-CoV nsp3 and nsp4 from separate plasmids and the 2D imaging of the resulting membrane structures. The observation of maze-like bodies and circular double-membrane profiles, which were interpreted to probably represent tubular structures, led these authors to conclude that co-expression of SARS-CoV nsp3 and nsp4 was not sufficient for DMV formation. Using ET (Fig. 6), we could now show that the circular profiles observed in these maze-like bodies are in fact DMVs, suggesting that the basic capability of nsp3 and nsp4 to induce DMV formation probably is a common feature of betacoronaviruses. These findings also highlight the importance of 3D analysis as a tool to fully characterize the ultrastructure of membranous viral ROs.

Interestingly, in the case of the arterivirus EAV, nsp2 and nsp3 were found to be required and sufficient for DMV formation (24, 180). At least to a certain extent, these proteins can be considered the functional equivalents of coronavirus nsp3 and nsp4, respectively as they share a number of features like the presence of multiple membrane-spanning domains and a papain-like protease in the upstream protein that cleaves the junction between the two subunits. They also occupy comparable positions in the replicase polyproteins, suggesting there may also be similarities in terms of the relative order in which these subunits are synthesized, released, and targeted to the membranes they transform (16). These functional similarities and the potential to trigger DMV formation may thus be shared by these proteins of all corona- and arteriviruses, and possibly extends to other branches of the order *Nidovirales*, like the poorly studied ronivirus and mesonivirus families.

Our findings also shed more light on DMV biogenesis, for which two models have been proposed that are not mutually exclusive. The first has been termed “double budding”, where a vesicle would first bud into the ER lumen and then bud out again to acquire a second membrane. The alternative model is based on “enwrapping”: membranes would first pair or “zipper”, then curve and finally form a closed DMV after a membrane fission event (88, 180). The frequent observation of zippered ER after co-expression of nsp3 and nsp4, and multiple EM images in which zippered ER seemed to wrap into a DMV (e.g. Fig. 3B), suggest that this structure is a DMV precursor. Interestingly, whereas the uncleaved nsp3-4 precursor was able to induce the pairing of ER membranes, DMV formation only occurred upon cleavage of the nsp3/nsp4 junction, which strongly suggests that membrane pairing is an early step in DMV formation. Our findings contrast with what was observed previously for arteriviruses where cleavage of the nsp2/3 junction was not required for the formation of DMVs in an expression system (89). Together our observations favor the enwrapping model for DMV formation and, even though the existence in parallel of a double budding mechanism cannot be formally ruled out, the current data adds to the mounting evidence pointing towards double-membrane enwrapping as the central mechanism for DMV formation. For the distantly related arteriviruses (180, 196) and the unrelated picornaviruses (56, 65), putative enwrapping intermediates have been described, indicating that this might be a common mechanism of DMV-biogenesis among +RNA viruses.

Several steps are required for DMV biogenesis: pairing of membranes, membrane curvature (both positive and negative), and fission (88, 180). In the enwrapping model for DMV biogenesis membrane pairing is an early step that may be mediated directly by interactions between the viral proteins inducing DMV formation. The interaction(s) between nsp3 and nsp4 that we described here for MERS-CoV may be sufficient to facilitate membrane pairing. Similar observations have been made for SARS-CoV and MHV (28, 96). The most likely candidate regions for this kind of interactions are the luminal loops of nsp3 and nsp4 (182, 183) that are located in the TM1 and TM2 regions respectively, as these could interact with their counterparts on the opposite side of the ER cisterna, thus inducing membrane pairing. This view is partly supported by a study on MHV for which a truncated nsp3 lacking the region upstream of TM1 co-expressed with nsp4 was sufficient to induce membrane pairing but not the formation of DMVs (96). This suggests that, although the cytosolic N-terminal region of nsp3 is required for complete DMV formation, the TM1 region (together with nsp4) may be sufficient to induce membrane pairing. In addition, the liberation (by PL^{pro}-mediated cleavage of the nsp3/nsp4 junction) and presumed membrane insertion of the hydrophobic N-terminal domain of nsp4 may be an important determinant of the ultimate trans-membrane configuration of this protein, potentially with direct implications for the transformation of zippered ER into DMVs. However, we found no major differences between DMVs induced by expression of self-cleaving MERS-CoV nsp3-4 compared to co-expression of nsp3 and nsp4, suggesting that nsp4 is properly inserted in the membrane when individually expressed. The concentric zippered ER observed after expression of the uncleaved nsp3-4 polyprotein could then reflect an intermediate stage in which the lack of nsp3/nsp4 cleavage prevents proper membrane remodeling. The proximal (and largest) luminal loop of nsp4 contains a N-linked glycosylation site (N2985 in MERS-CoV), similar to the glycosylation site(s) in SARS-CoV and MHV (95, 185, 188). Analysis of the use of that site in proteolytically processed nsp4 and the uncleaved nsp3-4 precursor could provide insight in the sequence of events leading to the membrane insertion of MERS-CoV nsp4.

Although our data establish that expression of nsp3 and nsp4 suffices for coronaviral DMV formation, the precise role in this process – if any – of the nsp6 transmembrane subunit remains unclear. Our current data suggest that, compared to cells expressing MERS-CoV nsp3 and nsp4 only, co-expression of cleaved nsp6 does not affect DMV formation, nor does it lead to the formation of additional structures like CM or spherules. However, co-expression of SARS-CoV nsp3, nsp4, and nsp6 was previously shown to induce CM formation (in addition to DMVs) (28). When MERS-CoV nsp6 was retained in an unprocessed nsp4-6 precursor (Fig. 4B), DMVs were no longer formed and membrane clusters appeared that resemble cubic membranes. It has been proposed that the CM formed by coronaviruses are in fact a form of cubic membranes (197). This might be related to observations that, compared to DMVs, CM are mostly formed relatively late in infection (21, 127) when (viral) proteins or polyprotein fragments accumulate. It is conceivable that such accumulation could lead to aggregation, misfolding, and/or impaired polyprotein processing resulting in the formation of cubic membranes. In other words, there could be a link between the status of polyprotein processing in the nsp4-6 region and the membrane structures formed. This

idea is supported by observations made for an unrelated DMV-forming virus, HCV, for which it was recently shown that DMV formation became less efficient when the proteolytic cleavage of the NS4B/5A site in the viral polyprotein was accelerated (39).

The existence of different proteolytic processing intermediates containing nsp5 is well documented for arterivirus infection (84), although the role of the different precursors in DMV formation has not been studied so far. Unfortunately, the kinetics of polyprotein processing by M^{pro} in MERS-CoV and SARS-CoV are still largely unknown. M^{pro}'s enzymatic activity has mainly been assessed using recombinant nsp5 and peptide substrates *in vitro* (76, 177, 179, 194), but an analysis of the kinetics in a large(r) polyprotein setting is mostly lacking. Most information on the processing of the coronavirus nsp4-nsp10 region is derived from studies on other coronaviruses, such as MHV, IBV and HCoV-229E (the latter two being a gamma- and alphacoronavirus, respectively) (76, 198, 199). An in-depth analysis of the kinetics of polyprotein maturation during coronavirus infection, the identification of nsp6-containing processing intermediates, and the investigation of their possibly distinct roles in membrane remodeling could help to unravel the mechanisms underlying the formation of the coronavirus ROs.

Acknowledgements

Gijs Versteeg (Max F. Perutz Laboratories, Vienna, Austria), Michael Buchmeier (University of California, Irvine, USA), Ralf Bartenschlager (Heidelberg University, Heidelberg, Germany), and Ron Fouchier (Erasmus Medical Center, Rotterdam, the Netherlands) are cordially acknowledged for providing reagents. Anja de Jong (EM section, Leiden University Medical Center) is thanked for technical assistance, and LUMC colleagues Peter Bredenbeek and Alexander Gorbalenya are thanked for helpful discussions.

MATERIALS AND METHODS

Cells, viruses, and antibodies

HuH-7 cells (kindly provided by Dr. Ralf Bartenschlager; Heidelberg University) were grown in Dulbecco's modified Eagle's medium (DMEM; Lonza) supplemented with 8% (v/v) FCS (Bodinco), 2 mM L-glutamine (PAA Laboratories) and non-essential amino acids (PAA Laboratories). 293T cells (kindly provided by Virgin lab; Washington University School of Medicine in St. Louis) were cultured in DMEM with 10% (v/v) FCS. All cell culture media contained 100 U/ml penicillin and 100 µg/ml streptomycin. Infection of HuH-7 cells with MERS-CoV (EMC/2012 strain kindly provided by Ron Fouchier; Erasmus Medical Center, The Netherlands; (12, 173)) was performed as previously described (128).

Primary antibodies used were mouse α-HA (Clone HA.C5; Abcam), mouse α-β-actin (Clone AC-74; Sigma), mouse α-V5 (Clone 2F11F7; Thermo Fisher). A rabbit serum recognizing SARS-CoV-nsp3 that cross-reacts with MERS-CoV nsp3 has been previously described (106, 128). A polyclonal rabbit serum was used against a combination of two MERS-CoV nsp5 peptides; SGLVKMSHPSGDVEAC (amino acids 3248-3263 of pp1a) and CPADQLSDPNYDALLI (3291-3306) which was produced by Eurogentec.

Plasmid construction and transfection

Human codon-optimized coding sequences of MERS-CoV nsp3-6 were designed using GeneART™ and ordered from Thermo Fisher in four fragments and subsequently assembled in low-copy vector pACNR1180 (200) using conventional cloning. The precise parts of MERS-CoV pp1a used for polyprotein constructs are outlined in Table S1. The nsp4 construct included the 21 C-terminal aa of nsp3 to prevent the N-terminal hydrophobic region of nsp4 from acting as a signal sequence, which could result in improper membrane insertion. In all constructs with a C-terminal myc- or V5-tag, the C-terminal glutamine of the viral sequence was omitted to prevent the removal of the tag by M^{pro}. The SARS-CoV nsp3 gene (Frankfurt 1 strain, pp1a amino acids 819-2740) was synthesized by Bio Basic Inc. (Ontario Canada). Coding sequences were transferred to the pCAGGS expression vector (Addgene) for expression. pCAGGS-SARS-nsp4 was described previously (28). 293T cells were transfected using Lipofectamine 2000 (Thermo Fisher) according to the manufacturer's instructions. HuH-7 cells were transfected using a Nucleofector 2b device (Lonza) with Nucleofector Kit T (Lonza) in 6x106 cells and 12 µg of plasmid DNA per transfection. Co-transfections were carried out with equimolar amounts of plasmids.

Western blotting

Cells were lysed in 2x Laemmli sample buffer (50 mM Tris-HCl, pH 6.8; 20% (v/v) glycerol; 4% (w/v) sodium dodecyl sulfate (SDS); 20 mM dithiothreitol; 0.02 mg/ml bromophenol blue) and separated by electrophoresis on SDS-polyacrylamide gels. Proteins were transferred to polyvinylidene fluoride membranes (Amersham) using a Trans-Blot Turbo transfer system (Bio-Rad). Blots were blocked with 5% (w/v) ELK skimmed milk powder (Campina) in phosphate-buffered saline (PBS) supplemented with 0.05% (v/v) Tween-20. Secondary HRP-conjugated antibodies (DAKO) and ECL Plus Western blotting substrate (Thermo Fisher) were used to visualize protein signal.

Immunofluorescence microscopy

After electroporation, HuH-7 were seeded on coverslips and fixed 24 hours later with 3% (w/v) paraformaldehyde in PBS. Samples were permeabilized with 0.2% (v/v) Triton X-100 and incubated with antibodies, including fluorescent conjugates, diluted in 5% (w/v) bovine serum albumin (BSA) in PBS. Nuclei were stained with 1 µg/ml Hoechst 33258. After embedding with Prolong Gold (Thermo Fisher), samples were analyzed with a Leica TCS SP8 confocal laser scanning microscope, which was equipped with a 63x objective (NA 1.40; 1 Airy Unit) and a Leica HyD hybrid detector.

Metabolic labeling and immunoprecipitation

293T cells were metabolically labeled with 100 µCi/mL [^{35}S]methionine and [^{35}S]cysteine (EXPRE35S35S Protein Labeling Mix; Perkin-Elmer) from 4 hours post-transfection onwards. Cells were lysed at 18 hours post-transfection in 20 mM Tris-HCl (pH 7.6), 150 mM NaCl, 0.5% (w/v) deoxycholic acid, 1% (v/v) Nonidet P-40, and 0.1% (w/v) SDS. Lysates were diluted in immunoprecipitation (IP) buffer (20 mM Tris-HCl (pH 7.6), 150 mM NaCl, 5 mM EDTA, 0.1% (w/v) DOC, 0.5% (v/v) NP-40, and 0.5% (w/v) SDS) and incubated with

antibody overnight. Antibody-protein complexes were then pulled down using Protein A and Protein G sepharose beads (GE healthcare), which were first blocked with 2% (w/v) BSA in PBS, and incubated for several hours. After repeated washing of the beads with IP buffer, proteins were eluted by heating in 2x Laemmli sample buffer. After separation on large 10% polyacrylamide gels and gel drying, signal was visualized using an Imaging Screen-K (Bio-Rad) and a Typhoon 9410 scanner (GE Healthcare).

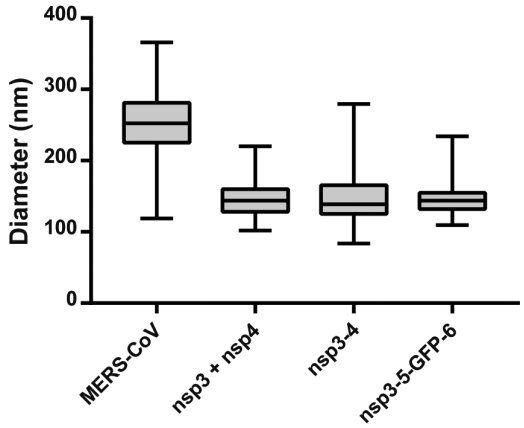
Electron microscopy

Transfected HuH-7 or 293T cells were fixed 24 hours post-transfection in 1,5% (w/v) glutaraldehyde in 0.10 M cacodylate buffer (pH 7.4) for 1 hour at room temperature. After washing in 0.14 M cacodylate buffer, samples were post-fixed and stained at 4°C with 1% (w/v) osmium tetroxide in 0.10 M cacodylate buffer for 1 hour. After washing with 0.14 M cacodylate and Milli-Q water, cells were scraped and stained with 1% (w/v) tannic acid in Milli-Q water on a 3D rotator for 1 hour at room temperature. Following washing with Milli-Q water, cells were spun down in heated 3% (w/v) agar in PBS and after solidification pellets were excised, cut into small blocks and dehydrated in increasing concentrations of ethanol. Samples were embedded in epoxy resin (LX-112; Ladd Research) and after polymerization 100-nm sections were placed on mesh-100 copper EM grids covered with a carbon-coated pioloform layer. Following post-staining with 7% (w/v) uranyl acetate and Reynolds lead citrate samples were analyzed on an FEI Tecnai 12 BioTwin equipped with an Eagle cooled slow-scan charge-coupled device (CCD) camera (FEI) and operated at 120 kV. Measurements of circular profiles from 2D-EM images were done with ImageJ software and Aperio Imagescope software (Leica). Circular profiles were measured over their longest and shortest axis and the geometric mean of those values was used as the diameter. 100 circular profiles were measured for each condition.

Electron tomography

Sections of 150 nm thickness were cut from the resin-embedded blocks of transfected HuH-7 or 293T cells prepared as described above. Prior to post-staining, colloidal gold particles of 10 nm were applied to both sides of the EM grid to serve later as fiducial markers for alignment. Tomography data was recorded on an Eagle CCD camera (FEI) in an FEI Tecnai 12 BioTwin (HuH-7 samples) or a Twin (293T samples) electron microscope operated at 120 kV, with the grids mounted on a 2040 Fischione tomography holder. Dual-axis tilt series of the regions of interest were collected using Xplore3D software (FEI) at magnifications that resulted in a pixel size of 1.7 nm (BioTwin data) or 1.4 nm (Twin data). The angular coverage for each single-axis tilt series was 130 degrees sampled in increments of 1 degree. Alignment of the tilt series and tomogram reconstruction by weighted backprojection were performed in IMOD (170).

SUPPLEMENTARY MATERIAL



Supplementary fig. 1. Structures induced by MERS-CoV nsp3 and nsp4 are smaller than those observed during MERS-CoV infection. *The size of circular profiles was determined for MERS-CoV infected cells (10 h p.i.), for nsp3-4 expressing nsp3 and nsp4, the nsp3-4 self-cleaving precursor, and the nsp3-5-GFP-6 construct. 100 profiles were measured for each condition and plotted as a box and whiskers plot. The boxes show the 25th to 75th percentile and the whiskers the total range of the measurements.*

Construct	N-terminal tag	Polyprotein Start	Polyprotein End	C-terminal tag
nsp3-4	HA	854	3246	V5
nsp3	HA	854	2739	c-myc
nsp4	-	2720	3246	V5
nsp3-6	HA	854	3844	V5
nsp3-6-GFP[1]	HA	854	3850	GFP
nsp3-5-GFP	HA	854	3558	GFP
nsp3-5-GFP-6[2]	HA	854	3560	GFP
nsp5-6	-	3242	3844	V5

Table S1. Details of MERS-CoV expression constructs. *The parts of MERS-CoV pp1a used for the different expression constructs are listed in the table. Amino acid numbers are based on pp1a of MERS-CoV EMC/2012 strain. The coding sequence was human codon optimized unless otherwise indicated. (1) Amino acids 3561 – 3850 were not codon-optimized but the MERS-CoV sequence. (2) GFP was followed by MERS-CoV pp1a amino acids 3548-3844 fused to a V5-tag at the C-terminus.*

Supplementary movies

Tomographic reconstructions of areas showing membrane structures induced by coronavirus nsps. HuH-7 cells co-transfected with constructs expressing MERS-CoV nsp3 and nsp4 (Movie S3) or transfected with a construct expressing the self-cleaving nsp3-4 precursor (Movie S4) were analyzed by ET. The movies move along the Z-axis in consecutive virtual slices of 1.67 nm thickness. Five DMVs that are fully reconstructed in the tomogram are indicated with green dots. The distinctive feature that unambiguously identifies a vesicle in a tomogram is a circular profile that is largest at the vesicle's equator and decreases in diameter when moving up or down from that plane through successive tomographic slices until, if the vesicle is fully contained in the section, it disappears. Scale bars represent 500 nm.

293T cells co-transfected with SARS-CoV nsp3 and nsp4 constructs were also analyzed by ET. Two areas are shown, one with relatively more zippered-ER (Movie S5) and the other with more DMVs (Movie S6). The movies progress first in the Z-axis along consecutive slices (1.42 nm thick) and then loops back marking with green dots all the DMVs that were fully reconstructed within the tomogram (i.e. originally fully contained in the cell section). Scale bars represent 500 nm. The movies will be available with the online version of the article that has been accepted for publication in mBio (mBio 8(6) e01658-17).

Chapter 5

Regulation of the innate immune system by ubiquitin and ubiquitin-like modifiers

Diede Oudshoorn, Gijs A. Versteeg & Marjolein Kikkert

Published in Cytokine Growth Factor Rev. 2012 Dec;23(6):273-82

ABSTRACT

Detection of invading pathogens by pattern recognition receptors (PRRs) is crucial for the activation of the innate immune response. These sensors signal through intertwining signaling cascades which result in the expression of pro-inflammatory cytokines and type I interferons. Conjugation, or binding, of ubiquitin and ubiquitin-like modifiers (UBLs) to a plethora of immune signaling molecules forms a common theme in innate immune regulation. Numerous E3 ligases and deubiquitinating enzymes (DUBs) actively modify signaling components in order to achieve a balanced activation of the innate immune system. This review will discuss how this balance is achieved and which questions remain regarding innate immune regulation by ubiquitin and UBLs.

INTRODUCTION

The innate immune response is the first line of defense against invading pathogens and is a crucial part of the immune system. It bridges the time between infection and the delayed activation of the adaptive immune response (Fig. 1A,B). Moreover, cells of the innate immune response, such as monocytes, dendritic cells and NK-cells assist in the proper activation of the adaptive immune response. In order to activate the immune system, recognition of pathogens is required, followed by the secretion of cytokines that induce an antiviral state in the area and recruit innate immune cells. Some of the most critical cytokines that control viral infections are type I and type III interferons, both of which signal through different receptors, yet activate the same downstream signaling partners. Type I interferon can be produced by most cell types, whereas type III interferon production is predominantly restricted to epithelial cells in the intestine (201). The importance of interferons is underpinned by the numerous studies demonstrating that animals lacking the receptors for these cytokines are hyper-susceptible to infection with numerous different microbes and succumb to infection before mounting an effective adaptive response (202).

Activation of the innate immune response relies on the detection of incoming pathogens by cellular sensors such as Toll-like- and RIG-I-like receptors (TLRs and RLRs respectively). These sensors, through various signaling cascades, activate the pro-inflammatory

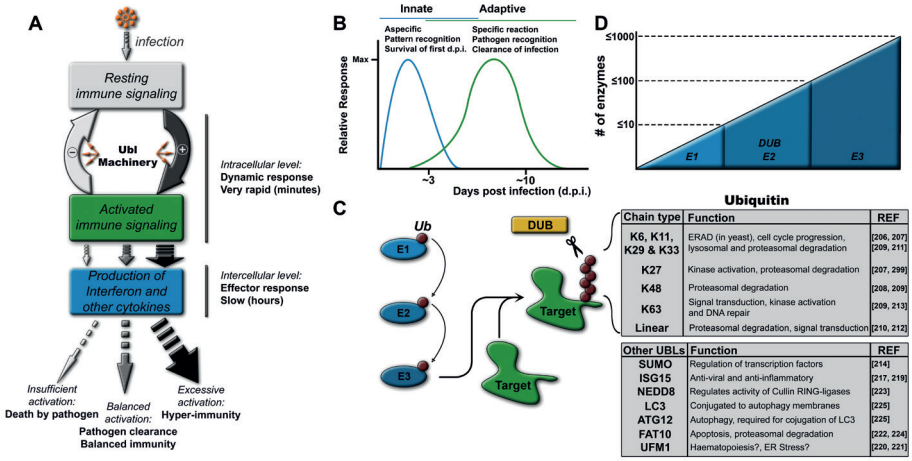


Fig. 1. Overview of innate immunity and ubiquitination. (A) *Infection triggers the activation of the innate immune signaling. Insufficient activation leads to uncontrolled infection, but hyper-immunity is detrimental to the host. A balanced activation of the innate immune signaling, at least partly regulated by UBLs, is required for pathogen clearance and host survival.* **(B)** *The innate immune response is a swift response, which is required for control of the initial infection and activation of the adaptive immune response.* **(C,D)** *Conjugation of UBLs involves sequential activity of three classes of enzymes, E1-activating enzymes, E2-conjugases and E3-ligases. DUBs remove conjugated UBLs from substrates. The functions of different ubiquitin chain linkages are listed with corresponding references, as well as the general functions of the other UBLs.*

transcription factors AP-1, NF-κB and/or one or more members of the interferon-regulatory factor (IRF) family. This ultimately results in the release of pro-inflammatory cytokines and interferons (IFNs). These signaling cascades are divergent and intertwine at several steps. Regulation of innate immune signaling relies on post-translational modifications such as conjugation of ubiquitin and UBLs. This topic has recently been reviewed in (203-205), however the focus of this review will be on how innate immune signaling is more a dynamic response instead of a sequential signaling pathway and that signaling through the innate immune pathways requires an equilibrium of ubiquitin and UBL conjugation and deconjugation.

THE UBIQUITIN SYSTEM

Ubiquitin is a small 8-kDa protein of 76 amino acids, which is conjugated by covalent attachment of its C-terminal glycine residue to lysine side chains or the N-terminus of substrate proteins. Differently linked ubiquitin chains can be formed, free or on protein substrates, by ubiquitination of one of the internal lysines in ubiquitin itself (K6, K11, K27, K29, K33, K48, or K63) or on the N-terminal methionine of ubiquitin (M1).

The significance of each of the different ubiquitin chain topologies is not yet fully understood, although several common themes have been established so far (206, 207). For example, substrates modified with a chain of at least four K48-linked ubiquitin units are selectively degraded by the 26S proteasome, which is an integral part of protein turnover and cellular homeostasis (208, 209). Although most chain types have since been implicated in proteasomal and/or lysosomal degradation to some extent, K48 linkages are believed to be the predominant proteasomal degradation signal in the cell (210, 211). In contrast, K63- and linear chains are often implicated in the regulation of signaling pathways and in the activation of signaling kinases (Fig. 1C) (212, 213).

Ubiquitin-like modifiers

Since the discovery of ubiquitin, more ubiquitin-like modifiers have been identified, among which are ISG15 and SUMO (209, 214, 215), each showing limited sequence homology with ubiquitin, yet sharing conserved structural features, such as the ubiquitin fold and one or two C-terminal glycines for conjugation (Fig. 1C) (216). SUMOylation requires a consensus sequence in substrates (ψKXE), where ψ is a hydrophobic residue and X is any amino acid. SUMOylation of transcription factors generally results in transcriptional repression, but it can also affect nuclear import and export of proteins (214). ISG15 is a potent antiviral molecule, which is produced after interferon signaling (217). It is conjugated co-translationally to newly synthesized proteins to inhibit viral replication, however it also likely has anti-inflammatory effects (218, 219). General functions of all UBLs are listed in fig. 1C (220-225).

Conjugation

Conjugation of ubiquitin and UBLs is a multi-step process involving a cascade of E1-activating, E2-conjugating and E3 ligase enzymes (209, 226, 227). There is an astounding degree of diversity in ubiquitination enzymes, and mammalian genomes have been estimated to contain ≤10 E1 enzymes, ≤100 E2 enzymes and ≤ 1000 different E3 ligases (Fig. 1D) (228).

Not only conjugation of ubiquitin and UBLs regulates innate immune responses, deconjugation is also a critical component of the system. Approximately 100 ubiquitin and UBL deconjugating enzymes (DUBs) have been identified in the human genome (229). DUBs are required for generating the mature forms of ubiquitin and UBLs by cleavage of precursor proteins, thereby exposing the C-terminal glycine residue required for conjugation. Additionally, DUBs function in the reversion of regulatory ubiquitin and UBL conjugation (Fig. 1C). They are often specific for a certain UBL, the ubiquitin chain topology and the substrate (229). DUBs are therefore an integral part of the regulation of the signaling cascades in which ubiquitin conjugation plays a role, which includes several innate immune response pathways. Several classes of DUBs have been recognized (230), and in the case of innate immune regulation, the ovarian tumor domain-containing (OTU) DUBs seem to play a major role. Among them are DUBA, OTUB1, OTUB2 and A20 (231-233). Another DUB that is critical in the regulation of the innate immune response is CYLD, which belongs to the USP DUB class (234). Since so many enzymes are involved in the conjugation and deconjugation, post-translational modification by ubiquitin and UBLs allows for precise and dynamic adjustment of signaling pathways and their ultimate effect in the (infected) organism.

PRR SIGNALING PATHWAYS

Recognition of incoming pathogens by PRRs is essential for the innate immune response (235). The best-studied PRRs include TLRs at the plasma membrane and endosomes, as well as Nod-Like Receptors (NLRs), RLRs and DNA sensors in the cytosol (Fig. 2). Upon recognition of pathogen associated molecular patterns (PAMPs) by specific PRRs, one or more of several signaling cascades are initiated. PAMPs, such as LPS, 5'triphosphate ssRNA and dsRNA are microbe-specific, and can thus be distinguished from cellular 'self' components by PRRs.

NLRs are cytosolic leucine rich repeat (LRR) proteins which mainly recognize bacterial antigens and signal either to activate the AP-1 and NF-κB transcription factors or to activate Caspase-1 and the inflammasome (236). TLRs are transmembrane PRRs that recognize PAMPs from viruses, bacteria and/or fungi and are expressed mainly by cells of hematopoietic origin (237). Upon ligand binding, all TLRs signal through the adaptor proteins MyD88 and/or TRIF to activate NF-κB, AP-1 and, in the case of endosomal TLRs, also IRF3/7 (238, 239).

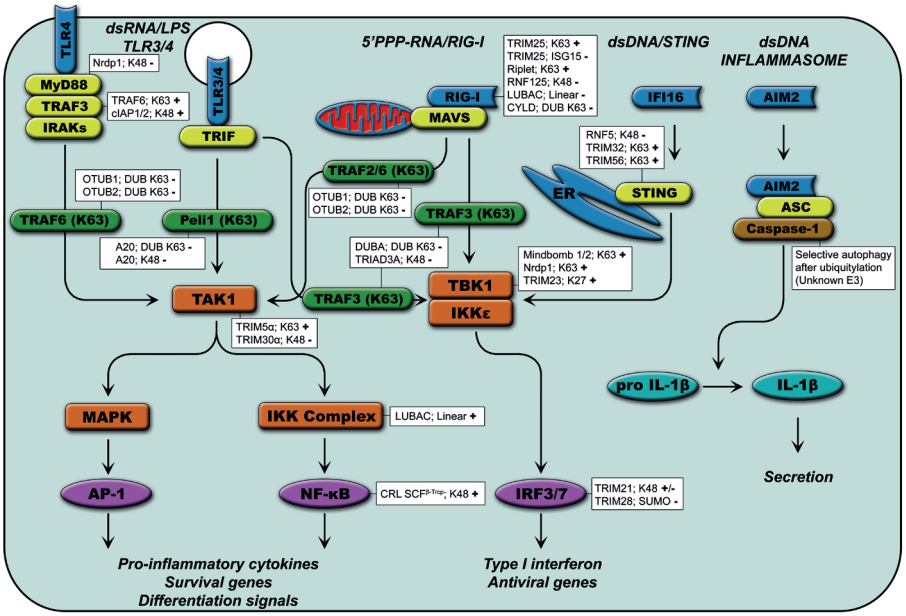


Fig. 2. PRR signaling pathways and their regulation by ubiquitin. *PRR signaling pathways are heavily regulated by UBLs. Basic components of the pathways are shown here, more detailed sub-pathways are depicted in Fig. 3. PRRs are shown in blue, adaptor proteins in yellow, the most important E3 ligases in green, kinases in orange and transcription factors in purple. Other E3 ligases and DUBs that influence PRR signaling are listed along with their chain specificity or UBL and effect (+/-) on the outcome of the signaling cascade.*

RLRs are ubiquitously expressed cytosolic RNA helicases that recognize viral RNA and signal through the mitochondrial adaptor MAVS (240, 241). Members of the RLR family include RIG-I, which recognizes 5'triphosphate RNA and dsRNA (242), and MDA5, which can be activated by (viral) ssRNA cleaved by RNase L (243), as well as (synthetic) dsRNA (244).

DNA sensors, such as IFI16 and AIM2 recognize dsDNA in the cytosol (245, 246). IFI16 signals through the ER signaling adaptor STING to activate IRFs as well as NF-κB (247). AIM2 activation does not result in the activation of transcription factors, but instead activates the inflammasome to produce mature IL-1β.

The next step in most of the TLR and RLR pathways that follow the activation of PRRs and their adaptors is the recruitment and activation of the TAK1 kinase complex. This complex acts as a Mitogen Activated Protein Kinase Kinase Kinase (MAPKKK) to activate the AP-1 transcription factor. It also activates the classical IKK complex, which subsequently phosphorylates the inhibitor of the NF-κB transcription factor (IκBα), ultimately resulting in its degradation and release of active NF-κB (238, 248).

In addition to the activation of the TAK1 complex, both the intracellular TLR and RLR signaling pathways also activate the IKK-related kinases TBK1 and IKKε. These kinases subsequently phosphorylate members of the IRF transcription factor family, which mediate

type I interferon production (249, 250). Interferon signals neighboring cells through the Interferon α/β Receptor (IFNAR) to induce expression of interferon stimulated genes (ISGs), many of which have potent antiviral activity (251).

Innate immunity in diseases

Although the ability to effectively mount an immune response during infection is critical for survival, prolonged or excessive -activation of the innate immune system can have detrimental effects. For example, highly pathogenic influenza virus strains, such as the 1918 H1N1 'Spanish flu' virus and several highly pathogenic H5N1 viruses, are potent activators of pro-inflammatory genes. The resulting 'cytokine storm' during infection is thought to contribute to the high mortality associated with these viruses (252). In addition, regulation of the innate immune system is important to prevent the development of auto-immunity. Several immune disorders, such as Systemic Lupus Erythematosus (SLE), Crohn's Disease, Blau syndrome, type I diabetes, multiple sclerosis and rheumatoid arthritis, have been linked to dysregulation of the innate immune system (253, 254). Only for a few of these diseases some aspects of the underlying immune dysregulation have been identified. For example, a link between mutations in the cytosolic NOD2 sensor and susceptibility for developing Crohn's disease and Blau syndrome has been found (253, 255). Also, increased levels of IFN-α have been detected in SLE patients, which correlated with severity of the disease (256). Onset of type I diabetes could be delayed in non-obese diabetic (NOD) mice, which spontaneously develop type I diabetes, by blocking the IFNAR, suggesting that IFN signaling plays a role in determining type I diabetes onset and progression (257). In these mice, plasmacytoid dendritic cells in the pancreatic draining lymph nodes produced higher levels of IFN-α compared to control mice, which led to activation of CD4 T Cells and subsequent development of disease (257). Determining what activates the type I interferon system and why it has adverse effects involved in these diseases will help in the development of new, more specific treatments with less side-effects than current immunosuppressive drugs used to treat some of these diseases.

To facilitate mounting of an effective immune response during infection, but also subsequent restoration to a resting state once the infection is cleared, the type I IFN system should be dynamically regulated. This dynamic nature ensures a balance between the extremes of insufficient activation, (resulting in death or persistent infection by the pathogen) on the one hand, and over-activation, resulting in hyper-inflammation and tissue damage on the other hand (Fig. 1A).

Cross-talk between different cells and cell types is one of the main ways to balance pro- and anti-inflammatory signals at the inter-cellular level. The response time resulting from the time it takes to produce and secrete the cytokines is in the range of minutes to hours. However, at the intra-cellular level, post-translational modifications of signaling components ensure even more rapid response times in the range of seconds to minutes. The sum of these signals ultimately determines the cytokine repertoire and functional fate of each particular cell during the immune response.

Phosphorylation and dephosphorylation form a main regulatory mechanism by which innate immune signaling cascades are controlled. In addition, many studies in recent years have established a very significant role for post-translational, covalent modification ubiquitin and UBL modifiers in the regulation of innate immunity.

Regulation of RIG-I by ubiquitin-mediated signals

Activation of the cytosolic sensor RIG-I by microbial RNA ultimately results in synthesis of the type I IFN and NF-κB-regulated pro-inflammatory pathways. RIG-I is comprised of two CARD domains at its N-terminus, which are responsible for downstream signaling to the critical mitochondrial adaptor molecule MAVS. Downstream of the CARD domains resides an RNA helicase domain for unwinding of the RNA, followed by a C-terminal regulatory domain (Fig. 3A).

Four different E3 ligases have been described to bind RIG-I and regulate its activation: Riplet, TRIM25, RNF125 and LUBAC. Riplet and TRIM25 promote RIG-I signaling, whereas RNF125 and LUBAC negatively affect RIG-I function. The regulatory domain can recognize the 5′-triphosphate on viral RNA, after which this domain is ubiquitinated by Riplet with a K63 chain (Fig. 2, 3A) (241, 258). This leads to a conformational change in the RIG-I molecule followed by exposure of the N-terminal CARD domains. TRIM25 subsequently binds to the first CARD domain via its SPRY domain and is required for downstream signaling (259). Direct K63 ubiquitin linkage by TRIM25 onto K172, located in the second CARD domain of RIG-I has been reported to be required for RIG-I activation (260).

However, a recent study using a completely *in vitro* reconstituted IFN induction pathway, demonstrated that K172 is a critical structural residue, required for the CARD domains to function as a ubiquitin-binding domain (UBD). Specific binding of the CARDs to short unanchored K63 chains was reported to be critical for RIG-I multimerization into a functional hetero-tetrameric complex of four RIG-I molecules and four unanchored K63 chains (Fig.3A) (261, 262). Consistently, when cell lysates were treated with the DUB Isopeptidase T, which only cleaves free ubiquitin chains by recognizing the free C-terminus, the ability to activate RIG-I signaling *in vitro* was completely lost (261, 263).

Thus, K172 of RIG-I was found to be structurally important for multimerization of RIG-I molecules with free ubiquitin-chains *in vitro*, while the significance of covalent ubiquitination of K172 for downstream signaling was determined in tissue culture systems. One possibility to explain this apparent discrepancy could be that ubiquitin chains covalently attached to K172 facilitate the binding or synthesis of unanchored ubiquitin chains, and therefore both observations may not be necessarily mutually exclusive to describe the mechanism of RIG-I regulation by ubiquitin. Mutation of K172 decreased RIG-I ubiquitination (260), which is seemingly more consistent with a model of covalent ubiquitin conjugation to this lysine in RIG-I. Apart from the suggested role of TRIM25 in the ubiquitin conjugation to K172 (260) however, also Riplet was reported to conjugate K63-chains to K154, K164 and K172 in the CARD domains of RIG-I, which was required for downstream signaling (264), and which could therefore also explain the loss of ubiquitination after K172 mutation.

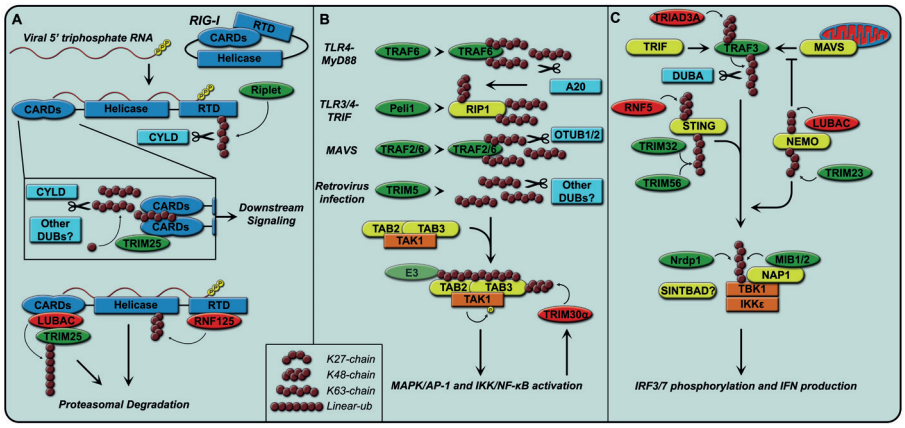


Fig.3. Ubiquitin-mediated regulation of RIG-I, TAK1 and TBK1/IKKε. (A) *Viral 5′-triphosphate RNA is recognized by RIG-I, which leads to a conformational change and then multimerization for downstream signaling (top part). Activation of RIG-I signaling is regulated by several distinct ubiquitination mechanisms.* **(B)** *The TAK1 complex can be activated by K63 chains (bound or free) from a variety of inputs as listed. Once the TAB2 and TAB3 subunits bind K63 chains, TAK1 auto-phosphorylates and initiates downstream signaling.* **(A-C)** *Activating E3 ligases are shown in green, deactivating in red and DUBs in light blue. For more detailed descriptions the reader is referred to the main text.*

The exact role of Riplet-mediated modification of the CARD domains remains uncertain, because it was not required for the *in vitro* RIG-I activation (261). One possibility is that, due to the nature of *in vitro* experiments, not all factors are present and Riplet-mediated conjugation might serve to alleviate inhibition by (non ubiquitin-mediated) negative regulators such as NLRX1 and gC1qR (265, 266). Moreover, knockout mouse models have shown that both TRIM25 and Riplet are both pivotal in the innate immune defense against RNA viruses and loss of either of these E3 ligases abolishes IFN production after viral infection (260, 267).

MDA5 functions similarly to RIG-I, although it does not have a C-terminal regulatory domain. After substrate recognition it also binds to short unanchored K-63 chains to assemble a hetero-tetrameric complex and initiate downstream signaling (262).

Negative regulation of ubiquitin-mediated RLR signaling is accomplished by RNF125, LUBAC, as well as the DUB CYLD. The first two molecules function as E3 ligases, whereas the latter specifically cleaves K63 linked ubiquitin chains from RIG-I and is also able to disassemble free ubiquitin chains (Fig. 3A) (213, 234).

RNF125 expression is induced by RIG-I signaling after which it modifies RIG-I and MDA5 with K48 linked ubiquitin chains, targeting them for proteasomal degradation (268). LUBAC inhibits RIG-I function by two distinct mechanisms. The HOIL-1 subunit of this E3 ligase complex binds to the CARD domains to limit activation, and the HOIP subunit binds to and modifies TRIM25 with a linear ubiquitin chain, which results in proteasomal degradation of TRIM25 (Fig. 3A) (269).

Another proposed mechanism for negative TRIM25 regulation is mediated by auto-ISGylation of TRIM25 with the ubiquitin like modifier ISG15, potentially though competition with ubiquitin (270). Taken together, it seems clear RIG-I signaling is regulated by multiple ubiquitin-dependent mechanisms, however how exactly these are related and temporally and spatially determine the activity of RIG-I *in vivo* remains to be elucidated.

TAK1 signal transduction

The TAK1 complex is an essential signaling complex in many innate immune pathways and is activated by RIG-I/MAVS and TLRs. It consists of the TAB2 and TAB3 accessory proteins and the TAK1 kinase. The TAK1 complex acts upstream of NF-κB and AP-1 (Fig. 2, 3B) (271, 272). It is not only involved in PRR signaling, but is a component in many pathways, such as TNFα, T-Cell Receptor, and IL-1 signaling. The TAK1 kinase subunit can be activated by auto-phosphorylation, which requires binding of TAB2 and TAB3 to K63-linked ubiquitin chains (Fig. 3B) (213). Interestingly, free K63 chains are sufficient for activation of TAK1 *in vitro*, however, K63 chains conjugated to a substrate are also potent activators of the TAK1 complex (213).

Depending on the signaling pathway involved, the K63 chains can originate from different sources (Fig. 2, 3B). For example in the case of MyD88-mediated TLR4 signaling, the E3-ligase TRAF6 synthesizes the K63 chains either free or on itself. In the case of TRIF-mediated TLR signaling the E3-ligase Peli1 attaches K63 chains to RIP1. Additionally, there is evidence that TRAF2 and/or TRAF6 mediate MAVS signaling to the TAK1 complex through K63-linked Ub chains (273-279).

TRIM5 is a potent cytosolic restriction factor for HIV. It restricts HIV by binding the HIV capsid, thereby interfering with uncoating of the viral genome and subsequent reverse transcription. Recent work suggests that TRIM5 may act as a PRR for the retrovirus capsid lattice, which in turn results in NF-κB and AP-1 activation. The authors demonstrated that upon HIV-1 infection, TRIM5 promoted unanchored K63 chain formation in cooperation with the Uev1A-Ubc13 E2 enzyme complex *in vitro* (280). Subsequently, these synthesized Ub chains bound and activated TAK1 (Fig. 3B).

Even though the TAK1 complex activates two distinct signaling cascades, mediated by either MAPK/AP-1 complex or IKK complex/NF-κB, their activation is spatially and temporally separated (Fig. 2) (248). In the case of MyD88-mediated TLR4 signaling, activation of the IKK complex by TAK1 occurs at the plasma membrane whereas MAPK signaling is initiated later on in the cytosol after the TAK1 complex has been released from the membrane-bound signaling complex. TRAF6 is anchored to the TLR signaling complex at the plasma membrane by IRAK proteins and by TRAF3, which in that case has a role as a scaffolding protein distinct from its E3 ligase functions (Fig. 2) (281). TRAF3, and possibly the IRAK proteins as well, are then modified with a K48 chain. This targets them for degradation by the E3-ligases cIAP1 and cIAP2, which are themselves activated by TRAF6-mediated attachment of a K63 chain (Fig. 2).

The many signals that activate the TAK1 complex can also be terminated in several different ways. The signals transduced by TRAF6 and RIP1 can be discontinued by the OTU

DUB A20, which is induced by TAK1 signaling and specifically de-conjugates K63 chains (Fig. 3B) (233). A20 also possesses E3-ligase activity, which specifically modifies RIP1 with a K48 chain targeting it for proteasomal degradation, providing an interesting dual function of both E3-ligase and DUB to serve two complementary roles in negatively regulating TAK1 activation (282). Furthermore, the DUBs OTUB1 and OTUB2 also negatively regulate TAK1 signaling by removing K63 chains from TRAF6 after viral infection (Fig. 2, 3B) (231). After TAK1-mediated IKK and NF-κB activation, expression of TRIM30α is induced. This causes TAB2 to be degraded in a ubiquitin-dependent manner and TAK1 signaling to be terminated (Fig. 3B) (283).

Since free K63 chains have been found to regulate at least two distinct signaling components, one possible issue could be the signal specificity. Since free chains do not "encode" any other signal than the linkage specificity, the question arises: what makes chains from TRIM25 activate RIG-I and chains from TRIM5a activate the TAK1 complex? One possibility is that these free chains are very volatile signals that can rapidly activate a signaling complex and are subsequently degraded by the DUBs present in the cytosol. Since *in vitro* most DUBs can efficiently break down purified free ubiquitin chains (depending on chain topology in some cases) it is likely that free K63 chains are degraded rapidly after synthesis and present a very dynamic mechanism for signaling complex activation (284). Since DUBs have been reported as integral components of large ubiquitination complexes, it is also not unconceivable that ubiquitin chains function within the complexes they were synthesized in and do not 'float' around free in the cytosol where they could engage unintended targets. Along those lines, one would predict that the number and activity of the conjugating and de-conjugating enzymes within those complexes establish an equilibrium between continuous synthesis and degradation of ubiquitin chains. Such an equilibrium could be very transiently and rapidly shifted 'left' or 'right' by modifying the number and the activity of the different enzymes in the protein complex or disengaging the intended target of the ubiquitin chains.

The classical IKK complex

The final signaling component before the activation of NF-κB is the IKK complex, which is activated by TAK1 (Fig. 2). The ubiquitin-binding protein NEMO is part of the classical IKK complex together with IKKα and IKKβ. The latter is required for phosphorylation of IκBα, its K48 ubiquitination by the CRL (Cullin RING Ligase) complex $SCF^{\beta\text{-}Trcp}$I, and its subsequent degradation and release of active NF-κB (285). NEMO possesses an UBAN (Ubiquitin Binding in ABIN and NEMO) domain that preferentially binds to linear polyubiquitin chains, but can also interact with K63 and K48 chains (286, 287). Furthermore, NEMO itself can also be modified by LUBAC with a linear ubiquitin chain during TNFα signaling, which is required for NF-κB activation (212).

Recruitment of the IKK complex to the TLR or TNFR signaling complexes is thought to occur by interaction of NEMO with K63 ubiquitin chains (287). Since IKK is activated by phosphorylation of the IKKα/β subunits and TAK1 is capable of phosphorylating those subunits *in vitro* (a catalytic mutant was unable to do so), a model was proposed in which

TAK1 phosphorylates IKKβ (271). In contrast, activation and auto-phosphorylation of the IKK complex by binding of free ubiquitin chains to NEMO has been proposed based on *in vitro* studies (213). Contrary to the requirement of K63 chains for TAK1 activation, the activation of IKK was independent of K48 or K63 linked ubiquitin. Moreover, the E2-enzyme involved was identified as UbcH5 (instead of Uev1A-Ubc13), which forms chains of various linkages. This suggested that distinct ubiquitin chain types could be involved. Moreover, due to the ability of NEMO to both bind and be modified by linear ubiquitin chains, it is possible that chains bound to one NEMO subunit are recognized by another and then oligomerize due to this interaction. This could then lead to auto-phosphorylation of the bound IKKα/β subunits similarly to how TAK1 can activate itself *in vitro* (213). In conclusion, the function of the linear ubiquitin chains in the classical IKK complex activation has not been fully clarified yet.

Most studies involving NEMO and the IKK complex have been carried out in the "canonical" NF-κB signaling pathway downstream of the TNF receptor. One caveat to this approach is that it obscures the role of NEMO and the IKK complex in other parts of the signaling cascades controlling innate immunity. Most knowledge about the activation of the IKK complex is inferred from the canonical pathway, yet the exact functions of NEMO in each different pathway remain unclear. It is not unlikely that as a results of multiple signaling cascades culminating in the activation of the IKK complex (TNFα, TLR signaling, CD40, IL-1 etc.), each pathway differs slightly in its method for activating the IKK complex. Due to the promiscuity of the interaction of NEMO with different ubiquitin chain linkages, as well as the various modifications of the protein itself, different ubiquitin signals could provide an interesting angle for differential and dynamic IKK complex activation.

TBK1/IKKε dependent IRF activation

MAVS and TRIF are two key signaling molecules critical for the activation of IRFs and thus IFN-mediated antiviral immunity (Fig. 3C). TRAF3 is recruited to all MAVS- and TRIF-based signaling complexes to mediate the activation of the IKK-related kinases IKKε and TBK1. TRAF3 self-activates by covalent auto-polyubiquitination with K63 linked ubiquitin chains (281, 288). TRAF3 activation can in turn be negated by DUBA, a DUB specifically binding TRAF3 and deconjugating its K63 chains (232). Furthermore, the E3-ligase TRIAD3A can modify TRAF3 with a K48 chain to target it for degradation as another means of down-regulating MAVS-mediated signaling (Fig. 3C) (289).

Signaling through the ER adaptor STING also results in activation of TBK1. STING, which requires modification with K63 chains by the E3 ligases TRIM56 and TRIM32 for signaling (290, 291), is able to signal through TBK1 and IKKε to activate IRFs. After activation, STING is targeted for degradation by K48 chain modifications by the E3 ligase RNF5 (292).

The following steps in the pathways downstream of MAVS and STING are not entirely clear, but at least require the E2 enzyme Ubc5 and K63 polyubiquitin (293). The IRF family members require phosphorylation by the IKK related kinases TBK1 and IKKε (249). TBK1 and IKKε were discovered to function as kinases of IRFs with some redundancy. However, functions specific for either TBK1 or IKKε have been discovered since (249, 294). For example, results from IKKε knock-out mice have suggested a predominant role in the

activation of STAT1 following IFNAR signaling (294). While TBK1 has been linked to selective autophagy of intracellular pathogens such as Salmonella (295). How the functions of IKKε and TBK1 relate to each other and how their respective functions fit together remains to be elucidated. For downstream signaling, TBK1 also requires K63-ubiquitination by mind bomb proteins after dsRNA signaling and by Nrdp1 after LPS signaling (296, 297); yet the major activator for IKKε is still unknown (Fig. 3C). How these kinases are activated is also likely dependent on their assembly into a complex (297).

Several NEMO-like adaptor/scaffold proteins have been identified (TANK, NAP1 and SINTBAD) all of which can constitutively bind TBK1 and IKKε (298). These adaptor proteins contain UBDs similar to NEMO and therefore regulation by ubiquitin chains is a feasible possibility. It is worth mentioning that their ability to directly interact with the kinases, distinguishes them from NEMO, which itself does not interact with TBK1 and IKKε. It is TANK that mediates interaction of NEMO with the IKK-related kinases. Moreover, TRIM23-mediated K27-linked ubiquitination of NEMO is important in IRF activation, although the precise molecular mechanism behind this remains to be determined (Fig. 3C) (299, 300).

Recently, linearly ubiquitinated NEMO was reported to inhibit MAVS signaling by interfering with the interactions between MAVS and TRAF3/6 (Fig. 3C) (301). LUBAC was critical for the NEMO-MAVS interaction and subsequent interference with TRAF3/6 binding. Taken together, LUBAC has so far been found to positively regulate NF-κB signaling (Fig. 2), but negatively regulate antiviral signaling (Fig. 3A,C). These findings indicate that LUBAC is involved in directing the innate immune response to a more pro-inflammatory instead of antiviral response. An E3 Ligase that has the opposite effect is Nrdp1, which activates TBK1, but targets TLRs for degradation by K48-linked ubiquitination (296). This shifts the balance of the innate immune system more to an interferon instead of a pro-inflammatory response.

The IKK-related kinases and the classical IKK complex also influence each other. For example, TANK inhibits the classical IKK complex and subsequent NF-κB activation by the IKK-related kinases via its interaction with NEMO (302). Interestingly, K63 chains formed by TRAF3 activate the IKK-related kinases, whereas TRAF2 and/or TRAF6 also form K63 chains but activate the TAK1 complex. These E3-ligases all interact with MAVS, yet how specificity is achieved by their synthesized K63 chains in TAK1 or IKK-related kinase activation remains to be determined. The exact mechanisms regulating TBK1 and IKKε activation and the interactions with their adaptor proteins will likely be the subject of extensive studies in the near future.

IRF3 and IRF7 regulation by ubiquitin and SUMO

The IKK-related kinases phosphorylate two members of the IRF transcription factor family: IRF3 and IRF7, which are required for the production of type I interferons (Fig. 2) (249). IRF3 is ubiquitously expressed in most cell types whereas IRF7 is an ISG and is only expressed by leukocytes in the absence of infection (250). Phosphorylated IRF3 and IRF7 can form homo- or heterodimers, each of which has different promoter specificity. IRF3 homodimers are created when there is a low supply of IRF7 (so in the absence of ISG expression) and initiate

production of chemokines such as CXCL10 to attract innate immune cells. Conversely, IRF3/IRF7 dimers potently activate type I interferon production, but this can only occur in innate immune cells or cells already stimulated with type I interferon (250). IRF7 dimers regulate the expression of a subset of ISGs as well as type I IFN by binding to specific ISREs to ensure proper induction of the antiviral state in the absence of IFNAR signaling (303).

TRIM21 has been found to regulate both IRF3 and IRF7. Binding of TRIM21 to IRF3 stabilized IRF3, whereas it targets IRF7 for proteasomal degradation by K48 ubiquitination (304, 305). Studies using TRIM21 knockout mice found that loss of TRIM21 increases NF-κB dependent cytokine expression in embryonic fibroblasts, yet no effects were observed *in vivo* (306). The net result of TRIM21 activity is therefore still uncertain, and variations in cell types used or different isoforms of TRIM21 might explain its different functions. However, there are only very few examples of transcription factors being regulated by ubiquitination like this. Another far more common mechanism affecting transcription factors, including the ones involved in innate immune signaling, is SUMOylation.

Attenuation of transcription factors is very important for regulation of the innate immune system in order to prevent harmful auto- and hyper immunity. Both IRF3 and IRF7 contain SUMO consensus sequences, which have been shown to be SUMOylated during viral infection, thereby providing a mechanism for post-activation attenuation by transcriptional repression (307). TRIM28 was identified as the E3-ligase for IRF7 SUMOylation, yet a SUMO E3 ligase for IRF3 has hitherto not been identified (308). Protein inhibitor of activated STATγ (PIASγ) was also found to inhibit the transcriptional activity of both NF-κB as well as transcription factors binding the ISRE (IRF7 and ISGF3) (309). Members of the PIAS protein family are SUMO E3-ligases and are involved in the regulation of a variety of innate immunity transcription factors (310). The PIAS proteins were identified as inhibitors of STAT proteins, possibly by prohibiting interaction of STAT with DNA or other co-factors through protein-protein interactions. However, the biological relevance of the SUMO E3-ligase function of the PIAS proteins remains unclear. Since the exact mechanism by which SUMO functions as a transcriptional repressor is not yet fully understood, more factors affecting SUMO-dependent regulation of IRF3 and IRF7 are likely to exist.

PATHOGEN EVASION STRATEGIES TARGETING UBIQUITIN AND UBL REGULATION

In order for pathogens to establish a productive infection and to facilitate productive replication, evasion of innate immune responses is pivotal. Different pathogens employ different strategies and many affect the innate immune response by tampering with the ubiquitin machinery regulating this system. For example, several unrelated virus families encode DUBs to modulate innate immune signaling, among which are arteriviruses, coronaviruses, nairoviruses, picornaviruses, adenoviruses and herpesviruses (311-315).

Some of the DUBs identified in these viruses resemble members of the OTU family of ubiquitin deconjugating enzymes. They are often capable of deconjugating different

ubiquitin chain linkages as well as ISG15, whereas mammalian OTU domain-containing DUBs are ubiquitin chain specific (313). Ectopic expression of these viral DUBs increases global ubiquitin and ISG15 deconjugation, however, it remains to be determined how the promiscuous activity of these enzymes is regulated during infection. Viral proteases of arteriviruses are able to inhibit RIG-I activation by deconjugating the K63 chains required for RIG-I activation (316), and more targets within the innate immune response cascades are likely to exist. Other examples of viral proteins interfering with the function of E3-ligases exist, such as Influenza A Virus NS1, which specifically binds TRIM25 thereby inhibiting RIG-I activation (317). Some large DNA viruses, such as herpes- and poxviruses even encode their own E3 ligases. Herpesviral E3s target the cellular E3 ligases RNF8 and RNF168 for degradation, which has been proposed to facilitate reactivation from latency (318, 319). Given that viral enzymes are often hard to recognize purely based on their sequence, more viral E3 ligases and DUBs likely still remain undiscovered.

CLOSING COMMENTS

In the case of a severe infection, survival can hinge on the balanced activation of the innate immune response. In order to achieve that balance, numerous E3-ligases and DUBs actively regulate the outcome of the innate immune response. The basic components and signals of the signaling pathways are well characterized, but how the different components interact is less clearly understood. Often signaling molecules are assembled into large complexes. However, the stoichiometry and localization of the different molecules in these complexes in time have remained relatively poorly studied thus far. The sophistication in complex composition is one of the current obstacles that the scientific community will need to overcome in both *in vitro* and cell based systems.

Because the post-translational modifications of signaling components are transient signals in most cases, monitoring changes in those signals during infection and/or auto-immunity over time will likely yield crucial information in understanding the dynamics of this system. To study these events, advances in mass spectrometry, such as multiplex MS and analysis of ubiquitination levels and substrates in complex samples from relevant tissue culture or experimental animal models, will be very important (320, 321). These tools could be used to discern whether patients with autoimmune diseases that are related to type I interferons have a different state of activation of the signaling pathways involved in innate immunity.

Most knowledge on the functions of free ubiquitin chains in the regulation of RIG-I and TAK1 has been deducted from *in vitro* reconstituted systems (213, 261). These experiments allowed for precise control of the individual components in the signaling pathways and have been instrumental in unraveling the minimal signals for the pathways to function. Future work should focus to validate the findings of the *in vitro* systems in the relevant primary cell types and/or disease models. Discrepancies between *in vitro* experiments and experiments in cell culture, such as the mechanism of K172-mediated RIG-I activation, underline the

importance of exploiting the strengths of individual model systems and validating findings in others (260, 261).

A vast array of enzymes is involved in ubiquitin (de)conjugation of proteins. It seems logical that the interpretation of a ubiquitin signal by UBDs, of which over 150 types divided over ~20 classes have been discovered, would also be very specific (322). However, the affinity of UBDs for ubiquitin chains is often relatively low, which raises the question how signaling complexes are assembled by ubiquitinated proteins. Either multivalent interactions of multiple UBDs with multiple conjugated ubiquitin molecules or enhancement of a weak existing interaction between two proteins can be considered. Alternatively, the ubiquitin-UBD interactions could be less specific and/or very transient in dynamic molecular structures where a relatively high local ubiquitin (-chain) concentration can be maintained. Under such circumstances, target specificity could be achieved by target availability in the complex, or by *e.g.* specific interactions between the target and one or more UBLs that would bring it close to the regulating ubiquitin groups.

An interesting possibility is that long ubiquitin chains themselves could form structural 'meshes' on/in which UBLs and their interacting targets could 'dock' for interaction with other complex components. In depth characterization of the localization and composition of signaling complexes is required to further our knowledge about the plethora of effects ubiquitin and UBLs exert on the innate immune system.

The importance of ubiquitination in regulating cellular mechanisms is becoming more and more clear and the innate immune system is no exception. PRR signaling relies on the conjugation of K63 chains to activate key signaling components, which results in quick and dynamic activation of signaling cascades. Knowledge gained on the regulation of the innate immune system could very well be used to develop new vaccine adjuvants and new strategies to treat autoimmune diseases.

Chapter 6

Antiviral innate immune response interferes with the formation of replication-associated membrane structures induced by a +RNA virus

Diede Oudshoorn, Barbara van der Hoeven, Ronald W.A.L. Limpens, Corrine Beugeling, Eric J. Snijder, Montserrat Bárcena, Marjolein Kikkert

Published in mBio. 2016 Dec 6;7(6) e01991-16

ABSTRACT

Infection with nidoviruses like corona- and arteriviruses induces a reticulovesicular network of interconnected ER-derived double-membrane vesicles (DMVs) and other membrane structures. This network is thought to accommodate the viral replication machinery, and protect it from innate immune detection. We hypothesized that the innate immune response has tools to counteract the formation of these virus-induced replication organelles in order to inhibit virus replication. Here we have investigated the effect of type I interferon (IFN) treatment on the formation of arterivirus-induced membrane structures. Our approach involved ectopic expression of arterivirus non-structural proteins nsp2 and nsp3, which induce DMV formation in the absence of other viral triggers of the interferon response, such as replicating viral RNA. Thus, this set-up can be used to identify immune effectors that specifically target the (formation of) virus-induced membrane structures. Using large-scale electron microscopy mosaic maps, we found that IFN-β treatment significantly reduced the formation of the membrane structures. Strikingly, we also observed abundant stretches of double-membrane sheets (a proposed intermediate of DMV formation) in IFN-β-treated samples, suggesting the disruption of DMV biogenesis. Three interferon-stimulated gene products, two of which have been reported to target the hepatitis C virus replication structures, were tested for their possible involvement, but none of them affected membrane structure formation. Our study reveals the existence of a previously unknown innate immune mechanism that antagonizes the viral hijacking of host membranes. It also provides a solid basis for further research into the poorly understood interactions between the innate immune system and virus-induced replication structures.

Importance

Viruses with a positive-strand RNA genome establish a membrane-associated replication organelle by hijacking and remodeling intracellular host membranes, a process deemed essential for their efficient replication. It is unknown whether the cellular innate immune system can detect and/or inhibit the formation of these membrane structures, which could be an effective mechanism to delay viral RNA replication. In this study, using an expression system that closely mimics the formation of arterivirus replication structures, we show for the first time that IFN-β treatment clearly reduces the amount of induced membrane structures. Moreover, drastic morphological changes were observed among the remaining structures, suggesting that their biogenesis was impaired. Follow-up experiments suggested that host cells contain a hitherto unknown innate antiviral mechanism, which targets this common feature of +RNA virus replication. Our study provides a strong basis for further research into the interaction of the innate immune system with membranous viral replication organelles.

INTRODUCTION

All positive-strand RNA (+RNA) viruses of eukaryotes studied to date modify intracellular membranes into unique structures that presumably facilitate viral RNA synthesis. These can therefore be viewed as the "headquarters" of +RNA viral replication (17-19, 323). Elaborate interactions between virus and host are believed to form the basis for the striking, virus-induced remodeling of specific cellular organelles in the infected cell (35, 41, 45, 324). These replication organelles may consist of different sub-structures, such as spherules, tubules, convoluted membranes, paired membranes or double-membrane vesicles. Despite this diversity, two recurrent classes of replication organelles induced by +RNA viruses have been recognized. The first type consists of membrane invaginations that create small 'spherules' in the membranes of intracellular organelles or the plasma membrane. Neck-like connections between the cytosol and the interior of the spherule, in which RNA synthesis takes place, are presumed to facilitate transport of viral RNA products to the cytosol for translation and packaging. Spherules of this kind have been described for *e.g.* alphaviruses, some flaviviruses, nodaviruses, and bromoviruses (27, 48, 50, 60). The second type of structures is characterized by unique membrane tubules and/or vesicles that have a double membrane. During the past decade, this kind of membrane structures has been observed and characterized extensively by electron tomography for arteriviruses, coronaviruses, picornaviruses, and hepatitis C virus (HCV) (20-23, 56, 65). For some of these double-membrane vesicle (DMV)-forming viruses connections between the DMV interior and the cytosol have been observed (23, 56, 65). However, this was not the case for arteri- and coronaviruses, raising the question whether their RNA synthesis takes place inside these vesicles, by analogy with the replication spherules described above. In that scenario, it would be unclear how newly synthesized RNA molecules are exported to the cytosol for translation and packaging (20, 21).

Equine arteritis virus (EAV) is the prototype of the arterivirus family and induces the formation of an extensive reticulovesicular network (RVN) of DMVs, which is thought to be derived from the endoplasmic reticulum (ER) (20). Furthermore, EAV infection results in the formation of proteinaceous tubules containing the nucleocapsid (N) protein, which were found in close proximity of the DMVs and were suggested to be involved in nucleocapsid assembly (20, 115). The EAV replicase gene encodes two large polyproteins, pp1a and pp1ab, the second being a C-terminally extended version of the first produced by ribosomal frameshifting. These precursors are cleaved by internal proteases to yield at least 13 mature viral non-structural proteins (nsps) (reviewed in (4)). Previous studies from our laboratory provided the first detailed description of arterivirus-induced remodeling of host membranes and established that expression of the nsp2-7 part of the EAV replicase polyproteins suffices to induce the formation of DMVs strikingly similar to those formed in infected cells (88). Subsequent studies demonstrated that the same result can be achieved by expressing a polyprotein fragment encompassing nsp2 and nsp3, including the papain-like protease in nsp2 (PLP2) that cleaves the nsp2-nsp3 junction (24, 180). As for other +RNA viruses, the viral non-structural proteins directly involved in RNA synthesis, such as the

RNA-dependent-RNA-polymerase (RdRp), as well as the (presumed) double-stranded RNA (dsRNA) intermediates of viral RNA replication, co-localize with the membrane structures induced during EAV infection (18, 20, 88). When analyzed in more detail however, the dsRNA was mainly located in the core of the DMVs whereas the non-structural proteins were located mainly on the membranes of the vesicles as well as on surrounding membranes (20, 88), as was also observed for coronaviruses (21, 125).

How replication organelles are formed during infection is still largely unclear. One proposed mechanism for DMV biogenesis, termed "double budding", includes the acquisition of the double membrane by the sequential budding of vesicles into and out of the ER lumen. Alternatively, ER membranes may pair to form double-membrane sheets, which would then bend and undergo fission to produce closed vesicles, a process termed "enwrapping" (18, 88, 180). In a recent study, we detected intermediate structures compatible with both models. Putative intermediates consisting of double-membrane sheets that fitted different stages of enwrapping were, however, particularly prominent, suggesting that enwrapping could be a key biogenesis pathway for EAV-induced structures (180). In the current study, we will refer to any combination of EAV nsp-induced membrane structures, including these intermediates, as "double-membrane structures" (DMS), irrespective of whether they are formed in the context of viral infection or upon expression of viral proteins.

The exact benefits of +RNA viral replication organelles formation remain unclear, although several advantages have been proposed (17, 18, 36, 180, 323). Firstly, the replication organelles could constitute a suitable micro-environment for viral RNA synthesis by concentrating the necessary viral and host proteins. Secondly, they could play an important role in the spatio-temporal coordination of the different steps of the viral replication cycle, such as genome translation, replicase polyprotein processing, RNA synthesis, and virion assembly. The third proposed role is hiding viral RNA species from detection by innate immune sensors. These sensors recognize pathogen-associated molecular patterns (PAMPs) such as virus-derived nucleic acids, leading to the induction of inflammatory responses and the production of type I interferons such as IFN-β (29-31). These interferons then signal in autocrine and paracrine fashion to up-regulate the expression of interferon-stimulated genes (ISGs) inducing a so-called antiviral state that strongly restricts further spread of the infection (29-31). The antiviral activities of several of the hundreds of ISGs induced upon type I interferon signaling have been characterized to a certain extent and these impact diverse aspects of viral infection such as entry, genome replication, particle formation, or budding (325). Even though virus-induced replication organelles are a prominent feature of +RNA viruses, there is very limited evidence for a direct targeting of these replication organelles by the innate immune system. To our knowledge, in fact only two reports have described such effects, in both cases on the membranous web formed during HCV replication (326, 327); however, the underlying mechanisms remain to be fully characterized and data for any other +RNA virus are lacking.

We here studied the effects of type-I IFN-induced signaling on DMS formation induced by EAV nsp expression, measured using quantitative electron microscopy (EM) methods that allowed the direct evaluation of the impact of the innate immune response on the

formation of EAV-induced DMS. We observed that IFN-β treatment reduces the number of cell sections showing DMS and drastically changed the morphology of the remaining structures. In order to investigate the underlying mechanism, we evaluated the role of individual ISGs, including cholesterol 25-hydroxylase (CH25H) and viperin, which are known to inhibit HCV membranous web formation (326, 327). However, the candidates tested appear not to be involved in restricting EAV nsp-induced membrane remodeling. This suggests the existence of a previously unknown IFN-β-induced mechanism targeting the formation of the replication organelles induced by arteriviruses and – possibly – other +RNA viruses.

RESULTS

Experimental set-up for studying the interaction of the innate immune system with arterivirus-induced membrane structures

Our goal was to analyze whether the innate immune system responds to the formation of +RNA virus-induced replication organelles and we hypothesized that such a response could be linked to the type-I IFN signaling pathway, which has an important role in counteracting virus infections from their earliest stage onwards. Human liver carcinoma cells (HuH-7), which are susceptible to EAV infection (Fig. 1A; (180)) and produce high titers of infectious virus, were used based on their responsiveness to IFN-β treatment (Fig. 1B; (328)). When EAV-infected HuH-7 cells were fixed by high-pressure freezing followed by freeze substitution (HPF-FS) and subsequently analyzed by EM, DMS similar to those previously described upon EAV infection in other cell types were readily observed (Fig. 1C) (20, 180). DMVs with characteristic double membranes and cores were abundantly present (Fig. 1C, examples indicated with red arrows) as well as the N protein-containing tubules described previously (20) (Fig. 1C, examples indicated with black arrows). In order to establish whether EAV replication is sensitive to IFN-β treatment in HuH-7 cells, cells were infected with a recombinant GFP-expressing reporter virus (EAV-GFP (329); multiplicity of infection (MOI) of 10) and treated with IFN-β from 1 h p.i. onward. A clear dose-dependent reduction of the GFP signal was observed during a single cycle of infection (Fig. 1D).

Because DMS formation requires the accumulation of viral nsps (88) derived from the abundant replication and translation of the viral RNA genome, it is not possible to study the effect of IFN-β treatment on DMS formation directly in infected cells, since the treatment will inhibit overall viral replication and – consequently – nsp synthesis. Thus, to investigate innate immune responses specifically targeting DMS formation, the latter process needed to be mimicked in a system that does not depend on EAV replication. Previously, the co-expression of EAV nsp2 and nsp3 (as a self-cleaving nsp2-3 polyprotein fragment) has been shown to be both required and sufficient to induce DMV formation in transfected cells and such a system can thus be used as a 'surrogate' to mimic the formation of DMS outside the context of infection (24).

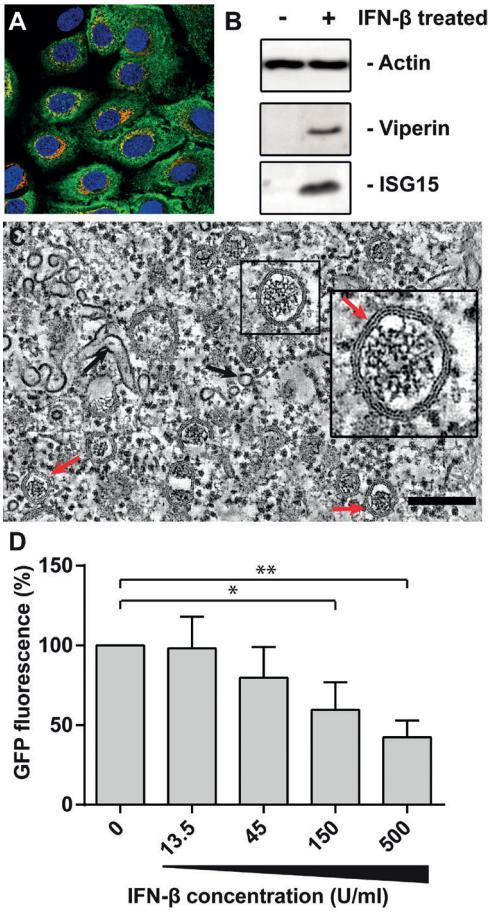


Fig. 1. (left page) EAV infection in HuH-7 cells is productive and sensitive to IFN-β treatment. **(A)** *HuH-7 cells infected with EAV were fixed and stained with antibodies specific for nsp2 (red) and nucleocapsid protein (N; green) at 12 h p.i. The nuclei were stained with Hoechst 33258 (blue).* **(B)** *Protein levels in HuH-7 cells were analyzed at by SDS-PAGE followed by western blotting after 12 hours of stimulation with 500 U/ml IFN-β or untreated control cells.* **(C)** *EAV infected HuH-7 cells were high-pressure frozen at 12 h p.i. Samples were freeze-substituted and analyzed by electron tomography as previously described (180). A virtual slice (2 nm thick) of a reconstructed tomogram is shown. The red arrows point at some of the multiple DMVs present in the field of view. The boxed DMV is enlarged in the inset to make the two tightly apposed DMV membranes more apparent. Black arrows indicate some of the N-containing tubules. The scale bar represents 200nm.* **(D)** *HuH-7 cells were infected with EAV-GFP in 96-wells black plates for 1 hour and after removal of the inoculum they were treated with the indicated dose of IFN-β. Cells were fixed at 16 h p.i. and GFP fluorescence was measured and normalized to a control infection. Error bars represent the standard deviation of 3 independent experiments and statistics was done with an unpaired student's t-test; * = $p<0.05$; ** = $p<0.01$.*

In order to develop a stable and inducible expression system, we generated polyclonal HuH-7 cell lines expressing EAV nsp2-3 with an HA-tag at the nsp2 N-terminus and a C-terminal GFP tag on nps3 under the control of a tetracycline-inducible CMV promoter (HuH-7/tetR/HA-nsp2-3GFP; Fig. 2A) (164). Induction of nsp2-3 expression in this cell line resulted in the formation of uniform DMVs (Fig. 2B), which appeared similar to those observed in HuH-7 infected cells, whereas such structures were not observed in non-induced cells. Although these DMVs were slightly larger than those found during EAV infection and (as expected) lacked the RNA-containing electron-dense core (compare Fig. 1C and Fig. 2B), electron tomography showed that their double-membrane architecture was identical (Fig. 2B). At 24 hours post tetracycline induction, many DMVs were found (Fig. 2B). The presence of the C-terminal GFP tag on nsp3 did not influence the morphology of DMVs, as they were indistinguishable from those induced by expression of HA-nsp2-3 lacking the GFP tag (180). The nsp2-3 expressed in HuH-7/tetR/HA-nsp2-3GFP cells localized to the perinuclear region (Fig. 2C), which is very

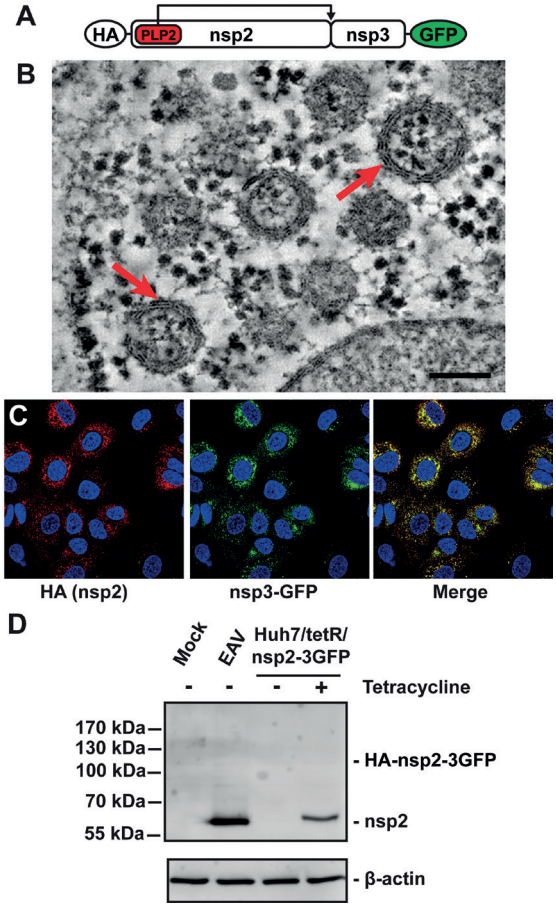
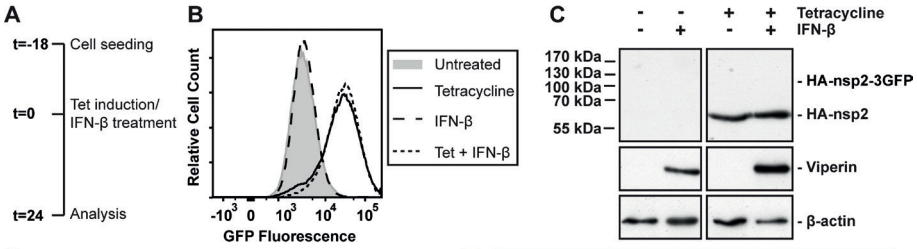


Fig. 2. (left page) Validation of the HuH-7/tetR/HA-nsp2-3GFP cell line. (A) *Schematic overview of the HA-nsp2-3GFP protein.* **(B)** *HuH-7/tetR/HA-nsp2-3GFP cells were high-pressure frozen, followed by freeze substitution and subsequently analyzed by electron tomography as described before (180). A 2-nm thick virtual slice of a reconstructed tomogram is shown. The red arrows indicate some of the DMVs that can be clearly observed. The scale bar represents 100 nm.* **(C)** *Immunofluorescence microscopy of HuH-7/tetR/HA-nsp2-3GFP cells treated with tetracycline for 24 hours to induce expression. Cells were stained with mouse-anti-HA and the HA-nsp2 signal was detected using a Cy3-conjugated antibody, whereas as nsp3-GFP could be visualized by virtue of its fluorescent tag.* **(D)** *EAV nsp2 expression was analyzed by western blotting during infection (12 h p.i.) and in induced HuH-7/tetR/HA-nsp2-3GFP cells (24 hours after induction).*

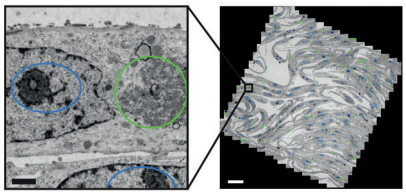
similar to their localization in EAV-infected cells (Fig. 1A). While the expression levels of nsp2 were somewhat lower in the tetracycline-induced HuH-7/tetR/HA-nsp2-3GFP cells compared to EAV-infected cells, the nsp2-3 polyprotein was correctly and efficiently cleaved by PLP2, as no precursor protein could be observed (Fig. 2D). In conclusion, this cell line could be used to reproducibly and quantitatively examine the specific interactions of arterivirus-induced membrane structures with the cell's innate immune responses.

IFN-β treatment disrupts the formation of double-membrane structures

We first checked whether the expression of nsp2-3GFP in HuH-7/tetR/HA-nsp2-3GFP cells and the resulting DMV formation by itself induced an innate immune response, which would imply that the structures can be sensed by the innate immune system. In our setup, this was not the case since no IFN-β or IFIT2 mRNA could be detected after induction of nsp2-3GFP expression in HuH7 or MEF cells (data not shown). We argued that in EAV-infected cells type



D



E

Exp	IFN-β	DMS+	Nuclei	Ratio	Change
#1	-	150	305	0.492	-33% **
	+	158	478	0.331	
#2	-	187	358	0.522	-23% *
	+	160	397	0.403	
#3	-	152	328	0.463	-33% **
	+	122	391	0.312	
#4	-	209	475	0.440	-20% n.s.
	+	125	355	0.352	

Fig. 3. IFN-β treatment reduces the number of double-membrane structures formed by EAV nsp2-3 while protein levels and nsp2-3 cleavage efficiency are not affected. (A) *Schematic overview of the experimental setup.* **(B)** *HuH-7/tetR/HA-nsp2-3GFP cells were analyzed by flow cytometry for GFP fluorescence after 24 hours of the indicated treatments.* **(C)** *Levels of the indicated proteins in HuH-7/tetR/HA-nsp2-3GFP cells were analyzed 24 hours after the indicated treatments, using Western blotting. The expected position of the HA-nsp2-3GFP precursor is indicated.* **(D)** *Example of a mosaic map (right) of a single mesh of an EM grid (tetracycline treated HuH-7/tetR/HA-nsp2-3GFP cells) composed of 1164 images (2048x2048 pixels each) acquired at 6800x magnification and binning 2, which corresponded to a pixel size of 3.2 nm. The close-up (left) was extracted from the mosaic map as indicated. Coloring represents annotations of nuclei (blue ovals) and EAV nsp2-3 induced DMS (green ovals) in this mesh. Scale bars represent 500 nm (left) and 20 μM (right) respectively.* **(E)** *In four independent experiments the number of cell profiles positive for DMS (DMS+) was quantified as well as the number of cell profiles containing a nucleus (Nuclei). Multiple mosaic maps were analyzed for each sample. Ratios are calculated as the number of DMS+ cell profiles divided by the number of cell profiles containing a nucleus and p-values were calculated using chi-square tests for each individual experiment; n.s. = not significant; * = p<0.05; ** = p<0.01. The average reduction over 4 experiments was 27% ± 7 (p=0.001).*

I IFN induction might be triggered by other viral PAMPs (e.g. viral RNA), which could affect the formation or function of the replication organelles by inducing the expression of particular ISGs and thus augmenting the general antiviral effect of the innate immune response. In order to address this possibility, we initially asked the question whether IFN-β treatment affects the number of EAV nsp2-3-induced DMS formed per cell. For this time-consuming quantitative analysis, we decided to use chemically fixed samples, which simplified the workflow while providing sufficient preservation to clearly assess the general morphology of the DMS induced upon nsp2-3 expression (see below). The HuH-7/tetR/HA-nsp2-3GFP cells were chemically fixed, scraped from the dish, pelleted, and embedded in an epoxy resin, after which thin sections suitable for transmission EM imaging were cut. By using cell pellets rather than monolayers, these sections represented random planes through the cells. We argued that if there would be a difference in the extent of DMS formation, this would be reflected in the number of cell profiles that contain DMS, as the fraction of random

sections containing structures would decrease. Importantly, we first checked the effect of IFN-β treatment on nsp2-3 expression levels and polyprotein cleavage in HuH-7/tetR/HA-nsp2-3GFP cells, since altered expression of nsp2-3 would likely affect DMS formation and possibly mask specific effects of the IFN-β treatment. Cells were treated with tetracycline and/or IFN-β (Fig. 3A), and nsp3-GFP expression was measured by flow cytometry. GFP signal increased after tetracycline induction, as expected, but was not affected by IFN-β treatment at the concentration used in our experiments (Fig. 3B). Likewise, polyprotein cleavage was not majorly affected since no HA-nsp2-3GFP precursor could be observed after IFN-β treatment, similar to the situation without IFN-β treatment (Fig. 3C).

After setting up this system for DMS quantification, the next step was to quantify nsp2-3-induced DMS in HuH-7/tetR/HA-nsp2-3GFP cells, treated with tetracycline alone or in combination with IFN-β. Using large mosaic maps of EM micrographs (330), we quantified the number of cell profiles positive for DMS as well as the total number of cell profiles showing a nucleus, which was used as a reference for normalizing the total number of cells analyzed (Fig. 3D). In four independent experiments, sections containing 300-500 cell profiles with a nucleus were analyzed for each condition. This revealed a consistent decrease (27% ± 7) in the number of cell profiles positive for nsp2-3-induced DMS after treatment with IFN-β (Fig. 3E). Because the nsp2-3 expression levels were very similar between the samples (Fig. 3B), our conclusion is that the induction of DMV formation by EAV nsp2 and nsp3 was substantially inhibited and that the type I interferon treatment restricts the hijacking of cellular membranes.

Besides the changes in their abundance caused by IFN-β treatment, we also analyzed the morphology of the DMS. As mentioned previously, tetracycline-induced HuH-7/tetR/HA-nsp2-3GFP cells mainly developed the DMV type of DMS (Fig. 4A). In 1% of the DMS-containing cell profiles, we also observed some double-membrane sheets, a presumed precursor of DMVs during their biogenesis (Fig. 4A; bottom panel; red arrow) (88, 180). These sheets were mostly found in the vicinity of DMVs and resembled the two tightly apposed membranes of the DMVs themselves, but they varied in shape depending in part on the sectioning plane for EM. When the tetracycline-induced HuH-7/tetR/HA-nsp2-3GFP cells were also treated with IFN-β, double-membrane sheets were found in much larger fraction of the DMS-containing cell profiles (36% ± 3) (Fig. 4B,C). With a few exceptions, the double-membrane sheets were found in cell profiles that also contained DMVs (Fig. 4B,C). They were often juxtaposed to intact DMVs and were usually strikingly more extensive than the double-membrane sheets observed without IFN-β treatment (compare Fig.4A (red arrow) and Fig. 4B). This strong increase in double-membrane sheet formation suggested a major effect in DMS biogenesis after IFN-β treatment.

Involvement of ISGs in inhibition of DMV formation

Likely, the effects of IFN-β treatment on DMS morphology and abundance is caused by the products of one or more ISGs, which are expressed as a result of the IFN-β treatment. Since EM is required to distinguish DMVs from double-membrane sheets, a high-throughput screen of the hundreds of ISG candidates was not feasible. Interestingly, two membrane-

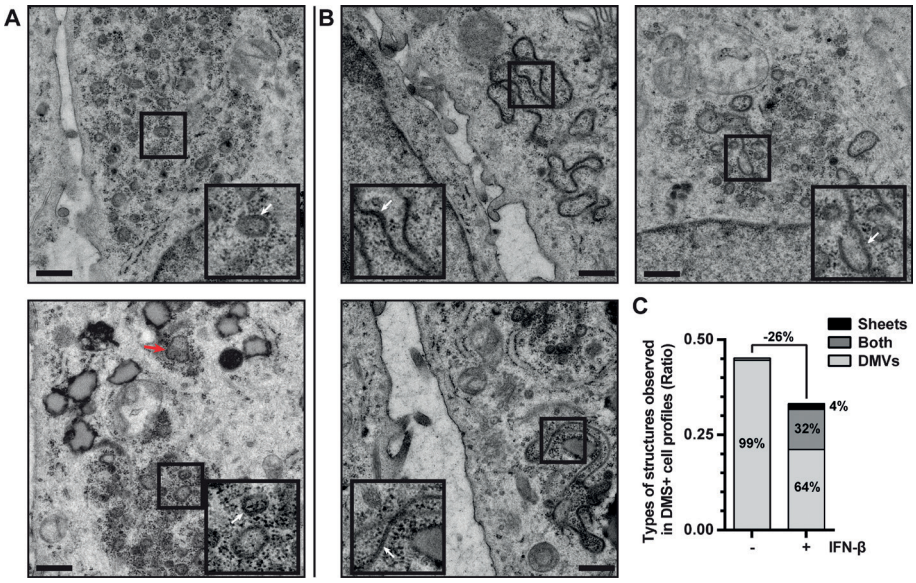
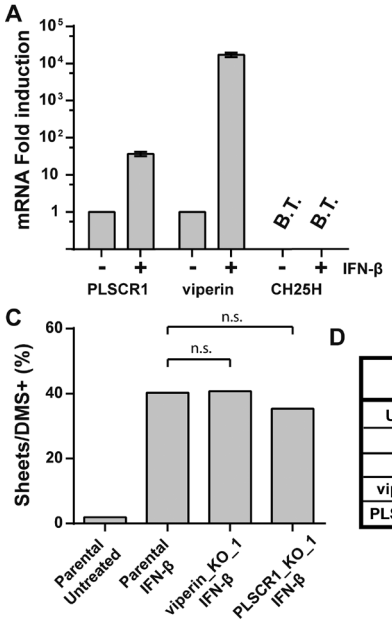


Fig. 4. IFN-β treatment blocks DMV formation and leads to the accumulation of double-membrane sheets. (A,B) *EM images of HuH-7/tetR/HA-nsp2-3GFP cells in which expression is induced with tetracycline for 24 hours. Cells represented in images of panel* **(B)** *were simultaneously treated with 500 U/ml IFN-β for 24 hours. Images were extracted from mosaic maps used for quantifications and scale bars represent 500 nm. Insets are 2x magnifications of areas where DMVs* **(A)** *or double-membrane sheets* **(B)** *are visible (indicated with white arrows). The different appearance of these samples relative to the data shown in Fig. 2 is the result of the different sample preparation approach (chemical fixation versus HPF-FS, respectively).* **(C)** *The occurrence of the different types of DMS (DMVs, double-membrane sheets or both) in the cell profiles is shown in control or IFN-β treated HuH-7/tetR/HA-nsp2-3GFP that were tetracycline-induced.*

associated ISGs, viperin (also called radical S-adenosyl methionine domain containing protein 2; RSAD2) and CH25H (the latter resulting in production of effector 25-hydroxy cholesterol (25HC)) were previously shown to influence HCV replication membranes, which have a similar double-membrane architecture as described for arteriviruses (36, 326, 327). Anggakusuma and co-workers expressed HCV NS3-5B proteins in HuH-7 cells, which resulted in the formation of membrane structures similar to those found upon HCV infection (23). Additional treatment of these cells with 25HC triggered, among other changes, the formation of smaller DMVs, leading to the conclusion that 25HC influences the HCV-induced membrane structures (326). The changed DMVs these authors observed were different from the double-membrane sheets that accumulate in our EAV nsp2-3 expression system upon IFN-β treatment.

In order to evaluate whether either of these ISGs may play a role in the biogenesis of EAV membrane structures, we first examined the expression of viperin, CH25H, and a third membrane-associated ISG, phospholipid scramblase 1 (PLSCR1), in parental HuH-7 cells upon IFN-β treatment. The mRNA of both viperin and PLSCR1 was strongly up-regulated,



D

	DMS+	Nuclei	Ratio	Change%	Sheets	Sheets%
Untreated	152	328	0.463	-	3	2.0%
IFN-β	122	391	0.312	-33%	46	37.7%
25HC	174	382	0.455	-0.8%	3	1.7%
viperin_KO_1	87	N.D.	N.D.	N.D.	36	41.4%
PLSCR1_KO_1	62	N.D.	N.D.	N.D.	22	35.5%

Fig. 5. CH25H, PLSCR1 and viperin are not involved in the inhibition of EAV nsp2-3 DMV formation by IFN-β. (A) *Relative induction of indicated ISG mRNAs in HuH-7 cells treated with IFN-β for 16 hours compared to untreated control cells, using RT-qPCR analysis. Indicated genes were amplified with gene-specific primers, error bars were based on three independent experiments. CH25H mRNA was below the threshold of detection (B.T.) in HuH-7 cells. The CH25H RT-qPCR was validated using cDNA of lipopolysaccharide-treated human dendritic cells.* **(B)** *Tetracycline-induced HuH-7/tetR/HA-nsp2-3GFP were treated with 500 U/ml IFN-β, 10μM of 25HC, or untreated, and analyzed by EM for the total number of cells positive for DMS (DMS+) as well as cell profiles positive for a nucleus (Nuclei). A section covering 300-500 cell profiles with a nucleus was analyzed for each sample. Ratios are calculated as the number of DMS+ cell profiles divided by the number of nuclei positive cell profiles as well as the % difference with the untreated control. The number of cell profiles positive for double-membrane sheets was also quantified and the ratio of sheets positive cell profiles compared to the total number DMS+ cell profiles was determined.* **(C)** *Tetracycline-induced CRISPR/Cas9 knock-out cell lines of indicated genes were treated with 500 U/ml IFN-β and compared to the parental control cells. The analysis was similar to that for panel (B), except that the DMS+/Nuclei ratio was not determined.* **(D)** *A table of the quantifications shown in panel B and C. N.D. = not determined. Statistics was done using chi-square tests. n.s. = not significant; ** = p<0.01*

whereas CH25H mRNA could not be detected, either with or without IFN-β treatment (Fig. 5A). Although the observation that CH25H was not expressed in HuH-7 cells after IFN-β treatment indicated that this factor could not be responsible for the observed effects in our experiments, we decided to test its impact on EAV nsp2-3-induced DMS, since this IFN-induced factor could be relevant during a natural infection if produced by immune cells. We treated HuH-7/tetR/HA-nsp2-3GFP with 10 μM 25HC, a concentration that partially inhibited EAV replication in parental HuH-7 cells (Fig. S1). We however found no significant

reduction in the number of DMS-containing cells nor did we observe an increase of double-membrane sheet formation as observed after IFN-β treatment (Fig. 5B,D). We therefore ruled out 25HC synthesis by CH25H as a mechanism that could be responsible for the effects we observed of IFN-β treatment on EAV nsp2-3-induced DMS.

To determine the impact of viperin and PLSCR1 on EAV nsp2-3GFP-induced DMS, we used CRISPR/Cas9 technology to knock-out either PLSCR1 or viperin expression in the HuH-7/tetR/HA-nsp2-3GFP cell line, which indeed abolished their expression upon IFN-β treatment (Fig. S2). If either viperin or PLSCR1 were required for the effects of IFN-β treatment we observed (Fig. 4), IFN-β treatment should no longer lead to the proliferation of double-membrane sheets in these respective knock-out cells. When the DMS in tetracycline-induced and IFN-β-treated knock-out cell lines were examined, we found no significant differences in the fraction of cells showing double-membrane sheets when compared to the parental HuH-7/tetR/HA-nsp2-3GFP cell line (Fig. 5C,D). Together, these data suggest that Viperin and PLSCR1 do not contribute to the disruption of nsp2-3-induced DMV biogenesis.

Strikingly, our results imply that, in the same cell line, HCV- and EAV-induced membrane structures, which both include DMVs, are targeted by different IFN-induced effectors. For HCV, 25HC treatment led to the formation of smaller DMVs whereas for EAV DMV biogenesis was not affected by 25HC. Our study thus suggests the existence of an alternative innate immune mechanism that antagonizes the viral hijacking of host membranes.

DISCUSSION

Modification of host membranes to accommodate the viral RNA replication machinery appears to be an essential and universal feature of +RNA virus infection. Our hypothesis was that – given their abundance in the cytosol of the infected cell – these structures are a likely target of the innate immune system. Disrupting the formation and/or function of virus-induced replication organelles would hamper viral replication and could therefore constitute an effective antiviral strategy for the cell. Our findings show that treatment of cells with IFN-β (mimicking the triggering of innate immunity after recognition of PAMPs such as viral nucleic acids) inhibits the formation of arterivirus-induced DMVs. We not only observed a decrease in the fraction of cells positive for EAV nsp2-3-induced DMS, but we also noticed the extensive accumulation of double-membrane sheets, which could be intermediates of DMV morphogenesis that become much more prevalent upon IFN-β treatment. This suggests that the membrane-curving and/or -fission events that could lead to DMV formation after initial membrane pairing (180) were inhibited by IFN-β treatment (Fig. 6). This conclusion is further supported by a preliminary experiment (data not shown) in which expression of nsp2-3GFP was first induced for 24 hours, to allow DMS formation, after which IFN-β treatment was performed for another 24 hours. In the latter experiment, the effect of IFN-β treatment on double-membrane sheet formation was markedly decreased: only 19.9% of the DMS-containing cell profiles contained sheets instead of 34.4% in cells

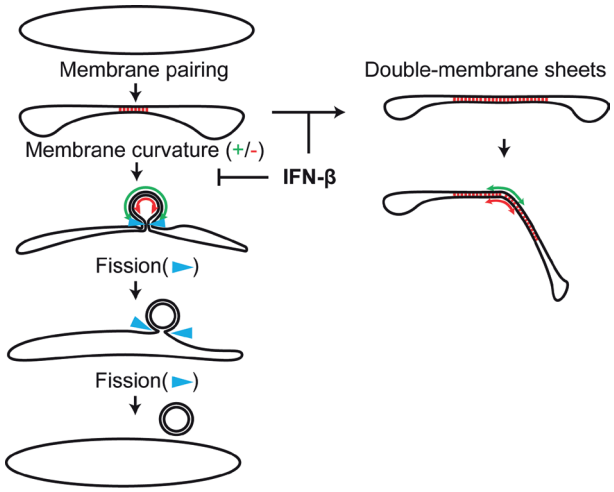


Fig. 6. Model for the inhibition of DMV formation by IFN-β treatment. *The enwrapping model for DMV formation. Membrane pairing is indicated with red dashes between the membranes. Positive and negative membrane curvature (green and red, respectively) are indicated with double arrows. The step proposed to be inhibited by IFN-β treatment and resulting in the formation of double-membrane sheets is indicated. Adapted from van der Hoeven et al. 2016 (180).*

treated with IFN-β from the moment of induction of nsp2-3GFP expression. This renders the alternative scenario, IFN-β treatment disrupting existing DMVs and converting them into double-membrane sheets, less likely and strongly suggests that IFN-β treatment indeed influences DMV biogenesis, although we cannot exclude some effects on existing structures. Our data may also shed more light on DMV morphogenesis, since it reinforces the notion that the enwrapping model is a prominent pathway for DMV formation (88, 180). The fact that DMVs were still present after IFN-β treatment suggests that either the enwrapping pathway was only partially blocked or that the remaining DMVs were formed via an alternative mechanism, for example double budding (180).

We tested the involvement of three selected candidate interferon-induced host factors, PLSCR1, viperin, and CH25H (331-333). When CRISPR/Cas9 knockout cells lacking viperin or PLSCR1 were IFN-β treated, the number of cells showing double-membrane sheets did not decrease. This indicated that, although those ISGs were abundantly expressed after IFN-β treatment, neither of them had any impact on DMS formation in our study. CH25H turned out not to be expressed after IFN-β signaling in HuH-7 cells and treatment of cells with 25HC, the antiviral metabolite synthesized by CH25H, did not visibly affect the EAV nsp2-3-induced DMS. Based on these observations, we concluded that the disruptive effect of IFN-β treatment on DMV formation was unlikely caused by PLSCR1, viperin, or CH25H.

In order to identify the IFN-β-induced factors sought, the best approach would be an unbiased screen of all ISGs expressed after IFN-β treatment. Because of the time-consuming type of EM analysis required to identify DMS, high-throughput EM analysis of all ISGs is not feasible and screening would have to rely on other methods such as pull-down assays or co-localization studies that could reveal promising candidates, which could then be analyzed by EM. A previous high-throughput ISG screen, in which the effect of individual ISGs on virus infection was evaluated using fluorescent reporter viruses, included EAV-

GFP (334). Most hits in that screen were well-characterized ISGs, such as the OAS proteins, which are known to affect other stages of the viral replication cycle or components in the innate immune signaling cascade, such as IRF1, which lead to the expression of a variety of ISGs. This study did not yield obvious candidates that could be responsible for the observed effects on EAV-induced membrane structures, although some of these could be tested to confirm this. Other possible candidates that we have not explored yet are transmembrane ISGs, such as members of the membrane-anchored IFITM protein family. Because their main mode of action seems to be the blocking of virus entry from endosomes (335), we do not consider these likely responsible for the effects on replication organelles at present.

Interestingly, the type II interferon (interferon gamma; IFN-γ) pathway has recently been shown to interact with the LC3 conjugating system, which is an established component of the autophagy machinery. LC3 was shown to label the vacuolar membrane of the parasite Toxoplasmosa gondii (336) and also the replication organelles induced by murine norovirus, another +RNA virus. This serves to recruit immunity-related GTPases induced by IFN-γ signaling to disrupt these membranes and control T. gondii and norovirus infections (336, 337). These pathogen-restricting effects did not depend on the degradative functions of autophagy, rather LC3 seems to function as a "flag" that labels foreign membrane structures. Whether similar mechanisms are also in play upon IFN-β treatment has not been investigated, but is an interesting possibility. Since LC3 (although in some cases also in its non-lipidated form) has been found to co-localize with nidovirus replication organelles (148, 150), it would be interesting to investigate whether this could be related to antiviral IFN-β or IFN-γ effects.

The impact of the disruption of DMS formation following IFN-β treatment still requires validation in infected cells, which would be most easily achieved if the responsible factor(s) were identified, because we could then evaluate the effect of this specific factor on replication organelles during infection. If the reduction in DMS prevalence that was observed after IFN-β treatment is representative for what happens during an infection, this could directly reduce overall replication efficiency. It should be noted though, that in the case of coronaviruses, the size and number of DMVs observed during infection was reported not to correlate with viral fitness in cell culture (131, 186). However, impairment of DMV biogenesis could also indirectly affect viral replication, based on their proposed role in the shielding viral PAMPs from cytosolic innate immune sensors. Even though the precise location of arterivirus RNA synthesis remains unclear, the interior of DMVs in EAV-infected cells labels strongly for dsRNA and is enriched for phosphorous, suggesting the abundant presence of viral RNA (20). The decrease of the number of closed DMVs, as observed after IFN-β treatment, could render this material accessible to cytosolic innate immune sensors and promote their recognition as a PAMP (338). Similarly, the exposure of viral RNA to the antiviral action of ISGs could be enhanced, for example to the ISGs that target viral RNA directly, such as the OAS proteins that indeed very effectively restrict EAV replication if over-expressed (334).

In future research, it would be interesting to investigate whether EAV and other +RNA viruses counteract innate immune responses targeted at virally induced membrane

structures, as so many other immune responses are counteracted by viral evasion mechanisms. Interestingly, the PLP2 protease in arterivirus nsp2 was shown to reverse post-translational conjugation of ubiquitin and ISG15 conjugation to cellular targets (165, 313, 338). Since both conjugation systems are thought to play a role in innate immune responses, these viral activities could be linked to countering the innate immune-triggered disruption of replication organelles.

In conclusion, we here describe a previously unknown effect of IFN-β treatment on viral replication organelles, which is distinct from earlier described effects on the HCV membranous web. This implies that the innate immune system possesses multiple ways to counteract the formation of replication organelles, thus augmenting the importance of these virally induced double-membrane structures as a target of the antiviral IFN-β response. HCV and EAV both belong to the DMV-forming class of viruses (19) and it would be very interesting if membrane structures formed by spherule-forming viruses are also targeted by the innate immune system. If so, the next question would be whether the same or different ISGs are involved. Given the rather large body of literature describing the ultrastructure of viral replication organelles, surprisingly little is known about their actual function during virus replication and the reasons why these replication organelles are such a conserved and prominent feature of +RNA virus replication. Further investigation of the interactions between antiviral innate immunity and replication organelles will likely provide clues on this matter.

Acknowledgements

Ralf Bartenschlager (Heidelberg University), Herbert Virgin (Washington University School of Medicine in St. Louis), Zhijan Chen (University of Texas Southwestern Medical Center), Ron Kopito (Stanford University), Stephen High (University of Manchester), Gijs Versteeg (Max F. Perutz Laboratories), Udeni Balasuriya (University of Kentucky), and Ernest Borden (Cleveland Clinic) are cordially acknowledged for providing reagents. Jessika Ruinaard, Jochem Pronk, and Leonie Hussaarts are thanked for technical assistance and Bram Koster for providing access to the facilities and training at the EM section in the LUMC.

This work was supported in part by the Netherlands Organization for Scientific Research through a TOP grant from the Council for Chemical Sciences (NWO-CW grant 700.57.301 to EJS and AJK) and a MEERVOUD grant (NWO-ALW grant 836.10.003 to MB) from the Council for Earth and Life Sciences.

MATERIALS & METHODS

Cells, viruses and antibodies

HuH-7 cells (Bartenschlager lab; Heidelberg University) were grown in Dulbecco's modified Eagle's medium (DMEM; Lonza) supplemented with 8% (v/v) FCS (Bodinco), 2 mM L-glutamine (PAA Laboratories, Pasching, Austria) and non-essential amino acids (PAA Laboratories). 293T cells (Virgin lab; Washington University School of Medicine in St. Louis) and wild type

C57BL/6 MEFs (Chen lab; University of Texas Southwestern Medical Center) were cultured in DMEM with 10% (v/v) FCS. All cell culture media contained 100 U/ml penicillin and 100 µg/ml streptomycin. EAV (Bucyrus strain) and recombinant EAV-GFP were grown on BHK-21 cells as described previously (329). Infections were carried out with MOI 10 unless otherwise indicated and incubated at 37°C. Innate immune stimulation was performed by addition of human Interferon-β (IFN-β; PBL) at a concentration of 500 U/ml unless otherwise indicated. 25HC (Sigma) was dissolved in ethanol before use at indicated concentrations. Cell viability assays were performed using CellTiter 96 AQueous Non-Radioactive Cell Proliferation Assay (Promega) according to the manufacturer's instructions. GFP and cell viability assays were analyzed using a Mithras LB940 (Berthold) in 96-well plates.

Primary antibodies used were mouse α-HA (Clone HA.C5; Abcam), mouse α-β-actin (Clone AC-74; Sigma), mouse α-viperin (Clone MaP.VIP; Millipore) and goat α-PLSCR1 (Clone N-17; Santa Cruz). The mouse α-ISG15 antibody was kindly provided by Ernest Borden (Cleveland Clinic). Antibodies recognizing EAV proteins were described previously: rabbit α-EAV-nsp2 (165) and mouse α-EAV-N (339).

Plasmid construction

Expression constructs that contain sequences that code for EAV nsp2 and nsp3 were assembled in pDONR201 (life technologies) with an HA-tag at the N-terminus of nsp2 and eGFP fused to the C-terminus of nsp3. The pDONR construct was then transferred using LR Clonase II (Life Technologies) to either pcDNA3.1-DEST or pLenti6.3/TO/V5-DEST (Life Technologies). Helper plasmids for lentivirus particle production have been described previously (340) and pLenti3.3/TR carrying the *tet*R gene was purchased from Life Technologies (164). To make CRISPR/Cas9 knock-out cell lines, the LentiCrisprv2 vector was used as previously described (341, 342). Guide RNA sequences are listed in Table S1 (343).

Production of lentivirus particles and creation of stable cell lines

293T cells were transiently transfected with the helper plasmids and either the pLenti3.3/TR vector, the pLenti6.3 expression constructs or pLentiCrisprv2 using PEI (Sigma). 72 hours after transfection the supernatant was harvested, spun down for 10 minutes at 2000 rpm, filtered through a 0.45 µm filter and stored at -80°C until use. Subconfluent HuH-7 cells were transduced with pLenti3.3/TR lentiviral particles in the presence of 8 µg/ml polybrene (Sigma-Aldrich) and after 48 hours cells were passaged and transduced cells were selected with 100 µg/ml G418 (Life technologies). After several passages the resulting cell line, named HuH-7/tetR, was transduced again with pLenti6.3 constructs containing the nsp2-3GFP (pLenti6.3/HA-nsp2-3GFP) coding sequence and cells were selected with 12,5 µg/ml Blasticidin S (PAA). Expression of transgenes was induced by the addition of 1 µg/ml tetracycline (Life Technologies) to the culture media for 24 hours. The resulting cell line, named HuH-7/tetR/HA-nsp2-3GFP, was transduced with lentivirus particles made with the pLentiCrisprv2 vector with guide RNA's targeting viperin or PLSCR1. All lentivirus transduced cells were maintained as polyclonal cell pools to avoid clonal differences

between control cell lines and knock-outs after serial transductions and selections, which could potentially delude the results. Cells were passaged at least 10 times before use in experiments to avoid lingering innate immune responses due to lentiviral transduction.

Western Blotting

Samples were lysed directly in 2x Laemmli sample buffer (50 mM Tris-HCl, pH 6.8; 20% (v/v) glycerol; 4% (w/v) sodium dodecyl sulfate (SDS); 20 mM dithiothreitol; 0.02 mg/ml bromophenol blue) and separated on SDS-polyacrylamide gels. Samples were transferred to PVDF membranes (Amersham) using a Trans-Blot Turbo Transfer System (Bio-Rad) and blocked with 5% (w/v) ELK (Campina) in phosphate buffered saline (PBS) supplemented with 0.05% Tween-20. After incubation with specific antibodies, signal was visualized using ECL Plus Western Blotting Substrate (Thermo-Fisher).

Immunofluorescence microscopy

Cells were grown on coverslips and fixed after 24 hours of tetracycline and/or IFN-β treatment, or 12 hours post infection (h p.i.) with 3% (w/v) paraformaldehyde (PFA) in PBS. After permeabilization in 0.2% (v/v) Triton X-100, coverslips were incubated with antibodies diluted in 5% (w/v) bovine serum albumin (BSA). Nuclei were visualized using 1 µg/ml Hoechst 33258 and samples were embedded using Prolong Gold (Life technologies). Samples were visualized using confocal laser scanning microscopy with a Leica TCS SP8 microscope, which was equipped with a 63x objective (NA 1.40; 1 Airy Unit) and a Leica HyD hybrid detector.

Flow cytometry

Cells were harvested using trypsin after 24 hours of tetracycline and/or IFN-β treatment and fixed in suspension in 3% (w/v) PFA in PBS. Cells were then washed with PBS and stored in PBS with 1% (w/v) BSA until analysis. Intracellular GFP levels were measured on a BD FACSCalibur and data was analyzed using Flowjo software (Flowjo Enterprise).

Reverse transcriptase quantitative real-time PCR

RNA was isolated from cells using the Nucleospin RNA kit (Machery Nagel) and converted into cDNA using RevertAid First Strand cDNA Synthesis Kit (Thermo) using Oligo(dT) 18 primers. Quantitative real-time PCR was performed using iQ SYBR green supermix (Bio-Rad) and a CFX384 Real-Time PCR detection system (Bio-Rad). Gene-specific primers were used to amplify interferon-stimulated genes as well as β-actin and GAPDH as reference genes (Table S1).

Electron microscopy

To compare in detail the DMS induced in the HuH-7/tetR/HA-nsp2-3GFP cell line with those present in EAV-infected HuH-7 cells, high-pressure frozen and freeze-substituted samples of both conditions were prepared and analyzed by electron tomography as described previously (180). All the samples used for quantifications in this study were fixed in 1.5%

(w/v) glutaraldehyde in 0.10 M cacodylate buffer (pH 7.4) for 1 hour at room temperature. After washing with 0.14 M cacodylate buffer, samples were post-fixed and stained with 1% (w/v) osmium tetroxide in 0.10 M cacodylate buffer for 1 hour at 4°C. Following subsequent washing with 0.14 M cacodylate buffer and milli-Q water cells were scraped and spun down in heated 3% (w/v) agar in PBS. After solidification, cell pellets were excised and cut into small blocks, dehydrated in increasing concentrations of ethanol, and embedded in an epoxy resin (LX-112, Ladd research). After polymerization, 100 nm sections were cut from the blocks and placed on mesh-100 electron microscopy grids, post-stained with 7% (w/v) uranyl acetate and Reynolds lead citrate and analyzed using a FEI Tecnai 12 BioTwin equipped with an Eagle cooled slow-scan charge-coupled device (CCD) camera (FEI). Mosaic maps were generated as previously described (330) at 6800x magnification and binning 2, which corresponded to a pixel size of 3.2 nm.

Quantification and statistical analysis

Mosaic maps of several meshes (approximately 170 µm x 170 µm per mesh) of an EM grid were analyzed for each sample. Cell profiles that were positive for arterivirus-associated DMS, cell profiles positive for double-membrane sheets, as well as cell profiles that contained a nucleus were annotated and counted using Aperio ImageScope software (Leica). Data of 3-4 meshes were combined and compared to parallel control samples. Datasets from individual experiments (e.g. control and IFN-β treated) were randomized prior to manual annotation to avoid detection bias. Statistical analysis of individual experiments was performed either using a chi-square test (one degree of freedom) comparing the ratios in different conditions of cell profiles positive for DMS (DMS+) over the total number of cell profiles containing a nucleus or the fraction of cell profiles containing double-membrane sheets out of all DMS+ cell profiles. Statistical analysis of replicate experiments was performed with an unpaired student's *t*-test.

Data availability

One mosaic map of each condition used in this study is available at the DANS data repository as an example (http://dx.doi.org/10.17026/dans-zku-4cgy).

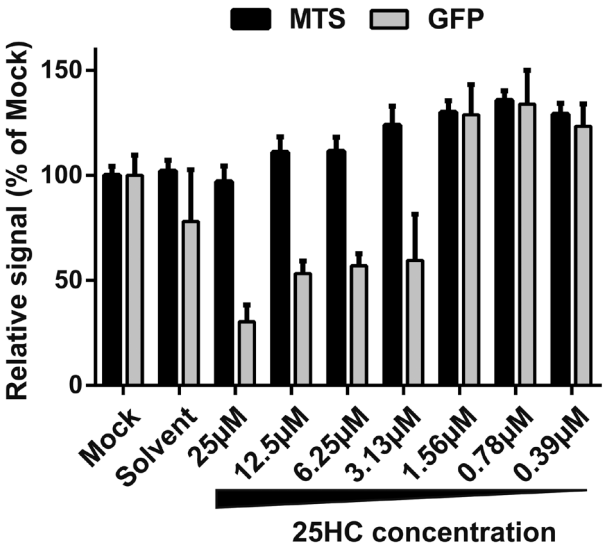


Fig. S1. EAV replication is affected by 25HC treatment. *HuH-7 cells were infected with EAV-GFP and from 1 hour after infection onwards cells were treated with the indicated concentrations of 25-hydroxy cholesterol (25HC). At 20 h p.i., cells were fixed and GFP levels determined. A non-infected control plate was used for a cell viability assay (MTS) performed at the time of fixation to check for cytotoxicity of 25HC treatment. 25HC treatment was verified with RT-qPCR of SREBF2. Error bars represent the standard deviation of quadruplets.*

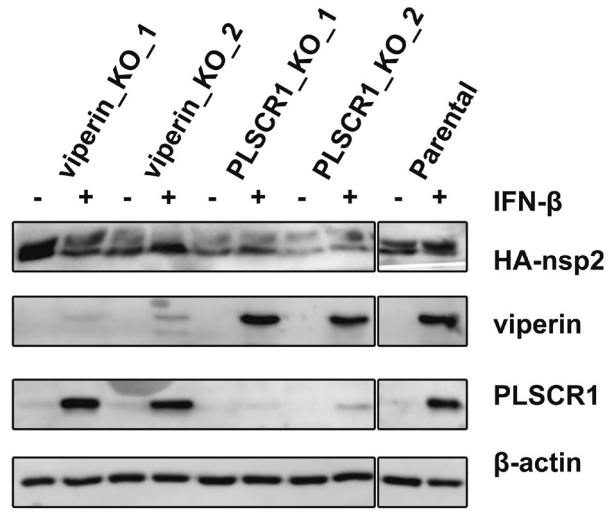


Fig. S2. CRISPR/Cas9 mediated knock-out of viperin and PLSCR1. *Protein expression of genes targeted using CRISPR/Cas9 was analyzed using western blotting. Expression of nsp2-3 was induced in all cells using 1 μg/ml tetracycline for 24 hours and samples were treated with 500 U/ml IFN-β as indicated. Two different guide RNAs targeting both ISGs were used, each leaving very little residual expression in the polyclonal cell pool. The cell pool with the lowest level of residual expression was used for EM analysis.*

CRISPR/Cas9 guide RNA's		
Target	Guide RNA #1	Guide RNA #2
Viperin	TGTCATTAATCGTTTCAACG	ATTGCTCACGATGCTCACGC
PLSCR1	TGTGTTGTGTGCAGCTGTTG	TGCTGTACCCGAAATTGCTG
RT-qPCR primers		
Target	Forward primer	Reverse primer
Actin	AGGCACCAGGGCGTGAT	GCCCACATAGGAATCCTTCTGAC
GAPDH	GCAAATTTCCATGGCACCGT	GCCCCACTTGATTTTGGAGG
Viperin	GAGCGCCACAAAGAAGTGTC	CCAGGATGGACTTGGAAGGG
PLSCR1	CCTCAGTATCCACCGACAGC	ACTGGCTGATTTGGGACAGG
CH25H	CATGCTGGTAGAGGGTCTGC	GATCCACCCTGACTTCTCGC
SREBF2	TCCAAAGCCTGGTGACATCC	TGTACTGTCTGCACCTGCTG

Table S1. Overview of primers and guide-RNA's used for RT-qPCR and CRISPR/Cas9.

Chapter 7

General discussion

DMV FORMATION OF ARTERIVIRUSES AND CORONAVIRUSES

The studies described in this thesis provide new insights regarding the biogenesis of nidovirus replication organelles (**Chapters 3-4**) as well as the cellular response to these unique membrane structures (**Chapter 6**). In **Chapter 3**, using EM and ET techniques, the formation of arterivirus ROs was investigated, both during EAV infection and in cell lines that express membrane-spanning viral nsps. Importantly, the DMVs formed after expression of EAV nsp2 and nsp3 (nsp2-3) share the same 3D membrane architecture as those formed during EAV infection. Moreover, co-expression of the EAV transmembrane protein nsp5 with nsp2-3 altered the size of the induced DMVs, but not their overall morphology, suggesting a regulatory rather than a "structural" role for nsp5 in DMV biogenesis. Also for the betacoronaviruses MERS-CoV and SARS-CoV, the expression of just two non-structural proteins (nsp3 and nsp4) suffices to induce the formation of DMVs (**Chapter 4**), whereas co-expressing the third transmembrane nsp (nsp6) did not seem to alter DMV morphology.

Using EM and ET, numerous membrane structures that provide novel insights into arterivirus and coronavirus DMV biogenesis were observed. In cells expressing EAV nsp2-3 or MERS-CoV nsp3-4, as well as in EAV-infected cells, we observed the accumulation of extensive double-membrane sheets, which we interpret as an intermediate stage of DMV biogenesis via an enwrapping mechanism (**Chapter 2**, Fig. 5). Double-membrane sheets were also found to accumulate when EAV nsp2-3 expressing cells were treated with IFN-β, which reduced the number of DMV positive cell profiles by about 27 percent. Assuming that IFN-β treatment somehow stalls or slows down DMV formation, this could be taken as additional support for double-membrane sheets being an intermediate stage in DMV biogenesis (**Chapter 6**). It should be noted though that both proposed mechanistic models for DMV formation, enwrapping and double-budding, would require the same fundamental membrane remodeling steps, albeit in a different order, and that in EAV-infected cells we also observed some structures that could be intermediates compatible with the double-budding model. The frequent observation of double-membrane sheets in different experimental setups suggests that enwrapping is a key mechanism for DMV biogenesis. Thus far, infected cells have been studied using ET for three other DMV-forming +RNA viruses, two picornaviruses (poliovirus and coxsackievirus B3 (CVB3)) and hepatitis C virus (HCV) (23, 56, 65). In the case of picornaviruses DMVs are formed later in infection and they are thought to arise by enwrapping of single-membrane tubules that are induced earlier during the infection, at the peak of RNA replication (56, 65). How the DMVs in HCV-infected cells are formed is currently unclear. One important distinction between nidovirus DMVs and those of picornaviruses and HCV is that in the case of those latter viruses the DMV interior occasionally was found to be connected to the cytosol. Although enwrapping may be a general mechanism for DMV biogenesis, the observed differences in terms of cytosolic connections could reflect fundamental differences that exist between different virus groups.

The findings in **Chapters 3 and 4** revealed striking similarities between DMV formation in cells infected with arteriviruses and coronaviruses. The nsps required for DMV

formation, arterivirus nsp2-3 and coronavirus nsp3-4, respectively, share a remarkable number of properties, despite considerable size differences (800-1400 amino acids (aa) in arteriviruses versus 2100-2500 aa in coronaviruses). First, their position in the viral replicase polyprotein, just upstream of the main protease, is comparable (see also **Chapter 2**, Fig. 1) (78, 344). The (predicted) membrane topology of arterivirus nsp2-3 and coronavirus nsp3-4 is similar as well. For example, arterivirus nsp2 and coronavirus nsp3 are mainly cytosolic. Furthermore, both arterivirus nsp3 and coronavirus nsp4 span the membrane four times, with the first transmembrane helix being adjacent to the N-terminal cleavage site and both proteins having two luminal domains, the N-terminal of which is the largest. Apart from their relative position in the polyprotein and membrane topology, they share some functional characteristics as well. Both arterivirus nsp2 and coronavirus nsp3 contain a papain-like protease (PLP) domain that processes the polyprotein junction at their C-terminus. Interestingly, although they belong to different protease classes (165, 190, 345, 346), both arterivirus PLP2 and coronavirus PLpro can also function as deubiquitinating enzyme (DUB) in order to inhibit type I IFN production, presumably by cleaving ubiquitin chains from cellular proteins, such as innate immune factors (165, 313, 347-350).

As described in **Chapters 3 and 4** of this thesis, nsp2-3 of EAV and nsp3-4 of both MERS-CoV and SARS-CoV also share the ability to induce DMV formation, adding another functional similarity between these distantly related proteins. Whether the roles of the third transmembrane protein in each virus (arterivirus nsp5 and coronavirus nsp6, respectively) are similar as well is still unclear. Findings in **Chapter 3** show that co-expression of EAV nsp5 (when present in a nsp5-7 precursor, as in infected cells (84)) can reduce DMV size. Although a role for arterivirus nsp6 and/or nsp7 in DMV formation cannot be formally excluded, the very hydrophobic nature of nsp5 suggests that it is this subunit that is responsible for the observed effects. MERS-CoV nsp6 did not affect DMV formation or size when it was co-expressed with nsp3-4 as an individual subunit. However, when MERS-CoV polyproteins encompassing the nsp3-6 region were expressed, polyprotein processing was found to be severely affected. In those nsp3-6 polyproteins, cleavage of the nsp3/4 junction remained intact, but the nsp4/5 and nsp5/6 cleavages were impaired. DMV formation was also impaired in those experiments, with cells showing the formation of elaborate cubic membranes (**Chapter 4**, Fig. 4), which can form for several reasons, including protein misfolding and/or overexpression of ER proteins leading to aggregates (193). Given the large impact of blocking the cleavage of the nsp3/4 junction on DMV formation (**Chapter 4**, Fig. 5), it is conceivable that impairment of the nsp4/5 cleavage could be equally sufficient to prevent DMV formation, and trigger cubic membrane formation instead. Expression of nsp3-5 polyproteins in which either M^{pro} in nsp5 is inactivated or the nsp4/5 junction is mutated may provide an answer to the question what triggers the formation of cubic membranes instead of DMVs. It is currently still unclear whether in infected cells MERS-CoV nsp6 is (mainly) present as a fully processed nsp or in the form of long-lived polyprotein fragments. In case of the latter, those processing intermediates could play a role in the formation of DMVs or the other types of membranous structures observed during coronavirus infection. So far, nsp6 has only been detected in infected cell lysates (by western blotting) for the

betacoronavirus mouse hepatitis virus (MHV) (184). In that case, nsp6 was observed as two distinct protein bands (23 and 27 kDa), suggesting either a post-translational modification, or perhaps the existence of a long-lived nsp6-7 precursor, given the relatively small size of nsp7. Moreover, also an nsp4-10 precursor was readily detected for MHV (184). Determining which membrane structures contain coronavirus nsp6, *e.g.* by immuno EM, should provide more insight and may help to clarify whether nsp6 plays a role in coronavirus RO formation.

Expression of multiple proteins as a large polyprotein is a very common strategy among +RNA viruses. Proteolytic processing of these precursors into smaller fragments is often tightly coordinated and can be directly related to subunit functionality, as was evident from interfering with the cleavage of the nsp3/4 junction in the case of MERS-CoV (**Chapter 4**). Other examples include the role of polyprotein cleavage in the temporal regulation of alphavirus replication (351, 352), and the decreased efficiency of DMV formation by HCV proteins after acceleration of the cleavage at the NS4B/NS5A junction (39). In the latter case, a clear relationship was observed between membrane structure formation and the degree of polyprotein cleavage. A similar functional requirement for cleavage(s) may also explain the existence of two distinct polyprotein processing pathways, as they are observed both in EAV-infected cells and pp1a expression systems (84). These processing pathways mainly differ with respect to the cleavage of either the N-terminal or the C-terminal junction of nsp5. The latter subunit may thus act as a membrane anchor for different adjacent nsps, a feature that may also play a role in RO biogenesis.

INNATE IMMUNE RESPONSES TARGETING DMVS

Whether cells have the means to counteract the hijacking of cellular membranes by +RNA viruses was explored for EAV in **Chapter 6**. Treatment of cells expressing EAV nsp2-3 with IFN-β resulted in a decrease of the fraction of cells showing double-membrane structures, leading to the general conclusion that the type I IFN response can indeed impair the formation of arterivirus ROs. Moreover, large numbers of double-membrane sheets accumulated in IFN-β-treated cells, adding to the notion that these may be intermediates of DMV biogenesis. Interestingly, for HCV at least one ISG has already been shown to affect DMV formation (326). This concerns CH25H, a host factor that could however not be linked to EAV DMV biogenesis (**Chapter 6**) suggesting the existence of multiple mechanisms by which the innate immune response targets the formation of ROs by different viruses. Also two other ISGs (PLSCR1 and viperin) that exert their antiviral effects through affecting lipid metabolism were found not to be involved in impairing EAV DMV formation (**Chapter 6**). **Chapter 6** briefly discusses possible future approaches to unravel the mechanism underlying the inhibition of DMV formation by IFN-β treatment, including a hypothesis pertaining to LC3-mediated tagging of aberrant intracellular membrane structures and the effector function of immunity-related GTPases (336, 337). Below I will outline two other hypotheses by which the innate immune response could inhibit RO formation and suggest approaches for future studies.

Could the membranes of viral ROs function as a PAMP?

The host cell's effector mechanism that inhibits DMV formation likely depends on recognition of a pathogen-associated molecular pattern (PAMP). One possibility would be that the innate immune system targets the tightly apposed membranes that are so typical of this class of viral RO structures. Another attractive option is that this pattern finds its basis in the lipid composition of the RO membranes. For example, for several +RNA viruses the phosphatidylinositol 4-kinases have been identified as important host factors in their replication (42-44), which are thought to drive the accumulation of phosphatidylinositol 4-phosphate (PI4P) lipids at sites of RO formation. Detection of increased local levels of PI4P lipids by the innate immune system could thus activate a cellular effector mechanism. Such 'membrane-associated' PAMPs could be what is recognized and/or targeted by the innate immune system to impair DMV formation. The observation that DMV formation by expression of nsp2-3 did not induce the production of IFN-β (**Chapter 6**) suggests that EAV nsp2-3 induced DMVs do not function as such PAMPs. However, it could very well be that this type of membrane-associated PAMP is only involved in effector mechanisms of the innate immune response, and not during the initial sensing of infection, as those molecular patterns also play important roles in normal cellular metabolism. For example, the formation of double membranes is a central part of the autophagy pathway (353) and PI4P lipids play a key role in several cellular signaling events (354). Recognition of such elements by the innate immune response during normal cell homeostasis would likely be detrimental for the cell in the absence of viral infection, but during an antiviral state induced by type I interferon it might be beneficial to antagonize such mechanisms to inhibit virus replication.

An innate immune effector mechanism targeting such membrane-associated PAMPs could either be activated to inhibit other players in virus replication (e.g. viral proteins or RNA), or target the membranes directly. The antiviral state induced by the innate immune response not only targets virus replication directly, but also greatly alters cellular metabolism to limit virus replication, which in turn could influence the integrity of viral ROs (355). A lipidomics approach using membrane fractions of cells expressing EAV nsp2-3 (or EAV-infected cells) with or without IFN-β treatment, could provide insight into changes in the lipid composition of RO membranes. Such changes could be the result of an innate effector mechanism directly targeting the RO membrane. Chemical compounds or inactivation of genes involved in lipid metabolism could then be used in attempts to mimic the effect of IFN-β treatment on specific parts of lipid metabolism, in order to determine whether such changes indeed play a role in antagonizing DMV formation.

Does ubiquitin play a role in the innate immune response targeted at ROs?

Interestingly, the PLP2-DUB protease in EAV nsp2 has been shown to have immune evasive activity (338). When EAV PLP2 was mutated in the virus in a way that prevented ubiquitin binding without affecting nsp2-3 cleavage (which is essential for infection), this resulted in increased IFN-β production in infected primary cells (165). The decreased in number of cell sections displaying double-membrane structures and the morphological changes

occurring after IFN-β treatment were, although consistently observed, rather modest (**Chapter 6**; Figs 4, 6). This could be interpreted as only limited support for the inhibitory effect of IFN signaling on RO formation in the infected cell or organism. It is however important to realize that viruses in general exhibit multiple activities that counteract or evade the antiviral responses of the cell.

The presence of a DUB in arterivirus nsp2 (and coronavirus nsp3) could also help to evade innate immune effector responses that target membrane structure formation if these would rely on post-translational modifications involving ubiquitin or ubiquitin-like modifiers. The cell could inhibit DMV formation by flagging relevant viral proteins involved with specific ubiquitin chain types (or ubiquitin-like modifiers), to either degrade them or inhibit their function. Such tagging could also result in the degradation of induced membrane structures containing these flagged proteins. This could resemble the use of ubiquitin as a flag in the degradation of intracellular bacteria by selective autophagy (139), or the labeling of aberrant membrane structures with LC3 to degrade them via immunity related GTPases (discussed in **Chapter 6**) (336, 337). On the other hand, the double-membrane sheets that are induced by EAV nsp2-3 expression after IFN-β treatment suggest that a block in DMV biogenesis is a more likely explanation for this phenomenon than the enhanced degradation of already formed structures.

The DUB function of EAV PLP2 might obviously counteract mechanisms as outlined in the previous paragraph, although apparently not in full as IFN-β treatment still interfered with the DMV formation induced by expression of EAV nsp2-3 containing an active PLP2-DUB (**Chapter 6**). To further test the role of the DUB activity in the context of the innate immune response against DMV formation, several cell lines inducibly expressing nsp2-3GFP carrying a DUB knock-out mutation (T312A/I313V/I353R) in PLP2 were created (165), in order to evaluate the effect of IFN-β treatment on DMV formation compared to the wild-type nsp2-3 construct (**Chapter 6**). If ubiquitin-based signaling would be involved and EAV PLP2 can no longer remove ubiquitin chains from nsp2-3, the observed effects of IFN-β treatment on DMV formation should become much more severe. In each of those cell lines nsp2-3GFP-DUB k/o expression levels decreased after IFN-β treatment, unlike what was observed in cell expressing the wild-type nsp2-3 (Fig. 1). This may have resulted from a decrease in transcription and/or translation of nsp2-3GFP mRNA; however, as the decrease was observed only upon expression of the DUB k/o construct, this data suggests that nsp2-3 was indeed directly targeted for ubiquitin-dependent degradation after IFN-β treatment. Due to the DUB function of nsp2 this was likely counteracted when expressing wild-type nsp2-3, resulting in unchanged nsp2-3 protein levels after IFN-β treatment.

The effect on nsp2-3 levels of mutations that knock out the PLP2-DUB function renders nsp2-3 DUB knock-out cell lines unsuitable for the kind of EM analysis used in **Chapter 6**. Any direct effect of IFN-β treatment on membrane structures, as observed in the wild-type nsp2-3-expressing cells, would be impossible to separate from the reduced or impaired formation of membrane structures that could simply result from the lower nsp2-3 expression level in DUB knock-out nsp2-3-producing cells treated with IFN-β. Determining the reason for this decrease could provide further insight into the innate immune response

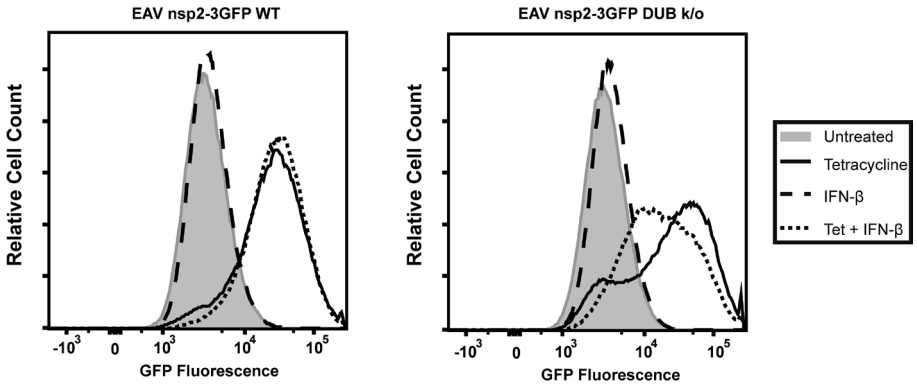


Fig. 1. EAV nsp2-3GFP DUB k/o protein levels decrease after IFN-β treatment. *HuH-7/tetR/HA-nsp2-3GFP (either wildtype PLP2 or the DUB k/o (T312A/I313V/I353R) (165)) cells were analyzed by flow cytometry after 24 hours of indicated treatments. For further experimental details, see methods section of* **Chapter 6**.

targeting DMV formation. One ISG that might be involved in this effect is ISG12a, which is an adapter for the SKP2 ubiquitin ligase and was shown to target HCV NS5A (one of the trans-membrane proteins required for HCV DMV formation) for degradation by K48 linked ubiquitination (356). If EAV nsp2-3 is indeed targeted directly by ISG12a (or any other ISG), mutating the lysine(s) targeted for ubiquitination in the nsp2-3 DUB knock-out construct could help reveal ubiquitin-dependent mechanisms involved in the inhibition of DMV formation.

CONCLUDING REMARKS

+RNA virus replication organelles have been an intriguing research topic over the last decades. Significant efforts were made to characterize the architecture and biogenesis of these membrane structures, which appear to be at the hub of cytoplasmic replication of +RNA viruses. Multiple hypotheses and models have been postulated regarding the structure-function relationships and design of replication organelles. For spherule-forming viruses, such models are relatively simple. Spherules by default provide a semi-closed compartment for efficient RNA replication, presumably away from RNA sensors such as RIG-I and MDA5, and newly synthesized genomes can exit through the relatively narrow openings that connect these compartments with the cytoplasm. For some DMV-forming viruses, such as HCV and picornaviruses, openings between the interior of some of their DMVs and the cytosol have been described. This provides a basis for a similar structure-function model, although the timeline of RO morphogenesis in general, and the appearance of open and closed structures in particular, remains to be investigated in more detail. Moreover, in the case of picornaviruses, DMV formation was most pronounced only after

the exponential phase of viral RNA replication (56, 65), raising the question whether DMVs actually have a key role in RNA replication in the first place.

The closed nature of nidovirus DMVs still confounds theories easily applicable to other +RNA viruses. The interior of arterivirus and coronavirus DMVs labels strongly for double-stranded RNA (20, 21), similar to what has been observed for other +RNA viruses. Recent EM studies (M. Bárcena *et al.*, personal communication) show that RNA replication is predominantly associated with DMVs, expanding the enigma of these closed vesicles. If the interior of closed DMVs is the site of replication, then newly made genomes and mRNAs, which need to be transported to the cytosol for translation and encapsidation, would either have to be translocated across two membranes through a protein channel or be released when a DMV would open up. Alternatively, virus replication could take place on the cytosolic face of the DMV outer membrane. In that scenario, however, most of the postulated benefits of compartmentalization and shielding of RNA replication intermediates inside vesicular structures would likely be minimal. Replication could also take place on both sides of the double membrane, but in that case RNA synthesis occurring on the inside would seem pointless if DMVs would remain closed.

Despite two decades of research on nidovirus-induced ROs, it remains very difficult to assess how important the reorganization of ER membranes, specifically into DMVs, really is. In some recent studies, the number of DMVs formed during coronavirus replication did not correlate very well with the efficiency of RNA replication, viral fitness, or pathogenesis (131, 357). On the other hand, our finding that the innate immune response targets DMV formation is promising, and suggests that membrane structure formation is a relevant step during virus infection that is "worth counteracting". Moreover, the knowledge gained on the viral proteins involved in arterivirus and coronavirus DMV formation will help to identify host factors involved in RO biogenesis, which in turn may aid to unravel why nidoviruses induce the formation of such extensive and unique membrane structures in infected cells.

REFERENCES

1. Zirkel F, Roth H, Kurth A, Drosten C, Ziebuhr J, Junglen S. 2013. Identification and characterization of genetically divergent members of the newly established family Mesoniviridae. Journal of virology 87:6346-6358.
2. Gorbalenya AE, snijder EJ, Cowley JA, Ziebuhr J, Faaberg K, Enjuanes L, Rottier PJ, de Groot RJ, Perlman S. 2011. Virus Taxonomy: The Classification and Nomenclature of Viruses – The 9th Report of the ICTV. Elsevier.
3. Lauber C, Goeman JJ, Parquet Mdel C, Nga PT, Snijder EJ, Morita K, Gorbalenya AE. 2013. The footprint of genome architecture in the largest genome expansion in RNA viruses. PLoS pathogens 9:e1003500.
4. Snijder EJ, Kikkert M, Fang Y. 2013. Arterivirus molecular biology and pathogenesis. The Journal of general virology 94:2141-2163.
5. Bryans JT, Crowe ME, Doll ER, McCollum WH. 1957. Isolation of a filterable agent causing arteritis of horses and abortion by mares; its differentiation from the equine abortion (influenza) virus. The Cornell veterinarian 47:3-41.
6. Balasuriya UB, Go YY, MacLachlan NJ. 2013. Equine arteritis virus. Veterinary microbiology 167:93-122.
7. Neumann EJ, Kliebenstein JB, Johnson CD, Mabry JW, Bush EJ, Seitzinger AH, Green AL, Zimmerman JJ. 2005. Assessment of the economic impact of porcine reproductive and respiratory syndrome on swine production in the United States. J Am Vet Med Assoc 227:385-392.
8. Han J, Zhou L, Ge X, Guo X, Yang H. 2017. Pathogenesis and control of the Chinese highly pathogenic porcine reproductive and respiratory syndrome virus. Veterinary microbiology.
9. Lunney JK, Fang Y, Ladinig A, Chen N, Li Y, Rowland B, Renukaradhya GJ. 2016. Porcine Reproductive and Respiratory Syndrome Virus (PRRSV): Pathogenesis and Interaction with the Immune System. Annu Rev Anim Biosci 4:129-154.
10. van Dinten LC, den Boon JA, Wassenaar AL, Spaan WJ, Snijder EJ. 1997. An infectious arterivirus cDNA clone: identification of a replicase point mutation that abolishes discontinuous mRNA transcription. Proceedings of the National Academy of Sciences of the United States of America 94:991-996.
11. Ge XY, Li JL, Yang XL, Chmura AA, Zhu G, Epstein JH, Mazet JK, Hu B, Zhang W, Peng C, Zhang YJ, Luo CM, Tan B, Wang N, Zhu Y, Crameri G, Zhang SY, Wang LF, Daszak P, Shi ZL. 2013. Isolation and characterization of a bat SARS-like coronavirus that uses the ACE2 receptor. Nature 503:535-538.
12. Zaki AM, van Boheemen S, Bestebroer TM, Osterhaus AD, Fouchier RA. 2012. Isolation of a novel coronavirus from a man with pneumonia in Saudi Arabia. The New England journal of medicine 367:1814-1820.
13. de Wit E, van Doremalen N, Falzarano D, Munster VJ. 2016. SARS and MERS: recent insights into emerging coronaviruses. Nature reviews. Microbiology 14:523-534.
14. Graham RL, Donaldson EF, Baric RS. 2013. A decade after SARS: strategies for controlling emerging coronaviruses. Nature reviews. Microbiology 11:836-848.
15. Zumla A, Chan JF, Azhar EI, Hui DS, Yuen KY. 2016. Coronaviruses – drug discovery and therapeutic options. Nature reviews. Drug discovery 15:327-347.
16. Angelini MM, Neuman BW, Buchmeier MJ. 2014. Untangling membrane rearrangement in the *nidovirales*. DNA and cell biology 33:122-127.
17. den Boon JA, Diaz A, Ahlquist P. 2010.

Cytoplasmic viral replication complexes. Cell host & microbe 8:77-85.

18. Miller S, Krijnse-Locker J. 2008. Modification of intracellular membrane structures for virus replication. Nature reviews. Microbiology 6:363-374.
19. Romero-Brey I, Bartenschlager R. 2016. Endoplasmic Reticulum: The Favorite Intracellular Niche for Viral Replication and Assembly. Viruses 8.
20. Knoops K, Barcena M, Limpens RW, Koster AJ, Mommaas AM, Snijder EJ. 2012. Ultrastructural characterization of arterivirus replication structures: reshaping the endoplasmic reticulum to accommodate viral RNA synthesis. Journal of virology 86:2474-2487.
21. Knoops K, Kikkert M, Worm SH, Zevenhoven-Dobbe JC, van der Meer Y, Koster AJ, Mommaas AM, Snijder EJ. 2008. SARS-coronavirus replication is supported by a reticulovesicular network of modified endoplasmic reticulum. PLoS biology 6:e226.
22. Maier HJ, Hawes PC, Cottam EM, Mantell J, Verkade P, Monaghan P, Wileman T, Britton P. 2013. Infectious bronchitis virus generates spherules from zippered endoplasmic reticulum membranes. mBio 4:e00801-00813.
23. Romero-Brey I, Merz A, Chiramel A, Lee JY, Chlanda P, Haselman U, Santarella-Mellwig R, Habermann A, Hoppe S, Kallis S, Walther P, Antony C, Krijnse-Locker J, Bartenschlager R. 2012. Three-dimensional architecture and biogenesis of membrane structures associated with hepatitis C virus replication. PLoS pathogens 8:e1003056.
24. Snijder EJ, van Tol H, Roos N, Pedersen KW. 2001. Non-structural proteins 2 and 3 interact to modify host cell membranes during the formation of the arterivirus replication complex. The Journal of general virology 82:985-994.
25. Suhy DA, Giddings TH, Jr., Kirkegaard K. 2000. Remodeling the endoplasmic reticulum by poliovirus infection and by individual viral proteins: an autophagy-like origin for virus-induced vesicles. Journal of virology 74:8953-8965.
26. Salonen A, Vasiljeva L, Merits A, Magden J, Jokitalo E, Kaariainen L. 2003. Properly folded nonstructural polyprotein directs the semliki forest virus replication complex to the endosomal compartment. Journal of virology 77:1691-1702.
27. Schwartz M, Chen J, Janda M, Sullivan M, den Boon J, Ahlquist P. 2002. A positive-strand RNA virus replication complex parallels form and function of retrovirus capsids. Molecular cell 9:505-514.
28. Angelini MM, Akhlaghpour M, Neuman BW, Buchmeier MJ. 2013. Severe acute respiratory syndrome coronavirus nonstructural proteins 3, 4, and 6 induce double-membrane vesicles. mBio 4.
29. Bowie AG, Unterholzner L. 2008. Viral evasion and subversion of pattern-recognition receptor signalling. Nature reviews. Immunology 8:911-922.
30. Gurtler C, Bowie AG. 2013. Innate immune detection of microbial nucleic acids. Trends in microbiology 21:413-420.
31. Yoneyama M, Onomoto K, Jogi M, Akaboshi T, Fujita T. 2015. Viral RNA detection by RIG-I-like receptors. Current opinion in immunology 32:48-53.
32. Sancho-Shimizu V, Perez de Diego R, Jouanguy E, Zhang SY, Casanova JL. 2011. Inborn errors of anti-viral interferon immunity in humans. Current opinion in virology 1:487-496.
33. Chan YK, Gack MU. 2016. Viral evasion of intracellular DNA and RNA sensing. Nature reviews. Microbiology 14:360-373.
34. Nielsen R, Bustamante C, Clark AG, Glanowski S, Sackton TB, Hubisz MJ, Fledel-Alon A, Tanenbaum DM, Civello D, White TJ, J JS, Adams MD, Cargill M. 2005. A scan for positively selected genes in the genomes of humans and chim-

panzees. PLoS biology 3:e170.

35. Paul D, Bartenschlager R. 2013. Architecture and biogenesis of plus-strand RNA virus replication factories. World journal of virology 2:32-48.
36. Romero-Brey I, Bartenschlager R. 2014. Membranous replication factories induced by plus-strand RNA viruses. Viruses 6:2826-2857.
37. Neufeldt CJ, Joyce MA, Van Buuren N, Levin A, Kirkegaard K, Gale M, Jr., Tyrrell DL, Wozniak RW. 2016. The Hepatitis C Virus-Induced Membranous Web and Associated Nuclear Transport Machinery Limit Access of Pattern Recognition Receptors to Viral Replication Sites. PLoS pathogens 12:e1005428.
38. Egger D, Wolk B, Gosert R, Bianchi L, Blum HE, Moradpour D, Bienz K. 2002. Expression of hepatitis C virus proteins induces distinct membrane alterations including a candidate viral replication complex. Journal of virology 76:5974-5984.
39. Romero-Brey I, Berger C, Kallis S, Kolovou A, Paul D, Lohmann V, Bartenschlager R. 2015. NS5A Domain 1 and Polyprotein Cleavage Kinetics Are Critical for Induction of Double-Membrane Vesicles Associated with Hepatitis C Virus Replication. mBio 6:e00759.
40. Nagy PD, Pogany J. 2012. The dependence of viral RNA replication on co-opted host factors. Nature reviews. Microbiology 10:137-149.
41. Belov GA, van Kuppeveld FJ. 2012. (+)RNA viruses rewire cellular pathways to build replication organelles. Current opinion in virology 2:740-747.
42. Reiss S, Rebhan I, Backes P, Romero-Brey I, Erfle H, Matula P, Kaderali L, Poenisch M, Blankenburg H, Hiet MS, Longerich T, Diehl S, Ramirez F, Balla T, Rohr K, Kaul A, Buhler S, Pepperkok R, Lengauer T, Albrecht M, Eils R, Schirmacher P, Lohmann V, Bartenschlager R. 2011. Recruitment and activation of a lipid kinase by hepatitis C virus NS5A is essential for integrity of the membranous replication compartment. Cell host & microbe 9:32-45.
43. Berger KL, Kelly SM, Jordan TX, Tartell MA, Randall G. 2011. Hepatitis C virus stimulates the phosphatidylinositol 4-kinase III alpha-dependent phosphatidylinositol 4-phosphate production that is essential for its replication. Journal of virology 85:8870-8883.
44. Hsu NY, Ilnytska O, Belov G, Santiana M, Chen YH, Takvorian PM, Pau C, van der Schaar H, Kaushik-Basu N, Balla T, Cameron CE, Ehrenfeld E, van Kuppeveld FJ, Altan-Bonnet N. 2010. Viral reorganization of the secretory pathway generates distinct organelles for RNA replication. Cell 141:799-811.
45. Diaz A, Ahlquist P. 2012. Role of host reticulon proteins in rearranging membranes for positive-strand RNA virus replication. Current opinion in microbiology 15:519-524.
46. Diaz A, Zhang J, Ollwerther A, Wang X, Ahlquist P. 2015. Host ESCRT proteins are required for bromovirus RNA replication compartment assembly and function. PLoS pathogens 11:e1004742.
47. Barcena M, Koster AJ. 2009. Electron tomography in life science. Seminars in cell & developmental biology 20:920-930.
48. Kopek BG, Perkins G, Miller DJ, Ellisman MH, Ahlquist P. 2007. Three-dimensional analysis of a viral RNA replication complex reveals a virus-induced mini-organelle. PLoS biology 5:e220.
49. Maier HJ, Cottam EM, Stevenson-Leggett P, Wilkinson JA, Harte CJ, Wileman T, Britton P. 2013. Visualizing the autophagy pathway in avian cells and its application to studying infectious bronchitis virus. Autophagy 9:496-509.
50. Welsch S, Miller S, Romero-Brey I, Merz A, Bleck CK, Walther P, Fuller SD, Antony C, Krijnse-Locker J, Bartenschlager R. 2009. Composition and three-dimensional architecture of the dengue virus replication and assembly sites. Cell host & microbe 5:365-375.

51. Gillespie LK, Hoenen A, Morgan G, Mackenzie JM. 2010. The endoplasmic reticulum provides the membrane platform for biogenesis of the flavivirus replication complex. Journal of virology 84:10438-10447.
52. Offerdahl DK, Dorward DW, Hansen BT, Bloom ME. 2012. A three-dimensional comparison of tick-borne flavivirus infection in mammalian and tick cell lines. PloS one 7:e47912.
53. Miorin L, Romero-Brey I, Maiuri P, Hoppe S, Krijnse-Locker J, Bartenschlager R, Marcello A. 2013. Three-dimensional architecture of tick-borne encephalitis virus replication sites and trafficking of the replicated RNA. Journal of virology 87:6469-6481.
54. Junjhon J, Pennington JG, Edwards TJ, Perera R, Lanman J, Kuhn RJ. 2014. Ultrastructural characterization and three-dimensional architecture of replication sites in dengue virus-infected mosquito cells. Journal of virology 88:4687-4697.
55. Fontana J, Lopez-Iglesias C, Tzeng WP, Frey TK, Fernandez JJ, Risco C. 2010. Three-dimensional structure of Rubella virus factories. Virology 405:579-591.
56. Limpens RW, van der Schaar HM, Kumar D, Koster AJ, Snijder EJ, van Kuppeveld FJ, Barcena M. 2011. The transformation of enterovirus replication structures: a three-dimensional study of single- and double-membrane compartments. mBio 2.
57. Cao X, Jin X, Zhang X, Li Y, Wang C, Wang X, Hong J, Wang X, Li D, Zhang Y. 2015. Morphogenesis of Endoplasmic Reticulum Membrane-Invaginated Vesicles during Beet Black Scorch Virus Infection: Role of Auxiliary Replication Protein and New Implications of Three-Dimensional Architecture. Journal of virology 89:6184-6195.
58. Grimley PM, Berezesky IK, Friedman RM. 1968. Cytoplasmic structures associated with an arbovirus infection: loci of viral ribonucleic acid synthesis. Journal of virology 2:1326-1338.
59. Froshauer S, Kartenbeck J, Helenius A. 1988. Alphavirus RNA replicase is located on the cytoplasmic surface of endosomes and lysosomes. The Journal of cell biology 107:2075-2086.
60. Kujala P, Ikaheimonen A, Ehsani N, Vihinen H, Auvinen P, Kaariainen L. 2001. Biogenesis of the Semliki Forest virus RNA replication complex. Journal of virology 75:3873-3884.
61. Frolova EI, Gorchakov R, Pereboeva L, Atasheva S, Frolov I. 2010. Functional Sindbis virus replicative complexes are formed at the plasma membrane. Journal of virology 84:11679-11695.
62. Laliberte JF, Sanfacon H. 2010. Cellular remodeling during plant virus infection. Annual review of phytopathology 48:69-91.
63. Diaz A, Gallei A, Ahlquist P. 2012. Bromovirus RNA replication compartment formation requires concerted action of 1a's self-interacting RNA capping and helicase domains. Journal of virology 86:821-834.
64. Ahlquist P. 2006. Parallels among positive-strand RNA viruses, reverse-transcribing viruses and double-stranded RNA viruses. Nature reviews. Microbiology 4:371-382.
65. Belov GA, Nair V, Hansen BT, Hoyt FH, Fischer ER, Ehrenfeld E. 2012. Complex dynamic development of poliovirus membranous replication complexes. Journal of virology 86:302-312.
66. Ferraris P, Beaumont E, Uzbekov R, Brand D, Gaillard J, Blanchard E, Roingeard P. 2013. Sequential biogenesis of host cell membrane rearrangements induced by hepatitis C virus infection. Cell Mol Life Sci 70:1297-1306.
67. Paul D, Hoppe S, Saher G, Krijnse-Locker J, Bartenschlager R. 2013. Morphological and biochemical characterization of the membranous hepatitis C virus replication compartment. Journal of virology 87:10612-10627.
68. Cowley JA, Dimmock CM, Walker PJ. 2002. Gill-associated nidovirus of Penaeus monodon prawns transcribes 3'-coterminal subgenomic

mRNAs that do not possess 5'-leader sequences. The Journal of general virology 83:927-935.

69. Knoops K, Swett-Tapia C, van den Worm SH, Te Velthuis AJ, Koster AJ, Mommaas AM, Snijder EJ, Kikkert M. 2010. Integrity of the early secretory pathway promotes, but is not required for, severe acute respiratory syndrome coronavirus RNA synthesis and virus-induced remodeling of endoplasmic reticulum membranes. Journal of virology 84:833-846.
70. Cavanagh D. 1997. *Nidovirales*: a new order comprising Coronaviridae and Arteriviridae. Archives of virology 142:629-633.
71. Lauck M, Sibley SD, Hyeroba D, Tumukunde A, Weny G, Chapman CA, Ting N, Switzer WM, Kuhn JH, Friedrich TC, O'Connor DH, Goldberg TL. 2013. Exceptional simian hemorrhagic fever virus diversity in a wild African primate community. Journal of virology 87:688-691.
72. Dunowska M, Biggs PJ, Zheng T, Perrott MR. 2012. Identification of a novel nidovirus associated with a neurological disease of the Australian brushtail possum (Trichosurus vulpecula). Veterinary microbiology 156:418-424.
73. Kuhn JH, Lauck M, Bailey AL, Shchetinin AM, Vishnevskaya TV, Bao Y, Ng TF, LeBreton M, Schneider BS, Gillis A, Tamoufe U, Diffo JL, Takuo JM, Kondov NO, Coffey LL, Wolfe ND, Delwart E, Clawson AN, Postnikova E, Bollinger L, Lackemeyer MG, Radoshitzky SR, Palacios G, Wada J, Shevtsova ZV, Jahrling PB, Lapin BA, Deriabin PG, Dunowska M, Alkhovsky SV, Rogers J, Friedrich TC, O'Connor DH, Goldberg TL. 2015. Reorganization and expansion of the nidoviral family Arteriviridae. Archives of virology.
74. Brierley I, Digard P, Inglis SC. 1989. Characterization of an efficient coronavirus ribosomal frameshifting signal: requirement for an RNA pseudoknot. Cell 57:537-547.
75. den Boon JA, Snijder EJ, Chirnside ED, de Vries AA, Horzinek MC, Spaan WJ. 1991. Equine arteritis virus is not a togavirus but belongs to the coronaviruslike superfamily. Journal of virology 65:2910-2920.
76. Ziebuhr J, Snijder EJ, Gorbalenya AE. 2000. Virus-encoded proteinases and proteolytic processing in the *Nidovirales*. The Journal of general virology 81:853-879.
77. Li Y, Tas A, Sun Z, Snijder EJ, Fang Y. 2014. Proteolytic processing of the porcine reproductive and respiratory syndrome virus replicase. Virus research.
78. Gorbalenya AE, Enjuanes L, Ziebuhr J, Snijder EJ. 2006. *Nidovirales*: evolving the largest RNA virus genome. Virus research 117:17-37.
79. Fang Y, Snijder EJ. 2010. The PRRSV replicase: exploring the multifunctionality of an intriguing set of nonstructural proteins. Virus research 154:61-76.
80. Lehmann KC, Snijder EJ, Posthuma CC, Gorbalenya AE. 2015. What we know but do not understand about nidovirus helicases. Virus research 202:12-32.
81. Lehmann KC, Gulyaeva A, Zevenhoven-Dobbe JC, Janssen GM, Ruben M, Overkleeft HS, van Veelen PA, Samborskiy DV, Kravchenko AA, Leontovich AM, Sidorov IA, Snijder EJ, Posthuma CC, Gorbalenya AE. 2015. Discovery of an essential nucleotidylating activity associated with a newly delineated conserved domain in the RNA polymerase-containing protein of all nidoviruses. Nucleic acids research 43:8416-8434.
82. Gorbalenya AE, Koonin EV, Donchenko AP, Blinov VM. 1989. Coronavirus genome: prediction of putative functional domains in the non-structural polyprotein by comparative amino acid sequence analysis. Nucleic acids research 17:4847-4861.
83. Vatter HA, Di H, Donaldson EF, Radu GU, Maines TR, Brinton MA. 2014. Functional analyses of the three simian hemorrhagic fever virus nonstructural protein 1 papain-like proteases. Journal of

virology 88:9129-9140.

84. Wassenaar AL, Spaan WJ, Gorbalenya AE, Snijder EJ. 1997. Alternative proteolytic processing of the arterivirus replicase ORF1a polyprotein: evidence that NSP2 acts as a cofactor for the NSP4 serine protease. Journal of virology 71:9313-9322.
85. Li Y, Tas A, Snijder EJ, Fang Y. 2012. Identification of porcine reproductive and respiratory syndrome virus ORF1a-encoded non-structural proteins in virus-infected cells. The Journal of general virology 93:829-839.
86. van Aken D, Zevenhoven-Dobbe J, Gorbalenya AE, Snijder EJ. 2006. Proteolytic maturation of replicase polyprotein pp1a by the nsp4 main proteinase is essential for equine arteritis virus replication and includes internal cleavage of nsp7. The Journal of general virology 87:3473-3482.
87. Faaberg KS, Plagemann PG. 1996. Membrane association of the C-terminal half of the open reading frame 1a protein of lactate dehydrogenase-elevating virus. Archives of virology 141:1337-1348.
88. Pedersen KW, van der Meer Y, Roos N, Snijder EJ. 1999. Open reading frame 1a-encoded subunits of the arterivirus replicase induce endoplasmic reticulum-derived double-membrane vesicles which carry the viral replication complex. Journal of virology 73:2016-2026.
89. Posthuma CC, Pedersen KW, Lu Z, Joosten RG, Roos N, Zevenhoven-Dobbe JC, Snijder EJ. 2008. Formation of the arterivirus replication/transcription complex: a key role for nonstructural protein 3 in the remodeling of intracellular membranes. Journal of virology 82:4480-4491.
90. Kappes MA, Miller CL, Faaberg KS. 2015. Porcine reproductive and respiratory syndrome virus nonstructural protein 2 (nsp2) topology and selective isoform integration in artificial membranes. Virology 481:51-62.
91. Snijder EJ, Wassenaar AL, Spaan WJ, Gorbalenya AE. 1995. The arterivirus Nsp2 protease. An unusual cysteine protease with primary structure similarities to both papain-like and chymotrypsin-like proteases. The Journal of biological chemistry 270:16671-16676.
92. Kanjanahaluethai A, Baker SC. 2000. Identification of mouse hepatitis virus papain-like proteinase 2 activity. Journal of virology 74:7911-7921.
93. Ziebuhr J, Thiel V, Gorbalenya AE. 2001. The autocatalytic release of a putative RNA virus transcription factor from its polyprotein precursor involves two paralogous papain-like proteases that cleave the same peptide bond. The Journal of biological chemistry 276:33220-33232.
94. Harcourt BH, Jukneliene D, Kanjanahaluethai A, Bechill J, Severson KM, Smith CM, Rota PA, Baker SC. 2004. Identification of severe acute respiratory syndrome coronavirus replicase products and characterization of papain-like protease activity. Journal of virology 78:13600-13612.
95. Oostra M, te Lintelo EG, Deijs M, Verheije MH, Rottier PJ, de Haan CA. 2007. Localization and membrane topology of coronavirus nonstructural protein 4: involvement of the early secretory pathway in replication. Journal of virology 81:12323-12336.
96. Hagemeijer MC, Monastyrska I, Griffith J, van der Sluijs P, Voortman J, van Bergen en Henegouwen PM, Vonk AM, Rottier PJ, Reggiori F, de Haan CA. 2014. Membrane rearrangements mediated by coronavirus nonstructural proteins 3 and 4. Virology 458-459:125-135.
97. van Dinten LC, Wassenaar AL, Gorbalenya AE, Spaan WJ, Snijder EJ. 1996. Processing of the equine arteritis virus replicase ORF1b protein: identification of cleavage products containing the putative viral polymerase and helicase domains. Journal of virology 70:6625-6633.
98. van der Meer Y, van Tol H, Locker JK, Snijder EJ. 1998. ORF1a-encoded replicase subunits are

involved in the membrane association of the arterivirus replication complex. Journal of virology 72:6689-6698.

99. van Hemert MJ, de Wilde AH, Gorbalenya AE, Snijder EJ. 2008. The *in vitro* RNA synthesizing activity of the isolated arterivirus replication/transcription complex is dependent on a host factor. The Journal of biological chemistry 283:16525-16536.
100. Denison MR, Spaan WJ, van der Meer Y, Gibson CA, Sims AC, Prentice E, Lu XT. 1999. The putative helicase of the coronavirus mouse hepatitis virus is processed from the replicase gene polyprotein and localizes in complexes that are active in viral RNA synthesis. Journal of virology 73:6862-6871.
101. Shi ST, Schiller JJ, Kanjanahaluethai A, Baker SC, Oh JW, Lai MM. 1999. Colocalization and membrane association of murine hepatitis virus gene 1 products and De novo-synthesized viral RNA in infected cells. Journal of virology 73:5957-5969.
102. van der Meer Y, Snijder EJ, Dobbe JC, Schleich S, Denison MR, Spaan WJ, Locker JK. 1999. Localization of mouse hepatitis virus nonstructural proteins and RNA synthesis indicates a role for late endosomes in viral replication. Journal of virology 73:7641-7657.
103. Bost AG, Carnahan RH, Lu XT, Denison MR. 2000. Four proteins processed from the replicase gene polyprotein of mouse hepatitis virus colocalize in the cell periphery and adjacent to sites of virion assembly. Journal of virology 74:3379-3387.
104. Brockway SM, Clay CT, Lu XT, Denison MR. 2003. Characterization of the expression, intracellular localization, and replication complex association of the putative mouse hepatitis virus RNA-dependent RNA polymerase. Journal of virology 77:10515-10527.
105. Prentice E, McAuliffe J, Lu X, Subbarao K, Denison MR. 2004. Identification and characterization of severe acute respiratory syndrome coronavirus replicase proteins. Journal of virology 78:9977-9986.
106. Snijder EJ, van der Meer Y, Zevenhoven-Dobbe J, Onderwater JJ, van der Meulen J, Koerten HK, Mommaas AM. 2006. Ultrastructure and origin of membrane vesicles associated with the severe acute respiratory syndrome coronavirus replication complex. Journal of virology 80:5927-5940.
107. van Hemert MJ, van den Worm SH, Knoops K, Mommaas AM, Gorbalenya AE, Snijder EJ. 2008. SARS-coronavirus replication/transcription complexes are membrane-protected and need a host factor for activity *in vitro*. PLoS pathogens 4:e1000054.
108. Breese SSJ, McCollum WH. 1970. Electron microscopy characterization of equine arteritis virus, p. 133-139. In Bryans JT, Gerber H (ed.), Proceedings of the 2nd International Conference on Equine Infectious Diseases. S. Karger, Basel.
109. Wood O, Tauraso N, Liebhaber H. 1970. Electron microscopic study of tissue cultures infected with simian haemorrhagic fever virus. The Journal of general virology 7:129-136.
110. Stueckemann JA, Ritzi DM, Holth M, Smith MS, Swart WJ, Cafruny WA, Plagemann GW. 1982. Replication of lactate dehydrogenase-elevating virus in macrophages. 1. Evidence for cytocidal replication. The Journal of general virology 59:245-262.
111. Wada R, Fukunaga Y, Kondo T, Kanemaru T. 1995. Ultrastructure and immuno-cytochemistry of BHK-21 cells infected with a modified Bucyrus strain of equine arteritis virus. Archives of virology 140:1173-1180.
112. Weiland FH, Granzow M, Wieczorek-Krohmer M, Weiland E. 1995. Electron microscopic studies on the morphogeneis of PRRSV in infected cells -comparative studies, p. 499-502. In Schwyzer M, Ackermann M, Bertoni G, Kocherhands R,

McCullough K, Engels M, Wittek R, Zanoni R (ed.), Immunobiology of viral infections. Proceedings of the 3rd Congress of the European Society of Veterinary Virology.

113. Pol JM, Wagenaar F, Reus JE. 1997. Comparative morphogenesis of three PRRS virus strains. Veterinary microbiology 55:203-208.
114. Metwally S, Mohamed F, Faaberg K, Burrage T, Prarat M, Moran K, Bracht A, Mayr G, Berninger M, Koster L, To TL, Nguyen VL, Reising M, Landgraf J, Cox L, Lubroth J, Carrillo C. 2010. Pathogenicity and molecular characterization of emerging porcine reproductive and respiratory syndrome virus in Vietnam in 2007. Transboundary and emerging diseases 57:315-329.
115. Wieringa R, de Vries AA, van der Meulen J, Godeke GJ, Onderwater JJ, van Tol H, Koerten HK, Mommaas AM, Snijder EJ, Rottier PJ. 2004. Structural protein requirements in equine arteritis virus assembly. Journal of virology 78:13019-13027.
116. McDonald K. 2007. Cryopreparation methods for electron microscopy of selected model systems. Methods in cell biology 79:23-56.
117. Leapman RD, Aronova MA. 2007. Localizing specific elements bound to macromolecules by EFTEM. Methods in cell biology 79:593-613.
118. Friedman RM, Sreevalsan T. 1970. Membrane binding of input arbovirus ribonucleic acid: effect of interferon or cycloheximide. Journal of virology 6:169-175.
119. Kujala P, Ahola T, Ehsani N, Auvinen P, Vihinen H, Kaariainen L. 1999. Intracellular distribution of rubella virus nonstructural protein P150. Journal of virology 73:7805-7811.
120. Quinkert D, Bartenschlager R, Lohmann V. 2005. Quantitative analysis of the hepatitis C virus replication complex. Journal of virology 79:13594-13605.
121. Svoboda D, Nielson A, Werber A, Higginson J. 1962. An electron microscopic study of viral hepatitis in mice. The American journal of pathology 41:205-224.
122. David-Ferreira JF, Manaker RA. 1965. An Electron Microscope Study of the Development of a Mouse Hepatitis Virus in Tissue Culture Cells. The Journal of cell biology 24:57-78.
123. Orenstein JM, Banach B, Baker SC. 2008. Morphogenesis of Coronavirus HCoV-NL63 in Cell Culture: A Transmission Electron Microscopic Study. The open infectious diseases journal 2:52-58.
124. Lundin A, Dijkman R, Bergstrom T, Kann N, Adamiak B, Hannoun C, Kindler E, Jonsdottir HR, Muth D, Kint J, Forlenza M, Muller MA, Drosten C, Thiel V, Trybala E. 2014. Targeting membrane-bound viral RNA synthesis reveals potent inhibition of diverse coronaviruses including the middle East respiratory syndrome virus. PLoS pathogens 10:e1004166.
125. Gosert R, Kanjanahaluethai A, Egger D, Bienz K, Baker SC. 2002. RNA replication of mouse hepatitis virus takes place at double-membrane vesicles. Journal of virology 76:3697-3708.
126. Goldsmith CS, Tatti KM, Ksiazek TG, Rollin PE, Comer JA, Lee WW, Rota PA, Bankamp B, Bellini WJ, Zaki SR. 2004. Ultrastructural characterization of SARS coronavirus. Emerging infectious diseases 10:320-326.
127. Ulasli M, Verheije MH, de Haan CA, Reggiori F. 2010. Qualitative and quantitative ultrastructural analysis of the membrane rearrangements induced by coronavirus. Cellular microbiology 12:844-861.
128. de Wilde AH, Raj VS, Oudshoorn D, Bestebroer TM, van Nieuwkoop S, Limpens RW, Posthuma CC, van der Meer Y, Barcena M, Haagmans BL, Snijder EJ, van den Hoogen BG. 2013. MERS-coronavirus replication induces severe *in vitro* cytopathology and is strongly inhibited by cyclosporin A or interferon-alpha treatment. The Journal of general virology 94:1749-1760.
129. Hagemeijer MC, Vonk AM, Monastyrska I, Rottier

PJ, de Haan CA. 2012. Visualizing coronavirus RNA synthesis in time by using click chemistry. Journal of virology 86:5808-5816.

130. Neupert W, Herrmann JM. 2007. Translocation of proteins into mitochondria. Annu Rev Biochem 76:723-749.
131. Al-Mulla HM, Turrell L, Smith NM, Payne L, Baliji S, Zust R, Thiel V, Baker SC, Siddell SG, Neuman BW. 2014. Competitive fitness in coronaviruses is not correlated with size or number of double-membrane vesicles under reduced-temperature growth conditions. mBio 5:e01107-01113.
132. Diaz A, Wang X, Ahlquist P. 2010. Membrane-shaping host reticulon proteins play crucial roles in viral RNA replication compartment formation and function. Proceedings of the National Academy of Sciences of the United States of America 107:16291-16296.
133. Diaz A, Zhang J, Ollwerther A, Wang X, Ahlquist P. 2015. Correction: Host ESCRT Proteins Are Required for Bromovirus RNA Replication Compartment Assembly and Function. PLoS pathogens 11:e1004845.
134. Snijder EJ, Wassenaar AL, Spaan WJ. 1994. Proteolytic processing of the replicase ORF1a protein of equine arteritis virus. Journal of virology 68:5755-5764.
135. Stachowiak JC, Brodsky FM, Miller EA. 2013. A cost-benefit analysis of the physical mechanisms of membrane curvature. Nature cell biology 15:1019-1027.
136. de Wilde AH, Wannee KF, Scholte FE, Goeman JJ, Ten Dijke P, Snijder EJ, Kikkert M, van Hemert MJ. 2015. A Kinome-Wide Small Interfering RNA Screen Identifies Proviral and Antiviral Host Factors in Severe Acute Respiratory Syndrome Coronavirus Replication, Including Double-Stranded RNA-Activated Protein Kinase and Early Secretory Pathway Proteins. Journal of virology 89:8318-8333.
137. Stanley RE, Ragusa MJ, Hurley JH. 2014. The beginning of the end: how scaffolds nucleate autophagosome biogenesis. Trends in cell biology 24:73-81.
138. Yang Z, Klionsky DJ. 2010. Mammalian autophagy: core molecular machinery and signaling regulation. Current opinion in cell biology 22:124-131.
139. Stolz A, Ernst A, Dikic I. 2014. Cargo recognition and trafficking in selective autophagy. Nature cell biology 16:495-501.
140. Chiramel AI, Brady NR, Bartenschlager R. 2013. Divergent roles of autophagy in virus infection. Cells 2:83-104.
141. Kudchodkar SB, Levine B. 2009. Viruses and autophagy. Reviews in medical virology 19:359-378.
142. Kirkegaard K, Taylor MP, Jackson WT. 2004. Cellular autophagy: surrender, avoidance and subversion by microorganisms. Nature reviews. Microbiology 2:301-314.
143. Prentice E, Jerome WG, Yoshimori T, Mizushima N, Denison MR. 2004. Coronavirus replication complex formation utilizes components of cellular autophagy. The Journal of biological chemistry 279:10136-10141.
144. Cottam EM, Maier HJ, Manifava M, Vaux LC, Chandra-Schoenfelder P, Gerner W, Britton P, Ktistakis NT, Wileman T. 2011. Coronavirus nsp6 proteins generate autophagosomes from the endoplasmic reticulum via an omegasome intermediate. Autophagy 7:1335-1347.
145. Chen Q, Fang L, Wang D, Wang S, Li P, Li M, Luo R, Chen H, Xiao S. 2012. Induction of autophagy enhances porcine reproductive and respiratory syndrome virus replication. Virus research 163:650-655.
146. Liu Q, Qin Y, Zhou L, Kou Q, Guo X, Ge X, Yang H, Hu H. 2012. Autophagy sustains the replication of porcine reproductive and respiratory virus in host cells. Virology 429:136-147.
147. Sun MX, Huang L, Wang R, Yu YL, Li C, Li PP, Hu XC, Hao HP, Ishag HA, Mao X. 2012. Porcine reproductive and respiratory syndrome virus in-

duces autophagy to promote virus replication. Autophagy 8:1434-1447.

148. Monastyrska I, Ulasli M, Rottier PJ, Guan JL, Reggiori F, de Haan CA. 2013. An autophagy-independent role for LC3 in equine arteritis virus replication. Autophagy 9:164-174.

149. Zhao Z, Thackray LB, Miller BC, Lynn TM, Becker MM, Ward E, Mizushima NN, Denison MR, Virgin HWt. 2007. Coronavirus replication does not require the autophagy gene ATG5. Autophagy 3:581-585.

150. Reggiori F, Monastyrska I, Verheije MH, Cali T, Ulasli M, Bianchi S, Bernasconi R, de Haan CA, Molinari M. 2010. Coronaviruses Hijack the LC3-I-positive EDEMosomes, ER-derived vesicles exporting short-lived ERAD regulators, for replication. Cell host & microbe 7:500-508.

151. Jackson WT, Giddings TH, Jr., Taylor MP, Mulinyawe S, Rabinovitch M, Kopito RR, Kirkegaard K. 2005. Subversion of cellular autophagosomal machinery by RNA viruses. PLoS biology 3:e156.

152. Richards AL, Jackson WT. 2012. Intracellular vesicle acidification promotes maturation of infectious poliovirus particles. PLoS pathogens 8:e1003046.

153. Chen YH, Du W, Hagemeijer MC, Takvorian PM, Pau C, Cali A, Brantner CA, Stempinski ES, Connelly PS, Ma HC, Jiang P, Wimmer E, Altan-Bonnet G, Altan-Bonnet N. 2015. Phosphatidylserine vesicles enable efficient en bloc transmission of enteroviruses. Cell 160:619-630.

154. Cottam EM, Whelband MC, Wileman T. 2014. Coronavirus NSP6 restricts autophagosome expansion. Autophagy 10:1426-1441.

155. Zuber C, Cormier JH, Guhl B, Santimaria R, Hebert DN, Roth J. 2007. EDEM1 reveals a quality control vesicular transport pathway out of the endoplasmic reticulum not involving the COPII exit sites. Proceedings of the National Academy of Sciences of the United States of America 104:4407-4412.

156. Cali T, Galli C, Olivari S, Molinari M. 2008. Segregation and rapid turnover of EDEM1 by an autophagy-like mechanism modulates standard ERAD and folding activities. Biochem Biophys Res Commun 371:405-410.

157. Spuul P, Balistreri G, Kaariainen L, Ahola T. 2010. Phosphatidylinositol 3-kinase-, actin-, and microtubule-dependent transport of Semliki Forest Virus replication complexes from the plasma membrane to modified lysosomes. Journal of virology 84:7543-7557.

158. Bredenbeek PJ, Frolov I, Rice CM, Schlesinger S. 1993. Sindbis virus expression vectors: packaging of RNA replicons by using defective helper RNAs. Journal of virology 67:6439-6446.

159. de Boer P, Hoogenboom JP, Giepmans BN. 2015. Correlated light and electron microscopy: ultrastructure lights up! Nature methods 12:503-513.

160. Kukulski W, Schorb M, Welsch S, Picco A, Kaksonen M, Briggs JA. 2011. Correlated fluorescence and 3D electron microscopy with high sensitivity and spatial precision. The Journal of cell biology 192:111-119.

161. Pan J, Peng X, Gao Y, Li Z, Lu X, Chen Y, Ishaq M, Liu D, Dediego ML, Enjuanes L, Guo D. 2008. Genome-wide analysis of protein-protein interactions and involvement of viral proteins in SARS-CoV replication. PloS one 3:e3299.

162. Hagemeijer MC, Ulasli M, Vonk AM, Reggiori F, Rottier PJ, de Haan CA. 2011. Mobility and interactions of coronavirus nonstructural protein 4. Journal of virology 85:4572-4577.

163. Wang J, Ptacek JB, Kirkegaard K, Bullitt E. 2013. Double-membraned liposomes sculpted by poliovirus 3AB protein. The Journal of biological chemistry 288:27287-27298.

164. Yao F, Svensjo T, Winkler T, Lu M, Eriksson C, Eriksson E. 1998. Tetracycline repressor, tetR, rather than the tetR-mammalian cell transcription factor fusion derivatives, regulates induci-

ble gene expression in mammalian cells. Human gene therapy 9:1939-1950.

165. van Kasteren PB, Bailey-Elkin BA, James TW, Ninaber DK, Beugeling C, Khajehpour M, Snijder EJ, Mark BL, Kikkert M. 2013. Deubiquitinase function of arterivirus papain-like protease 2 suppresses the innate immune response in infected host cells. Proceedings of the National Academy of Sciences of the United States of America 110:E838-847.
166. Schonborn J, Oberstrass J, Breyel E, Tittgen J, Schumacher J, Lukacs N. 1991. Monoclonal antibodies to double-stranded RNA as probes of RNA structure in crude nucleic acid extracts. Nucleic acids research 19:2993-3000.
167. Weber F, Wagner V, Rasmussen SB, Hartmann R, Paludan SR. 2006. Double-stranded RNA is produced by positive-strand RNA viruses and DNA viruses but not in detectable amounts by negative-strand RNA viruses. Journal of virology 80:5059-5064.
168. Kukulski W, Schorb M, Welsch S, Picco A, Kaksonen M, Briggs JA. 2012. Precise, correlated fluorescence microscopy and electron tomography of lowicryl sections using fluorescent fiducial markers. Methods in cell biology 111:235-257.
169. Mastronarde DN. 2005. Automated electron microscope tomography using robust prediction of specimen movements. Journal of structural biology 152:36-51.
170. Kremer JR, Mastronarde DN, McIntosh JR. 1996. Computer visualization of three-dimensional image data using IMOD. Journal of structural biology 116:71-76.
171. Drosten C, Gunther S, Preiser W, van der Werf S, Brodt HR, Becker S, Rabenau H, Panning M, Kolesnikova L, Fouchier RA, Berger A, Burguiere AM, Cinatl J, Eickmann M, Escriou N, Grywna K, Kramme S, Manuguerra JC, Muller S, Rickerts V, Sturmer M, Vieth S, Klenk HD, Osterhaus AD, Schmitz H, Doerr HW. 2003. Identification of a novel coronavirus in patients with severe acute respiratory syndrome. The New England journal of medicine 348:1967-1976.
172. Ksiazek TG, Erdman D, Goldsmith CS, Zaki SR, Peret T, Emery S, Tong S, Urbani C, Comer JA, Lim W, Rollin PE, Dowell SF, Ling AE, Humphrey CD, Shieh WJ, Guarner J, Paddock CD, Rota P, Fields B, DeRisi J, Yang JY, Cox N, Hughes JM, LeDuc JW, Bellini WJ, Anderson LJ, Group SW. 2003. A novel coronavirus associated with severe acute respiratory syndrome. The New England journal of medicine 348:1953-1966.
173. van Boheemen S, de Graaf M, Lauber C, Bestebroer TM, Raj VS, Zaki AM, Osterhaus AD, Haagmans BL, Gorbalenya AE, Snijder EJ, Fouchier RA. 2012. Genomic characterization of a newly discovered coronavirus associated with acute respiratory distress syndrome in humans. mBio 3.
174. Perlman S, Netland J. 2009. Coronaviruses post-SARS: update on replication and pathogenesis. Nature reviews. Microbiology 7:439-450.
175. Snijder EJ, Decroly E, Ziebuhr J. 2016. The Nonstructural Proteins Directing Coronavirus RNA Synthesis and Processing. Advances in virus research 96:59-126.
176. Baez-Santos YM, St John SE, Mesecar AD. 2015. The SARS-coronavirus papain-like protease: structure, function and inhibition by designed antiviral compounds. Antiviral research 115:21-38.
177. Hilgenfeld R. 2014. From SARS to MERS: crystallographic studies on coronaviral proteases enable antiviral drug design. The FEBS journal 281:4085-4096.
178. Mielech AM, Chen Y, Mesecar AD, Baker SC. 2014. Nidovirus papain-like proteases: multifunctional enzymes with protease, deubiquitinating and deISGylating activities. Virus research 194:184-190.
179. Steuber H, Hilgenfeld R. 2010. Recent advances in targeting viral proteases for the discovery

of novel antivirals. Current topics in medicinal chemistry 10:323-345.

180. van der Hoeven B, Oudshoorn D, Koster AJ, Snijder EJ, Kikkert M, Barcena M. 2016. Biogenesis and architecture of arterivirus replication organelles. Virus research.

181. Avila-Perez G, Rejas MT, Rodriguez D. 2016. Ultrastructural characterization of membranous torovirus replication factories. Cellular microbiology 18:1691-1708.

182. Neuman BW. 2016. Bioinformatics and functional analyses of coronavirus nonstructural proteins involved in the formation of replicative organelles. Antiviral research 135:97-107.

183. Oostra M, Hagemeijer MC, van Gent M, Bekker CP, te Lintelo EG, Rottier PJ, de Haan CA. 2008. Topology and membrane anchoring of the coronavirus replication complex: not all hydrophobic domains of nsp3 and nsp6 are membrane spanning. Journal of virology 82:12392-12405.

184. Baliji S, Cammer SA, Sobral B, Baker SC. 2009. Detection of nonstructural protein 6 in murine coronavirus-infected cells and analysis of the transmembrane topology by using bioinformatics and molecular approaches. Journal of virology 83:6957-6962.

185. Clementz MA, Kanjanahaluethai A, O'Brien TE, Baker SC. 2008. Mutation in murine coronavirus replication protein nsp4 alters assembly of double membrane vesicles. Virology 375:118-129.

186. Beachboard DC, Anderson-Daniels JM, Denison MR. 2015. Mutations across murine hepatitis virus nsp4 alter virus fitness and membrane modifications. Journal of virology 89:2080-2089.

187. Sparks JS, Lu X, Denison MR. 2007. Genetic analysis of Murine hepatitis virus nsp4 in virus replication. Journal of virology 81:12554-12563.

188. Gadlage MJ, Sparks JS, Beachboard DC, Cox RG, Doyle JD, Stobart CC, Denison MR. 2010. Murine hepatitis virus nonstructural protein 4 regulates virus-induced membrane modifications and replication complex function. Journal of virology 84:280-290.

189. Miyazaki J, Takaki S, Araki K, Tashiro F, Tominaga A, Takatsu K, Yamamura K. 1989. Expression vector system based on the chicken beta-actin promoter directs efficient production of interleukin-5. Gene 79:269-277.

190. Bailey-Elkin BA, Knaap RC, Johnson GG, Dalebout TJ, Ninaber DK, van Kasteren PB, Bredenbeek PJ, Snijder EJ, Kikkert M, Mark BL. 2014. Crystal structure of the Middle East respiratory syndrome coronavirus (MERS-CoV) papain-like protease bound to ubiquitin facilitates targeted disruption of deubiquitinating activity to demonstrate its role in innate immune suppression. The Journal of biological chemistry 289:34667-34682.

191. Yang X, Chen X, Bian G, Tu J, Xing Y, Wang Y, Chen Z. 2014. Proteolytic processing, deubiquitinase and interferon antagonist activities of Middle East respiratory syndrome coronavirus papain-like protease. The Journal of general virology 95:614-626.

192. Norholm MH, Light S, Virkki MT, Elofsson A, von Heijne G, Daley DO. 2012. Manipulating the genetic code for membrane protein production: what have we learnt so far? Biochim Biophys Acta 1818:1091-1096.

193. Almsherqi ZA, Kohlwein SD, Deng Y. 2006. Cubic membranes: a legend beyond the Flatland* of cell membrane organization. The Journal of cell biology 173:839-844.

194. Kilianski A, Mielech AM, Deng X, Baker SC. 2013. Assessing activity and inhibition of Middle East respiratory syndrome coronavirus papain-like and 3C-like proteases using luciferase-based biosensors. Journal of virology 87:11955-11962.

195. Nagy PD, Pogany J. 2011. The dependence of viral RNA replication on co-opted host factors. Nature reviews. Microbiology 10:137-149.

196. Oudshoorn D, van der Hoeven B, Limpens RW, Beugeling C, Snijder EJ, Barcena M, Kikkert

M. 2016. Antiviral Innate Immune Response Interferes with the Formation of Replication-Associated Membrane Structures Induced by a Positive-Strand RNA Virus. mBio 7.

197. Deng Y, Almsherqi ZA, Ng MM, Kohlwein SD. 2010. Do viruses subvert cholesterol homeostasis to induce host cubic membranes? Trends in cell biology 20:371-379.

198. Lu XT, Sims AC, Denison MR. 1998. Mouse hepatitis virus 3C-like protease cleaves a 22-kilodalton protein from the open reading frame 1a polyprotein in virus-infected cells and *in vitro*. Journal of virology 72:2265-2271.

199. Ziebuhr J, Siddell SG. 1999. Processing of the human coronavirus 229E replicase polyproteins by the virus-encoded 3C-like proteinase: identification of proteolytic products and cleavage sites common to pp1a and pp1ab. Journal of virology 73:177-185.

200. Ruggli N, Tratschin JD, Mittelholzer C, Hofmann MA. 1996. Nucleotide sequence of classical swine fever virus strain Alfort/187 and transcription of infectious RNA from stably cloned full-length cDNA. Journal of virology 70:3478-3487.

201. Pott J, Mahlakoiv T, Mordstein M, Duerr CU, Michiels T, Stockinger S, Staeheli P, Hornef MW. 2011. IFN-lambda determines the intestinal epithelial antiviral host defense. Proceedings of the National Academy of Sciences of the United States of America 108:7944-7949.

202. Muller U, Steinhoff U, Reis LF, Hemmi S, Pavlovic J, Zinkernagel RM, Aguet M. 1994. Functional role of type I and type II interferons in antiviral defense. Science 264:1918-1921.

203. Jiang X, Chen ZJ. 2012. The role of ubiquitylation in immune defence and pathogen evasion. Nature reviews. Immunology 12:35-48.

204. Maelfait J, Beyaert R. 2012. Emerging role of ubiquitination in antiviral RIG-I signaling. Microbiol Mol Biol Rev 76:33-45.

205. Harhaj EW, Dixit VM. 2012. Regulation of NF-kappaB by deubiquitinases. Immunol Rev 246:107-124.

206. Malynn BA, Ma A. 2010. Ubiquitin makes its mark on immune regulation. Immunity 33:843-852.

207. Xu P, Duong DM, Seyfried NT, Cheng D, Xie Y, Robert J, Rush J, Hochstrasser M, Finley D, Peng J. 2009. Quantitative proteomics reveals the function of unconventional ubiquitin chains in proteasomal degradation. Cell 137:133-145.

208. Hershko A, Ciechanover A, Heller H, Haas AL, Rose IA. 1980. Proposed role of ATP in protein breakdown: conjugation of protein with multiple chains of the polypeptide of ATP-dependent proteolysis. Proceedings of the National Academy of Sciences of the United States of America 77:1783-1786.

209. Kerscher O, Felberbaum R, Hochstrasser M. 2006. Modification of proteins by ubiquitin and ubiquitin-like proteins. Annu Rev Cell Dev Biol 22:159-180.

210. Zhao S, Ulrich HD. 2010. Distinct consequences of posttranslational modification by linear versus K63-linked polyubiquitin chains. Proceedings of the National Academy of Sciences of the United States of America 107:7704-7709.

211. Dammer EB, Na CH, Xu P, Seyfried NT, Duong DM, Cheng D, Gearing M, Rees H, Lah JJ, Levey AI, Rush J, Peng J. 2011. Polyubiquitin linkage profiles in three models of proteolytic stress suggest the etiology of Alzheimer disease. The Journal of biological chemistry 286:10457-10465.

212. Tokunaga F, Sakata S, Saeki Y, Satomi Y, Kirisako T, Kamei K, Nakagawa T, Kato M, Murata S, Yamaoka S, Yamamoto M, Akira S, Takao T, Tanaka K, Iwai K. 2009. Involvement of linear polyubiquitylation of NEMO in NF-kappaB activation. Nature cell biology 11:123-132.

213. Xia ZP, Sun L, Chen X, Pineda G, Jiang X, Adhikari A, Zeng W, Chen ZJ. 2009. Direct activation of protein kinases by unanchored polyubiquitin chains. Nature 461:114-119.

214. Hay RT. 2005. SUMO: a history of modification.

Molecular cell 18:1-12.

215. Haas AL, Ahrens P, Bright PM, Ankel H. 1987. Interferon induces a 15-kilodalton protein exhibiting marked homology to ubiquitin. The Journal of biological chemistry 262:11315-11323.

216. Hochstrasser M. 2000. Evolution and function of ubiquitin-like protein-conjugation systems. Nature cell biology 2:E153-157.

217. Lenschow DJ, Lai C, Frias-Staheli N, Giannakopoulos NV, Lutz A, Wolff T, Osiak A, Levine B, Schmidt RE, Garcia-Sastre A, Leib DA, Pekosz A, Knobeloch KP, Horak I, Virgin HWt. 2007. IFN-stimulated gene 15 functions as a critical antiviral molecule against influenza, herpes, and Sindbis viruses. Proceedings of the National Academy of Sciences of the United States of America 104:1371-1376.

218. Durfee LA, Lyon N, Seo K, Huibregtse JM. 2010. The ISG15 conjugation system broadly targets newly synthesized proteins: implications for the antiviral function of ISG15. Molecular cell 38:722-732.

219. Werneke SW, Schilte C, Rohatgi A, Monte KJ, Michault A, Arenzana-Seisdedos F, Vanlandingham DL, Higgs S, Fontanet A, Albert ML, Lenschow DJ. 2011. ISG15 is critical in the control of Chikungunya virus infection independent of UbE1L mediated conjugation. PLoS pathogens 7:e1002322.

220. Tatsumi K, Yamamoto-Mukai H, Shimizu R, Waguri S, Sou YS, Sakamoto A, Taya C, Shitara H, Hara T, Chung CH, Tanaka K, Yamamoto M, Komatsu M. 2011. The Ufm1-activating enzyme Uba5 is indispensable for erythroid differentiation in mice. Nat Commun 2:181.

221. Lemaire K, Moura RF, Granvik M, Igoillo-Esteve M, Hohmeier HE, Hendrickx N, Newgard CB, Waelkens E, Cnop M, Schuit F. 2011. Ubiquitin fold modifier 1 (UFM1) and its target UFBP1 protect pancreatic beta cells from ER stress-induced apoptosis. PloS one 6:e18517.

222. Schmidtke G, Kalveram B, Groettrup M. 2009. Degradation of FAT10 by the 26S proteasome is independent of ubiquitylation but relies on NUB1L. FEBS Lett 583:591-594.

223. Watson IR, Irwin MS, Ohh M. 2011. NEDD8 pathways in cancer, Sine Quibus Non. Cancer Cell 19:168-176.

224. Raasi S, Schmidtke G, Groettrup M. 2001. The ubiquitin-like protein FAT10 forms covalent conjugates and induces apoptosis. The Journal of biological chemistry 276:35334-35343.

225. Schmid D, Munz C. 2007. Innate and adaptive immunity through autophagy. Immunity 27:11-21.

226. Pickart CM. 2001. Mechanisms underlying ubiquitination. Annu Rev Biochem 70:503-533.

227. Hershko A, Ciechanover A. 1998. The ubiquitin system. Annu Rev Biochem 67:425-479.

228. Schulman BA, Harper JW. 2009. Ubiquitin-like protein activation by E1 enzymes: the apex for downstream signalling pathways. Nature reviews. Molecular cell biology 10:319-331.

229. Love KR, Catic A, Schlieker C, Ploegh HL. 2007. Mechanisms, biology and inhibitors of deubiquitinating enzymes. Nat Chem Biol 3:697-705.

230. Nijman SM, Luna-Vargas MP, Velds A, Brummelkamp TR, Dirac AM, Sixma TK, Bernards R. 2005. A genomic and functional inventory of deubiquitinating enzymes. Cell 123:773-786.

231. Li S, Zheng H, Mao AP, Zhong B, Li Y, Liu Y, Gao Y, Ran Y, Tien P, Shu HB. 2010. Regulation of virus-triggered signaling by OTUB1- and OTUB2-mediated deubiquitination of TRAF3 and TRAF6. The Journal of biological chemistry 285:4291-4297.

232. Kayagaki N, Phung Q, Chan S, Chaudhari R, Quan C, O'Rourke KM, Eby M, Pietras E, Cheng G, Bazan JF, Zhang Z, Arnott D, Dixit VM. 2007. DUBA: a deubiquitinase that regulates type I interferon production. Science 318:1628-1632.

233. Boone DL, Turer EE, Lee EG, Ahmad RC, Wheeler MT, Tsui C, Hurley P, Chien M, Chai S, Hitotsumatsu O, McNally E, Pickart C, Ma A. 2004. The ubiquitin-modifying enzyme A20 is

required for termination of Toll-like receptor responses. Nature immunology 5:1052-1060.

234. Friedman CS, O'Donnell MA, Legarda-Addison D, Ng A, Cardenas WB, Yount JS, Moran TM, Basler CF, Komuro A, Horvath CM, Xavier R, Ting AT. 2008. The tumour suppressor CYLD is a negative regulator of RIG-I-mediated antiviral response. EMBO Rep 9:930-936.

235. Pichlmair A, Reis e Sousa C. 2007. Innate recognition of viruses. Immunity 27:370-383.

236. Chen G, Shaw MH, Kim YG, Nunez G. 2009. NOD-like receptors: role in innate immunity and inflammatory disease. Annu Rev Pathol 4:365-398.

237. Gay NJ, Gangloff M. 2007. Structure and function of Toll receptors and their ligands. Annu Rev Biochem 76:141-165.

238. Ostuni R, Zanoni I, Granucci F. 2010. Deciphering the complexity of Toll-like receptor signaling. Cell Mol Life Sci 67:4109-4134.

239. Kawai T, Akira S. 2011. Toll-like receptors and their crosstalk with other innate receptors in infection and immunity. Immunity 34:637-650.

240. Yoneyama M, Kikuchi M, Natsukawa T, Shinobu N, Imaizumi T, Miyagishi M, Taira K, Akira S, Fujita T. 2004. The RNA helicase RIG-I has an essential function in double-stranded RNA-induced innate antiviral responses. Nature immunology 5:730-737.

241. Loo YM, Gale M, Jr. 2011. Immune signaling by RIG-I-like receptors. Immunity 34:680-692.

242. Hausmann S, Marq JB, Tapparel C, Kolakofsky D, Garcin D. 2008. RIG-I and dsRNA-induced IFNbeta activation. PloS one 3:e3965.

243. Luthra P, Sun D, Silverman RH, He B. 2011. Activation of IFN-β expression by a viral mRNA through RNase L and MDA5. Proceedings of the National Academy of Sciences of the United States of America 108:2118-2123.

244. Kato H, Takeuchi O, Sato S, Yoneyama M, Yamamoto M, Matsui K, Uematsu S, Jung A, Kawai T, Ishii KJ, Yamaguchi O, Otsu K, Tsujimura T, Koh CS, Reis e Sousa C, Matsuura Y, Fujita T, Akira S. 2006. Differential roles of MDA5 and RIG-I helicases in the recognition of RNA viruses. Nature 441:101-105.

245. Unterholzner L, Keating SE, Baran M, Horan KA, Jensen SB, Sharma S, Sirois CM, Jin T, Latz E, Xiao TS, Fitzgerald KA, Paludan SR, Bowie AG. 2010. IFI16 is an innate immune sensor for intracellular DNA. Nature immunology 11:997-1004.

246. Rathinam VA, Jiang Z, Waggoner SN, Sharma S, Cole LE, Waggoner L, Vanaja SK, Monks BG, Ganesan S, Latz E, Hornung V, Vogel SN, Szomolanyi-Tsuda E, Fitzgerald KA. 2010. The AIM2 inflammasome is essential for host defense against cytosolic bacteria and DNA viruses. Nature immunology 11:395-402.

247. Ishikawa H, Barber GN. 2008. STING is an endoplasmic reticulum adaptor that facilitates innate immune signalling. Nature 455:674-678.

248. Matsuzawa A, Tseng PH, Vallabhapurapu S, Luo JL, Zhang W, Wang H, Vignali DA, Gallagher E, Karin M. 2008. Essential cytoplasmic translocation of a cytokine receptor-assembled signaling complex. Science 321:663-668.

249. Sharma S, tenOever BR, Grandvaux N, Zhou GP, Lin R, Hiscott J. 2003. Triggering the interferon antiviral response through an IKK-related pathway. Science 300:1148-1151.

250. Honda K, Takaoka A, Taniguchi T. 2006. Type I interferon [corrected] gene induction by the interferon regulatory factor family of transcription factors. Immunity 25:349-360.

251. Schoggins JW, Wilson SJ, Panis M, Murphy MY, Jones CT, Bieniasz P, Rice CM. 2011. A diverse range of gene products are effectors of the type I interferon antiviral response. Nature 472:481-485.

252. Kash JC, Tumpey TM, Proll SC, Carter V, Perwitasari O, Thomas MJ, Basler CF, Palese P, Taubenberger JK, Garcia-Sastre A, Swayne DE, Katze MG. 2006. Genomic analysis of increased host immune and cell death responses induced

by 1918 influenza virus. Nature 443:578-581.

253. Hugot JP, Chamaillard M, Zouali H, Lesage S, Cezard JP, Belaiche J, Almer S, Tysk C, O'Morain CA, Gassull M, Binder V, Finkel Y, Cortot A, Modigliani R, Laurent-Puig P, Gower-Rousseau C, Macry J, Colombel JF, Sahbatou M, Thomas G. 2001. Association of NOD2 leucine-rich repeat variants with susceptibility to Crohn's disease. Nature 411:599-603.

254. Crow MK. 2010. Type I interferon in organ-targeted autoimmune and inflammatory diseases. Arthritis Res Ther 12 Suppl 1:S5.

255. Miceli-Richard C, Lesage S, Rybojad M, Prieur AM, Manouvrier-Hanu S, Hafner R, Chamaillard M, Zouali H, Thomas G, Hugot JP. 2001. CARD15 mutations in Blau syndrome. Nat Genet 29:19-20.

256. Hooks JJ, Moutsopoulos HM, Geis SA, Stahl NI, Decker JL, Notkins AL. 1979. Immune interferon in the circulation of patients with autoimmune disease. The New England journal of medicine 301:5-8.

257. Li Q, Xu B, Michie SA, Rubins KH, Schreriber RD, McDevitt HO. 2008. Interferon-alpha initiates type 1 diabetes in nonobese diabetic mice. Proceedings of the National Academy of Sciences of the United States of America 105:12439-12444.

258. Oshiumi H, Matsumoto M, Hatakeyama S, Seya T. 2009. Riplet/RNF135, a RING finger protein, ubiquitinates RIG-I to promote interferon-beta induction during the early phase of viral infection. The Journal of biological chemistry 284:807-817.

259. Gack MU, Kirchhofer A, Shin YC, Inn KS, Liang C, Cui S, Myong S, Ha T, Hopfner KP, Jung JU. 2008. Roles of RIG-I N-terminal tandem CARD and splice variant in TRIM25-mediated antiviral signal transduction. Proceedings of the National Academy of Sciences of the United States of America 105:16743-16748.

260. Gack MU, Shin YC, Joo CH, Urano T, Liang C, Sun L, Takeuchi O, Akira S, Chen Z, Inoue S, Jung JU. 2007. TRIM25 RING-finger E3 ubiquitin ligase is essential for RIG-I-mediated antiviral activity. Nature 446:916-920.

261. Zeng W, Sun L, Jiang X, Chen X, Hou F, Adhikari A, Xu M, Chen ZJ. 2010. Reconstitution of the RIG-I pathway reveals a signaling role of unanchored polyubiquitin chains in innate immunity. Cell 141:315-330.

262. Jiang X, Kinch LN, Brautigam CA, Chen X, Du F, Grishin NV, Chen ZJ. 2012. Ubiquitin-Induced Oligomerization of the RNA Sensors RIG-I and MDA5 Activates Antiviral Innate Immune Response. Immunity.

263. Reyes-Turcu FE, Horton JR, Mullally JE, Heroux A, Cheng X, Wilkinson KD. 2006. The ubiquitin binding domain ZnF UBP recognizes the C-terminal diglycine motif of unanchored ubiquitin. Cell 124:1197-1208.

264. Gao D, Yang YK, Wang RP, Zhou X, Diao FC, Li MD, Zhai ZH, Jiang ZF, Chen DY. 2009. REUL is a novel E3 ubiquitin ligase and stimulator of retinoic-acid-inducible gene-I. PloS one 4:e5760.

265. Xu L, Xiao N, Liu F, Ren H, Gu J. 2009. Inhibition of RIG-I and MDA5-dependent antiviral response by gC1qR at mitochondria. Proceedings of the National Academy of Sciences of the United States of America 106:1530-1535.

266. Moore CB, Bergstralh DT, Duncan JA, Lei Y, Morrison TE, Zimmermann AG, Accavitti-Loper MA, Madden VJ, Sun L, Ye Z, Lich JD, Heise MT, Chen Z, Ting JP. 2008. NLRX1 is a regulator of mitochondrial antiviral immunity. Nature 451:573-577.

267. Oshiumi H, Miyashita M, Inoue N, Okabe M, Matsumoto M, Seya T. 2010. The ubiquitin ligase Riplet is essential for RIG-I-dependent innate immune responses to RNA virus infection. Cell host & microbe 8:496-509.

268. Arimoto K, Takahashi H, Hishiki T, Konishi H, Fujita T, Shimotohno K. 2007. Negative regulation of the RIG-I signaling by the ubiquitin ligase

RNF125. Proceedings of the National Academy of Sciences of the United States of America 104:7500-7505.

269. Inn KS, Gack MU, Tokunaga F, Shi M, Wong LY, Iwai K, Jung JU. 2011. Linear ubiquitin assembly complex negatively regulates RIG-I- and TRIM25-mediated type I interferon induction. Molecular cell 41:354-365.

270. Zou W, Wang J, Zhang DE. 2007. Negative regulation of ISG15 E3 ligase EFP through its autoISGylation. Biochem Biophys Res Commun 354:321-327.

271. Wang C, Deng L, Hong M, Akkaraju GR, Inoue J, Chen ZJ. 2001. TAK1 is a ubiquitin-dependent kinase of MKK and IKK. Nature 412:346-351.

272. Ninomiya-Tsuji J, Kishimoto K, Hiyama A, Inoue J, Cao Z, Matsumoto K. 1999. The kinase TAK1 can activate the NIK-I kappaB as well as the MAP kinase cascade in the IL-1 signalling pathway. Nature 398:252-256.

273. Yamamoto M, Okamoto T, Takeda K, Sato S, Sanjo H, Uematsu S, Saitoh T, Yamamoto N, Sakurai H, Ishii KJ, Yamaoka S, Kawai T, Matsuura Y, Takeuchi O, Akira S. 2006. Key function for the Ubc13 E2 ubiquitin-conjugating enzyme in immune receptor signaling. Nature immunology 7:962-970.

274. Deng L, Wang C, Spencer E, Yang L, Braun A, You J, Slaughter C, Pickart C, Chen ZJ. 2000. Activation of the IkappaB kinase complex by TRAF6 requires a dimeric ubiquitin-conjugating enzyme complex and a unique polyubiquitin chain. Cell 103:351-361.

275. Bhoj VG, Chen ZJ. 2009. Ubiquitylation in innate and adaptive immunity. Nature 458:430-437.

276. Xu LG, Wang YY, Han KJ, Li LY, Zhai Z, Shu HB. 2005. VISA is an adapter protein required for virus-triggered IFN-beta signaling. Molecular cell 19:727-740.

277. Chang M, Jin W, Sun SC. 2009. Peli1 facilitates TRIF-dependent Toll-like receptor signaling and proinflammatory cytokine production. Nature immunology 10:1089-1095.

278. Meylan E, Burns K, Hofmann K, Blancheteau V, Martinon F, Kelliher M, Tschopp J. 2004. RIP1 is an essential mediator of Toll-like receptor 3-induced NF-kappa B activation. Nature immunology 5:503-507.

279. Mikkelsen SS, Jensen SB, Chiliveru S, Melchjorsen J, Julkunen I, Gaestel M, Arthur JS, Flavell RA, Ghosh S, Paludan SR. 2009. RIG-I-mediated activation of p38 MAPK is essential for viral induction of interferon and activation of dendritic cells: dependence on TRAF2 and TAK1. The Journal of biological chemistry 284:10774-10782.

280. Pertel T, Hausmann S, Morger D, Zuger S, Guerra J, Lascano J, Reinhard C, Santoni FA, Uchil PD, Chatel L, Bisiaux A, Albert ML, Strambio-De-Castillia C, Mothes W, Pizzato M, Grutter MG, Luban J. 2011. TRIM5 is an innate immune sensor for the retrovirus capsid lattice. Nature 472:361-365.

281. Tseng PH, Matsuzawa A, Zhang W, Mino T, Vignali DA, Karin M. 2010. Different modes of ubiquitination of the adaptor TRAF3 selectively activate the expression of type I interferons and proinflammatory cytokines. Nature immunology 11:70-75.

282. Wertz IE, O'Rourke KM, Zhou H, Eby M, Aravind L, Seshagiri S, Wu P, Wiesmann C, Baker R, Boone DL, Ma A, Koonin EV, Dixit VM. 2004. De-ubiquitination and ubiquitin ligase domains of A20 downregulate NF-kappaB signalling. Nature 430:694-699.

283. Shi M, Deng W, Bi E, Mao K, Ji Y, Lin G, Wu X, Tao Z, Li Z, Cai X, Sun S, Xiang C, Sun B. 2008. TRIM30 alpha negatively regulates TLR-mediated NF-kappa B activation by targeting TAB2 and TAB3 for degradation. Nature immunology 9:369-377.

284. Reyes-Turcu FE, Ventii KH, Wilkinson KD. 2009. Regulation and cellular roles of ubiquitin-specific deubiquitinating enzymes. Annu Rev Biochem 78:363-397.

285. Maniatis T. 1999. A ubiquitin ligase complex essential for the NF-kappaB, Wnt/Wingless, and Hedgehog signaling pathways. Genes Dev 13:505-510.
286. Rahighi S, Ikeda F, Kawasaki M, Akutsu M, Suzuki N, Kato R, Kensche T, Uejima T, Bloor S, Komander D, Randow F, Wakatsuki S, Dikic I. 2009. Specific recognition of linear ubiquitin chains by NEMO is important for NF-kappaB activation. Cell 136:1098-1109.
287. Laplantine E, Fontan E, Chiaravalli J, Lopez T, Lakisic G, Veron M, Agou F, Israel A. 2009. NEMO specifically recognizes K63-linked poly-ubiquitin chains through a new bipartite ubiquitin-binding domain. The EMBO journal 28:2885-2895.
288. Hacker H, Tseng PH, Karin M. 2011. Expanding TRAF function: TRAF3 as a tri-faced immune regulator. Nature reviews. Immunology 11:457-468.
289. Nakhaei P, Mesplede T, Solis M, Sun Q, Zhao T, Yang L, Chuang TH, Ware CF, Lin R, Hiscott J. 2009. The E3 ubiquitin ligase Triad3A negatively regulates the RIG-I/MAVS signaling pathway by targeting TRAF3 for degradation. PLoS pathogens 5:e1000650.
290. Tsuchida T, Zou J, Saitoh T, Kumar H, Abe T, Matsuura Y, Kawai T, Akira S. 2010. The ubiquitin ligase TRIM56 regulates innate immune responses to intracellular double-stranded DNA. Immunity 33:765-776.
291. Zhang J, Hu MM, Wang YY, Shu HB. 2012. TRIM32 modulates type I interferon induction and cellular antiviral response by targeting MITA/STING for K63-linked ubiquitination. The Journal of biological chemistry.
292. Zhong B, Zhang L, Lei C, Li Y, Mao AP, Yang Y, Wang YY, Zhang XL, Shu HB. 2009. The ubiquitin ligase RNF5 regulates antiviral responses by mediating degradation of the adaptor protein MITA. Immunity 30:397-407.
293. Zeng W, Xu M, Liu S, Sun L, Chen ZJ. 2009. Key role of Ubc5 and lysine-63 polyubiquitination in viral activation of IRF3. Molecular cell 36:315-325.
294. Tenoever BR, Ng SL, Chua MA, McWhirter SM, Garcia-Sastre A, Maniatis T. 2007. Multiple functions of the IKK-related kinase IKKepsilon in interferon-mediated antiviral immunity. Science 315:1274-1278.
295. Wild P, Farhan H, McEwan DG, Wagner S, Rogov VV, Brady NR, Richter B, Korac J, Waidmann O, Choudhary C, Dotsch V, Bumann D, Dikic I. 2011. Phosphorylation of the autophagy receptor optineurin restricts Salmonella growth. Science 333:228-233.
296. Wang C, Chen T, Zhang J, Yang M, Li N, Xu X, Cao X. 2009. The E3 ubiquitin ligase Nrdp1 'preferentially' promotes TLR-mediated production of type I interferon. Nature immunology 10:744-752.
297. Li S, Wang L, Berman M, Kong YY, Dorf ME. 2011. Mapping a dynamic innate immunity protein interaction network regulating type I interferon production. Immunity 35:426-440.
298. Chau TL, Gioia R, Gatot JS, Patrascu F, Carpentier I, Chapelle JP, O'Neill L, Beyaert R, Piette J, Chariot A. 2008. Are the IKKs and IKK-related kinases TBK1 and IKK-epsilon similarly activated? Trends Biochem Sci 33:171-180.
299. Arimoto K, Funami K, Saeki Y, Tanaka K, Okawa K, Takeuchi O, Akira S, Murakami Y, Shimotohno K. 2010. Polyubiquitin conjugation to NEMO by triparite motif protein 23 (TRIM23) is critical in antiviral defense. Proceedings of the National Academy of Sciences of the United States of America 107:15856-15861.
300. Zhao T, Yang L, Sun Q, Arguello M, Ballard DW, Hiscott J, Lin R. 2007. The NEMO adaptor bridges the nuclear factor-kappaB and interferon regulatory factor signaling pathways. Nature immunology 8:592-600.
301. Belgnaoui S, Paz S, Goulet M, Sun Q, Iwai K, Dikic I, Hiscott J, lin R. 2012. Linear ubiquitination of

NEMO negatively regulates the IFN antiviral response through the disruption of the MAVS signalosome. Cell host & microbe 12:211-222.

302. Clark K, Takeuchi O, Akira S, Cohen P. 2011. The TRAF-associated protein TANK facilitates cross-talk within the IkappaB kinase family during Toll-like receptor signaling. Proceedings of the National Academy of Sciences of the United States of America 108:17093-17098.
303. Schmid S, Mordstein M, Kochs G, Garcia-Sastre A, Tenoever BR. 2010. Transcription factor redundancy ensures induction of the antiviral state. The Journal of biological chemistry 285:42013-42022.
304. Yang K, Shi HX, Liu XY, Shan YF, Wei B, Chen S, Wang C. 2009. TRIM21 is essential to sustain IFN regulatory factor 3 activation during antiviral response. Journal of immunology 182:3782-3792.
305. Higgs R, Lazzari E, Wynne C, Ni Gabhann J, Espinosa A, Wahren-Herlenius M, Jefferies CA. 2010. Self protection from anti-viral responses--Ro52 promotes degradation of the transcription factor IRF7 downstream of the viral Toll-Like receptors. PloS one 5:e11776.
306. Yoshimi R, Chang TH, Wang H, Atsumi T, Morse HC, 3rd, Ozato K. 2009. Gene disruption study reveals a nonredundant role for TRIM21/Ro52 in NF-kappaB-dependent cytokine expression in fibroblasts. Journal of immunology 182:7527-7538.
307. Kubota T, Matsuoka M, Chang TH, Tailor P, Sasaki T, Tashiro M, Kato A, Ozato K. 2008. Virus infection triggers SUMOylation of IRF3 and IRF7, leading to the negative regulation of type I interferon gene expression. The Journal of biological chemistry 283:25660-25670.
308. Liang Q, Deng H, Li X, Wu X, Tang Q, Chang TH, Peng H, Rauscher FJ, 3rd, Ozato K, Zhu F. 2011. Tripartite motif-containing protein 28 is a small ubiquitin-related modifier e3 ligase and negative regulator of IFN regulatory factor 7. Journal of immunology 187:4754-4763.
309. Zhang J, Xu LG, Han KJ, Wei X, Shu HB. 2004. PIASy represses TRIF-induced ISRE and NF-kappaB activation but not apoptosis. FEBS Lett 570:97-101.
310. Shuai K, Liu B. 2005. Regulation of gene-activation pathways by PIAS proteins in the immune system. Nature reviews. Immunology 5:593-605.
311. Balakirev MY, Jaquinod M, Haas AL, Chroboczek J. 2002. Deubiquitinating function of adenovirus proteinase. Journal of virology 76:6323-6331.
312. Gonzalez CM, Wang L, Damania B. 2009. Kaposi's sarcoma-associated herpesvirus encodes a viral deubiquitinase. Journal of virology 83:10224-10233.
313. Frias-Staheli N, Giannakopoulos NV, Kikkert M, Taylor SL, Bridgen A, Paragas J, Richt JA, Rowland RR, Schmaljohn CS, Lenschow DJ, Snijder EJ, Garcia-Sastre A, Virgin HWt. 2007. Ovarian tumor domain-containing viral proteases evade ubiquitin- and ISG15-dependent innate immune responses. Cell host & microbe 2:404-416.
314. Clementz MA, Chen Z, Banach BS, Wang Y, Sun L, Ratia K, Baez-Santos YM, Wang J, Takayama J, Ghosh AK, Li K, Mesecar AD, Baker SC. 2010. Deubiquitinating and interferon antagonism activities of coronavirus papain-like proteases. Journal of virology 84:4619-4629.
315. Wang D, Fang L, Li P, Sun L, Fan J, Zhang Q, Luo R, Liu X, Li K, Chen H, Chen Z, Xiao S. 2011. The leader proteinase of foot-and-mouth disease virus negatively regulates the type I interferon pathway by acting as a viral deubiquitinase. Journal of virology 85:3758-3766.
316. van Kasteren PB, Beugeling C, Ninaber DK, Frias-Staheli N, van Boheemen S, Garcia-Sastre A, Snijder EJ, Kikkert M. 2011. Arterivirus and nairovirus ovarian tumor domain-containing deubiquitinases target activated RIG-I to control innate immune signaling. Journal of virology.
317. Gack MU, Albrecht RA, Urano T, Inn KS, Huang IC,

Carnero E, Farzan M, Inoue S, Jung JU, Garcia-Sastre A. 2009. Influenza A virus NS1 targets the ubiquitin ligase TRIM25 to evade recognition by the host viral RNA sensor RIG-I. Cell host & microbe 5:439-449.

318. Lilley CE, Chaurushiya MS, Boutell C, Landry S, Suh J, Panier S, Everett RD, Stewart GS, Durocher D, Weitzman MD. 2010. A viral E3 ligase targets RNF8 and RNF168 to control histone ubiquitination and DNA damage responses. The EMBO journal 29:943-955.

319. Nerenberg BT, Taylor J, Bartee E, Gouveia K, Barry M, Fruh K. 2005. The poxviral RING protein p28 is a ubiquitin ligase that targets ubiquitin to viral replication factories. Journal of virology 79:597-601.

320. Kim W, Bennett EJ, Huttlin EL, Guo A, Li J, Possemato A, Sowa ME, Rad R, Rush J, Comb MJ, Harper JW, Gygi SP. 2011. Systematic and quantitative assessment of the ubiquitin-modified proteome. Molecular cell 44:325-340.

321. Ting L, Rad R, Gygi SP, Haas W. 2011. MS3 eliminates ratio distortion in isobaric multiplexed quantitative proteomics. Nature methods 8:937-940.

322. Dikic I, Wakatsuki S, Walters KJ. 2009. Ubiquitin-binding domains – from structures to functions. Nature reviews. Molecular cell biology 10:659-671.

323. Neuman BW, Angelini MM, Buchmeier MJ. 2014. Does form meet function in the coronavirus replicative organelle? Trends in microbiology 22:642-647.

324. Nagy PD, Barajas D, Pogany J. 2012. Host factors with regulatory roles in tombusvirus replication. Current opinion in virology 2:691-698.

325. Schneider WM, Chevillotte MD, Rice CM. 2014. Interferon-stimulated genes: a complex web of host defenses. Annual review of immunology 32:513-545.

326. Anggakusuma, Romero-Brey I, Berger C, Colpitts CC, Boldanova T, Engelmann M, Todt D, Perin PM, Behrendt P, Vondran FW, Xu S, Goffinet C, Schang LM, Heim MH, Bartenschlager R, Pietschmann T, Steinmann E. 2015. Interferon-inducible cholesterol-25-hydroxylase restricts hepatitis C virus replication through blockage of membranous web formation. Hepatology 62:702-714.

327. Helbig KJ, Eyre NS, Yip E, Narayana S, Li K, Fiches G, McCartney EM, Jangra RK, Lemon SM, Beard MR. 2011. The antiviral protein viperin inhibits hepatitis C virus replication via interaction with nonstructural protein 5A. Hepatology 54:1506-1517.

328. Melen K, Keskinen P, Lehtonen A, Julkunen I. 2000. Interferon-induced gene expression and signaling in human hepatoma cell lines. Journal of hepatology 33:764-772.

329. van den Born E, Posthuma CC, Knoops K, Snijder EJ. 2007. An infectious recombinant equine arteritis virus expressing green fluorescent protein from its replicase gene. The Journal of general virology 88:1196-1205.

330. Faas FG, Avramut MC, van den Berg BM, Mommaas AM, Koster AJ, Ravelli RB. 2012. Virtual nanoscopy: generation of ultra-large high resolution electron microscopy maps. The Journal of cell biology 198:457-469.

331. Helbig KJ, Beard MR. 2014. The role of viperin in the innate antiviral response. Journal of molecular biology 426:1210-1219.

332. Sahu SK, Gummadi SN, Manoj N, Aradhyam GK. 2007. Phospholipid scramblases: an overview. Archives of biochemistry and biophysics 462:103-114.

333. Cyster JG, Dang EV, Reboldi A, Yi T. 2014. 25-Hydroxycholesterols in innate and adaptive immunity. Nature reviews. Immunology 14:731-743.

334. Schoggins JW, MacDuff DA, Imanaka N, Gainey MD, Shrestha B, Eitson JL, Mar KB, Richardson RB, Ratushny AV, Litvak V, Dabelic R, Manicassamy B, Aitchison JD, Aderem A, Elliott

RM, Garcia-Sastre A, Racaniello V, Snijder EJ, Yokoyama WM, Diamond MS, Virgin HW, Rice CM. 2014. Pan-viral specificity of IFN-induced genes reveals new roles for cGAS in innate immunity. Nature 505:691-695.

335. Diamond MS, Farzan M. 2013. The broad-spectrum antiviral functions of IFIT and IFITM proteins. Nature reviews. Immunology 13:46-57.

336. Choi J, Park S, Biering SB, Selleck E, Liu CY, Zhang X, Fujita N, Saitoh T, Akira S, Yoshimori T, Sibley LD, Hwang S, Virgin HW. 2014. The parasitophorous vacuole membrane of Toxoplasma gondii is targeted for disruption by ubiquitin-like conjugation systems of autophagy. Immunity 40:924-935.

337. Park S, Choi J, Biering SB, Dominici E, Williams LE, Hwang S. 2016. Targeting by AutophaGy proteins (TAG): Targeting of IFNG-inducible GTPases to membranes by the LC3 conjugation system of autophagy. Autophagy:0.

338. van Kasteren PB, Beugeling C, Ninaber DK, Frias-Staheli N, van Boheemen S, Garcia-Sastre A, Snijder EJ, Kikkert M. 2012. Arterivirus and nairovirus ovarian tumor domain-containing Deubiquitinases target activated RIG-I to control innate immune signaling. Journal of virology 86:773-785.

339. MacLachlan NJ, Balasuriya UB, Hedges JF, Schweidler TM, McCollum WH, Timoney PJ, Hullinger PJ, Patton JF. 1998. Serologic response of horses to the structural proteins of equine arteritis virus. Journal of veterinary diagnostic investigation : official publication of the American Association of Veterinary Laboratory Diagnosticians, Inc 10:229-236.

340. Carlotti F, Bazuine M, Kekarainen T, Seppen J, Pognonec P, Maassen JA, Hoeben RC. 2004. Lentiviral vectors efficiently transduce quiescent mature 3T3-L1 adipocytes. Molecular therapy : the journal of the American Society of Gene Therapy 9:209-217.

341. Shalem O, Sanjana NE, Hartenian E, Shi X, Scott DA, Mikkelsen TS, Heckl D, Ebert BL, Root DE, Doench JG, Zhang F. 2014. Genome-scale CRISPR-Cas9 knockout screening in human cells. Science 343:84-87.

342. Sanjana NE, Shalem O, Zhang F. 2014. Improved vectors and genome-wide libraries for CRISPR screening. Nature methods 11:783-784.

343. Kusano S, Eizuru Y. 2012. Human phospholipid scramblase 1 interacts with and regulates transactivation of HTLV-1 Tax. Virology 432:343-352.

344. V'Kovski P, Al-Mulla H, Thiel V, Neuman BW. 2015. New insights on the role of paired membrane structures in coronavirus replication. Virus research 202:33-40.

345. Ratia K, Saikatendu KS, Santarsiero BD, Barretto N, Baker SC, Stevens RC, Mesecar AD. 2006. Severe acute respiratory syndrome coronavirus papain-like protease: structure of a viral deubiquitinating enzyme. Proceedings of the National Academy of Sciences of the United States of America 103:5717-5722.

346. Sulea T, Lindner HA, Purisima EO, Menard R. 2005. Deubiquitination, a new function of the severe acute respiratory syndrome coronavirus papain-like protease? Journal of virology 79:4550-4551.

347. Barretto N, Jukneliene D, Ratia K, Chen Z, Mesecar AD, Baker SC. 2005. The papain-like protease of severe acute respiratory syndrome coronavirus has deubiquitinating activity. Journal of virology 79:15189-15198.

348. Lindner HA, Fotouhi-Ardakani N, Lytvyn V, Lachance P, Sulea T, Menard R. 2005. The papain-like protease from the severe acute respiratory syndrome coronavirus is a deubiquitinating enzyme. Journal of virology 79:15199-15208.

349. Devaraj SG, Wang N, Chen Z, Chen Z, Tseng M, Barretto N, Lin R, Peters CJ, Tseng CT, Baker SC, Li K. 2007. Regulation of IRF-3-dependent innate immunity by the papain-like protease domain of the severe acute respiratory syndrome coronavirus. The Journal of biological chemis-

try 282:32208-32221.

350. Sun Z, Chen Z, Lawson SR, Fang Y. 2010. The cysteine protease domain of porcine reproductive and respiratory syndrome virus nonstructural protein 2 possesses deubiquitinating and interferon antagonism functions. Journal of virology 84:7832-7846.

351. Lemm JA, Rumenapf T, Strauss EG, Strauss JH, Rice CM. 1994. Polypeptide requirements for assembly of functional Sindbis virus replication complexes: a model for the temporal regulation of minus- and plus-strand RNA synthesis. The EMBO journal 13:2925-2934.

352. Shirako Y, Strauss JH. 1994. Regulation of Sindbis virus RNA replication: uncleaved P123 and nsP4 function in minus-strand RNA synthesis, whereas cleaved products from P123 are required for efficient plus-strand RNA synthesis. Journal of virology 68:1874-1885.

353. Kaur J, Debnath J. 2015. Autophagy at the crossroads of catabolism and anabolism. Nature reviews. Molecular cell biology 16:461-472.

354. D'Angelo G, Vicinanza M, Di Campli A, De Matteis MA. 2008. The multiple roles of PtdIns(4)P -- not just the precursor of PtdIns(4,5)P2. Journal of cell science 121:1955-1963.

355. Fritsch SD, Weichhart T. 2016. Effects of Interferons and Viruses on Metabolism. Frontiers in immunology 7:630.

356. Xue B, Yang D, Wang J, Xu Y, Wang X, Qin Y, Tian R, Chen S, Xie Q, Liu N, Zhu H. 2016. ISG12a restricts hepatitis C virus infection through ubiquitination-dependent degradation pathway. Journal of virology.

357. Maier HJ, Neuman BW, Bickerton E, Keep SM, Alrashedi H, Hall R, Britton P. 2016. Extensive coronavirus-induced membrane rearrangements are not a determinant of pathogenicity. Sci Rep 6:27126.

Samenvatting

Curriculum vitae

List of publications

SAMENVATTING

Virussen kunnen levensbedreigende infecties veroorzaken, ondanks het feit dat ze relatief simpel in elkaar zitten. Het virusdeeltje bestaat uit het genoom dat is ingepakt in een of meerdere eiwitten. Bij veel virussen bevat het deeltje ook een membraan, met daarin verankerd de eiwitten waarmee het virusdeeltje aan een receptor kan binden om een gastheercel te infecteren. Na dit moment van infectie, interacteren virussen op allerlei vlakken met de gastheercel om uiteindelijk nieuwe virusdeeltjes te kunnen maken. Dit stapsgewijze proces wordt de replicatiecyclus genoemd, en tussen virusfamilies en -groepen bestaat aanzienlijke variatie waar het de details van deze cyclus betreft. In het geval van de positiefstrengige (+) RNA-virussen bestaat het virale genoom uit een enkelstrengs mRNA molecuul dat direct na het binnendringen in de cel wordt afgelezen door ribosomen om zo de eerste virale eiwitten te produceren. Deze eiwitten zorgen ervoor dat het genoom wordt vermenigvuldigd en kan worden verpakt in nieuwe virusdeeltjes.

Dit proefschrift richt zich op de een specifiek aspect van de replicatie van de arterivirussen en de coronavirussen (twee +RNA-virusfamilies), namelijk de vorming van zogenaamde replicatieorganellen in het cytoplasma van de geïnfecteerde cel. Arterivirussen en coronavirussen zijn evolutionair verwant en behoren tot de orde van de nidovirussen. Arterivirussen veroorzaken vooral problemen in de veterinaire wereld, terwijl coronavirussen ook humane infecties kunnen veroorzaken. De bekendste coronavirussen zijn het severe acute respiratory syndrome coronavirus (SARS-CoV) en Middle East respiratory syndrome coronavirus (MERS-CoV), die beiden dodelijke respiratoire infecties in de mens kunnen veroorzaken. Hoewel het genoom van coronavirussen twee tot drie keer groter is dan dat van arterivirussen, is de genoomorganisatie en replicatiecyclus van deze twee virusfamilies in grote lijnen vergelijkbaar. De voor mensen ongevaarlijke arterivirussen worden daarom mede gebruikt als model om de replicatiecyclus van levensbedreigende coronavirussen in kaart te brengen.

+RNA virale replicatieorganellen zijn structuren die aangemaakt worden in de geïnfecteerde gastheercel op basis van een samenspel tussen virale en cellulaire spelers. De basis van de replicatieorganellen wordt gevormd door membranen die 'gestolen' worden van de gastheercel. De transformatie van deze membranen tot unieke membraanstructuren wordt aangestuurd door specifieke +RNA virale transmembraaneiwitten, vermoedelijk in nauwe samenwerking met gastheerceleiwitten. De omvangrijke wetenschappelijke literatuur over +RNA-virale replicatieorganellen wordt samengevat in **hoofdstuk 2**. In de wetenschappelijke literatuur is veel gespeculeerd over de functie van deze replicatieorganellen tijdens virusinfectie. Ten eerste wordt gedacht dat deze structuren een "micromilieu" vormen ter bevordering van de enzymatische reacties die nodig zijn tijdens de reproductie van het virale genoom. Ook zouden deze structuren kunnen bijdragen aan de regulatie van de replicatiecyclus, door verschillende processen te compartimentaliseren. Tot slot wordt aangenomen dat de replicatieorganellen ervoor zorgen dat de gastheercel het binnengedrongen virus niet (of pas later) kan herkennen. De structuren zouden een soort schild vormen om het virale genoom af te schermen van het zogenaamde aangeboren

immuunsysteem. Replicatieorganellen worden niet alleen in nidovirus- geïnfecteerde cellen gevormd, maar in alle eukaryote cellen die geïnfecteerd zijn met een +RNA-virus, hoewel de soort membraanstructuren en het als membraandonor gebruikte cellulaire compartiment sterk kunnen vetschillen. De vorming van deze membraanstructuren is daarmee één van de meest karakteristieke elementen van de replicatiecyclus van deze grote virusgroep. Voorbeelden van de replicatieorganellen van arterivirussen en coronavirussen zijn afgebeeld in **hoofdstuk 2** figuur 2 en 4. Arterivirus-geïnduceerde replicatieorganellen bestaan uit "double-membrane vesicles" (DMVs), gesloten blaasjes die zijn omgeven met twee gepaarde membranen (**hoofdstuk 2**, figuur 2B). Deze DMVs zijn via hun buitenmembraan met elkaar verbonden en vormen zo een netwerk. Coronavirussen vormen naast DMVs ook nog enkele andere membraanstructuren zoals "convoluted membranes", "spherules" en "vesicle packets".

Bij nidovirussen wordt de vorming van de replicatieorganellen geïnduceerd door de virale eiwitten die gemaakt worden door translatie van het virale genoom. Deze eiwitten worden gemaakt als onderdeel van twee lange poly-eiwitten, die intern gekliefd worden tot losse eenheden (nonstructural proteins, nsps) door proteases die in deze poly-eiwitten aanwezig zijn. Doordat de replicatiecyclus van een virus een complex proces is, is het lastig om specifieke onderdelen van de virale replicatiemachine te modificeren zonder dat de replicatie zelf verstoord wordt of verloren gaat. Door bijvoorbeeld mutaties aan te brengen in de nsps die de vorming van replicatieorganellen induceren zou men kunnen bestuderen hoe de organellen gevormd worden en welke gastheercelfactoren daarvoor nodig zijn. Maar als door zulke mutaties essentiële aspecten van de replicatiecyclus niet meer functioneren worden de virale eiwitten die de vorming van membraanstructuren aansturen überhaupt niet meer gemaakt, waardoor er geen replicatieorganellen worden gevormd. **hoofdstuk 3** beschrijft onderzoek naar de vorming van arterivirus replicatieorganellen. Sinds 2001 was bekend dat de expressie van twee arterivirale nsps (nsp2 en nsp3) voldoet om - buiten de context van virusreplicatie - de vorming van membraanstructuren te induceren. Deze 'surrogaat'structuren lijken sterk op de replicatieorganellen die gevormd worden tijdens arterivirusinfectie. Omdat nsp5, naast nsp2 en nsp3, het enige andere arterivirale transmembraan nsp is, was het aannemelijk dat nsp5 ook een rol speelt in de vorming van DMVs, en ook dit is in dit hoofdstuk bestudeerd. De DMVs die werden gevormd na gezamenlijke expressie van nsp2, nsp3 en nsp5 waren kleiner en uniformer, maar de globale structuur van de DMVs veranderde niet. Dit wijst erop dat nsp5 waarschijnlijk een regulerende rol heeft. Ook is in dit onderzoek een driedimensionale reconstructie gemaakt van de 'surrogaat' DMVs, om meer inzicht te krijgen in hun biogenese. Daaruit bleek dat waarschijnlijk eerst twee membranen worden gepaard, die daarna tot DMVs worden getransformeerd.

Het was lang onbekend welke coronavirale eiwitten nodig zijn om DMVs (en de andere structuren van het coronavirus replicatieorganel) te vormen. In 2013 beschreven Angelini *et al*. dat voor SARS-CoV nsp3, nsp4 en nsp6 nodig zijn voor de vorming van DMVs. Coronavirus nsp3, nsp4 en nsp6 zijn te vergelijken met arterivirus nsp2, nsp3 en nsp5 (zie ook **hoofdstuk 2**, figuur 1). In **hoofdstuk 4** laten we echter zien dat voor zowel SARS-CoV

als MERS-CoV expressie van nsp3 en nsp4 voldoende is om DMV-vorming te induceren, en dat MERS-CoV nsp6 geen rol lijkt te spelen bij DMV-vorming. Ook dit onderzoek werd uitgevoerd met behulp van gedetailleerde driedimensionale reconstructies op basis van elektrontomografie, en laat zien dat arterivirussen en coronavirussen vergelijkbare mechanismen gebruiken om DMVs te vormen. Zoals eerder vermeld maken de coronavirus nsps deel uit van een groot poly-eiwit, dat door interne proteases tot individuele nsps wordt gekliefd. Deze proteases bevinden zich in nsp3 en nsp5. In dit onderzoek is ook gekeken naar de rol in DMV-vorming van de klieving tussen nsp3 en nsp4 door het protease in nsp3. De klieving tussen nsp3 en nsp4 bleek essentieel om DMV-vorming op gang te brengen. Als deze klieving werd geblokkeerd, werden de membranen nog wel gepaard, maar in plaats van DMVs accumuleerden dubbele membranen, vaak in de vorm van concentrische structuren. Deze resultaten geven aan dat de klieving van het virale poly-eiwit een integrale rol kan spelen in de regulatie van de vorming van +RNA virale replicatieorganellen.

Cellen hebben een breed scala aan sensoren om de aanwezigheid van een virus te detecteren. Deze sensoren herkennen bijvoorbeeld het virale genoom, virale eiwitten of virusdeeltjes. Herkenning is gebaseerd op bepaalde ongebruikelijke moleculaire patronen, en is niet gericht op een specifiek pathogenen, zoals dat wel het geval is bij de adaptieve immuunrespons. Als een cel een binnengedrongen virus heeft gesignaleerd, wordt het aangeboren immuunsysteem geactiveerd. Dit zorgt ervoor dat zowel in de geïnfecteerde cel als in nabijgelegen cellen een antivirale modus aangeschakeld wordt, die deze cellen moeilijker te infecteren maakt en virusreplicatie remt. Dit signaal wordt onder meer overgedragen door interferon eiwitten. Ook zorgt de antivirale modus ervoor dat witte bloedcellen worden gerekruteerd om het adaptieve immuunsysteem te activeren. Deze mechanismen, en hoe ze gereguleerd worden, worden toegelicht in **hoofdstuk 5**. Om toch te kunnen repliceren hebben virussen verschillende methoden ontwikkeld om te voorkomen dat ze herkend worden of om de cellulaire respons te blokkeren of te vertragen. Dit resulteert in een constante wapenwedloop tussen het aangeboren immuunsysteem en virussen.

De resultaten beschreven in **hoofdstuk 6** toonden aan dat het aangeboren immuunsysteem arterivirus DMV-vorming, door expressie van virale eiwitten geïnduceerd, kan remmen. In dit onderzoek zijn cellen die arterivirus nsp2 en nsp3 tot expressie brengen behandeld met interferon om de antivirale modus te activeren. Aangezien interferonbehandeling virusreplicatie op meerdere fronten remt, is dit onderzoek uitgevoerd buiten de context van virusinfectie om specifiek een effect van het aangeboren immuunsysteem op DMV-vorming te kunnen onderzoeken. In deze proefopzet zorgde interferonbehandeling ervoor dat minder cellen DMVs vormden. Daarnaast werden er na interferon behandeling meer gepaarde membranen gevonden (die geen DMVs vormden) in vergelijking met onbehandelde cellen. Deze bevindingen wijzen op remming van DMV-biogenese door het aangeboren immuunsysteem. De antivirale respons die door interferon wordt geactiveerd leidt tot verhoogde expressie van minstens driehonderd verschillende genen. Van drie van deze genen (CH25H, viperin en PLSCR1) is getest of ze invloed hebben op DMV-vorming door arterivirus nsp2 en nsp3, omdat elders vergelijkbare effecten van hun

genproducten waren beschreven. CH25H, viperin en PLSCR1 bleken echter niet betrokken bij de remming van arterivirale DMV-vorming door het aangeboren immuunsysteem, wat suggereert dat dit gebeurt via een tot op heden onbekend mechanisme.

Het werk in dit proefschrift verschaft nieuwe inzichten in de biogenese van replicatieorganellen van arterivirussen en coronavirussen. Ook is nu duidelijk dat cellen actief proberen de vorming van deze replicatieorganellen tegen te gaan. Als in toekomstig onderzoek het mechanisme van de remming van DMV-vorming door het aangeboren immuunsysteem opgehelderd wordt, kan deze kennis bijvoorbeeld gebruikt worden om selectieve antivirale strategieën te ontwikkelen.

CURRICULUM VITAE

Diede Oudshoorn werd 5 februari 1989 geboren te Warmond. In 2005 behaalde hij zijn gymnasiumdiploma aan het Stedelijk Gymnasium in Leiden. Vervolgens begon hij aan de opleiding Biomedische Wetenschappen aan de Universiteit Leiden. Tijdens de bachelor fase nam hij deel aan een uitwisselingsprogramma met het Karolinska Instituut in Stockholm, Zweden. Tijdens de onderzoeksspecialisatie in de master fase heeft Diede zijn eerste stageproject uitgevoerd bij de afdeling Medische Microbiologie (LUMC) onder begeleiding van Kazimier Wannee, M.Sc. en dr. ir. Marjolein Kikkert. De afstudeerstage werd uitgevoerd in New York bij het Department of Microbiology van de Icahn School of Medicine at Mount Sinai, onder supervisie van dr. Gijs Versteeg en prof. dr. Adolfo García-Sastre. Daar werkte hij aan ISG15 (interferon-stimulated gene 15) van de muis. Direct na het behalen van zijn masterdiploma (*cum laude*) begon hij aan een promotietraject bij de LUMC-afdeling Medische Microbiologie, onder begeleiding van promotor prof. dr. Eric Snijder en zijn voormalige stagebegeleider dr. ir. Marjolein Kikkert. Zijn onderzoek richtte zich in eerste instantie op de interactie tussen het aangeboren immuunsysteem en virale replicatie en breidde zich gedurende het project uit naar de vorming van virusgeïnduceerde membraanstructuren onder begeleiding van dr. Montserrat Bárcena.

LIST OF PUBLICATIONS

1. **Oudshoorn D**, Rijs K, Limpens RWAL, Groen K, Koster AJ, Snijder EJ, Kikkert M, Bárcena M. 2017. Expression and Cleavage of Middle East Respiratory Syndrome Coronavirus nsp3-4 Polyprotein Induce the Formation ofDouble-Membrane Vesicles That MimicThose Associated with Coronaviral RNA Replication. mBio 8(6) e01658-17.
2. **Oudshoorn D**, van der Hoeven B, Limpens RW, Beugeling C, Snijder EJ, Bárcena M, Kikkert M. 2016. Antiviral Innate Immune Response Interferes with the Formation of Replication-Associated Membrane Structures Induced by a Positive-Strand RNA Virus. mBio 7(6) e01991-16.
3. van der Hoeven B*, **Oudshoorn D***, Koster AJ, Snijder EJ, Kikkert M, Bárcena M. 2016. Biogenesis and architecture of arterivirus replication organelles. Virus Res 220:70-90.
4. de Wilde AH, Raj VS, **Oudshoorn D**, Bestebroer TM, van Nieuwkoop S, Limpens RW, Posthuma CC, van der Meer Y, Bárcena M, Haagmans BL, Snijder EJ, van den Hoogen BG. 2013. MERS-coronavirus replication induces severe *in vitro* cytopathology and is strongly inhibited by cyclosporin A or interferon-alpha treatment. J Gen Virol 94:1749-1760.
5. **Oudshoorn D**, Versteeg GA, Kikkert M. 2012. Regulation of the innate immune system by ubiquitin and ubiquitin-like modifiers. Cytokine Growth Factor Rev 23:273-282.
6. **Oudshoorn D**, van Boheemen S, Sanchez-Aparicio MT, Rajsbaum R, Garcia-Sastre A, Versteeg GA. 2012. HERC6 is the main E3 ligase for global ISG15 conjugation in mouse cells. PLoS One 7:e29870.

*Authors contributed equally tot his study

